CRUSTAL STRUCTURE OF THE MARIANA ISLAND ARC SYSTEM AND OLD PACIFIC PLATE FROM SEISMIC REFRACTION DATA

A THESIS SUBMITTED TO THE GRADUATE DIVISION OF THE UNIVERSITY OF HAWAII IN PARTIAL FULFILLMENT OF THE REQUIREMENTS FOR THE DEGREE OF

MASTER OF SCIENCE

IN GEOLOGY AND GEOPHYSICS

MAY 1978

By

Sharon L. LaTraille

Thesis Committee:

Donald M. Hussong, Chairman
Ralph Moberly
Mark E. Odegard

We certify that we have read this thesis and that in our opinion it is satisfactory in scope and quality as a thesis for the degree of Master of Science in Geology and Geophysics.

THESIS COMMITTEE

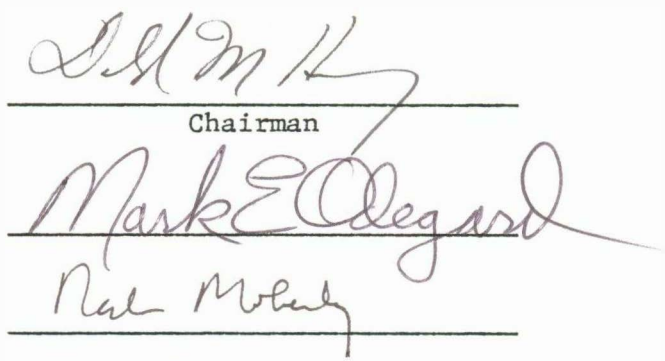

Chairman

ACKNOWLEDGMENTS

The author wishes to thank her advisor Dr. D. M. Hussong for suggesting the topic and for critical discussions and guidance on the project. Data analysis could not have proceeded smoothly without the aid of L. Wipperman, J. Tuttle and Dr. M. E. Odegard, among others. Portions of the draft were typed by B. Ambos, J. Miller, K. Mansfield and K. Lee, while S. Dang and K. Mansfield did much of the artwork. The author also wishes to thank her husband for his understanding and encouragement throughout the project.

While the work was in progress, the author was supported under the grants OCE 76-02187, ONR N00014-75-C-0209P08 and CU-H 125903A2. Refraction seismic data were collected under the latter grant.

ABSTRACT

Twenty-six new explosion refraction profiles from the Mariana island arc system and old Pacific plate along a 750 km east-west line at about 18°N latitude are analyzed to determine crustal structure across the Mariana basin (old Pacific plate), arc-trench gap, Mariana ridge and Mariana trough. The Pacific plate east of the Mariana trench has a crustal thickness of 6.8 km, similar to that of average Pacific ocean crust, but has thicker than average layers 2A and 2B. This is most likely due to lower velocity material introduced by local seamount volcanism. Large scale vertical faulting in the arc-trench gap is supported by the data in this study, while plate accretion is not. Thick sequences of low-velocity material are also found in the arc-trench gap, and no mantle velocities are found. Crustal structure on the Mariana ridge is roughly similar to that of the arc-trench gap. There is evidence here of arrivals from a relatively high velocity body under the ridge, possibly a volcanic plug or sill. In the Mariana trough, an average crustal thickness of 5 km is found, with evidence of crustal thinning toward the center of the trough. These data, together with depth-age and depth-heat flow relationships, indicate crustal formation in the Mariana marginal basin differs considerably from that at mid-ocean ridges. Crust which forms in the marginal basin is thinner, cools faster and sinks more quickly than oceanic crust.

TABLE OF CONTENTS

LIST OF TABLES

LIST OF ILLUSTRATIONS

LIST OF ILLUSTRATIONS (continued)

LIST OF ILLUSTRATIONS (continued)

INTRODUCTION

This thesis describes the first crustal structure interpretation across the entire Mariana island arc system using seismic refraction data. Twenty-six new seismic refraction profiles, extending from the Mariana trough eastward onto the old Pacific plate, are analyzed. While the Mariana island arc system was extensively studied using other geophysical techniques, such as heat flow measurements, reflection profiling, dredging and DSDP coring (Karig, 1971a), there have been no published seismic refraction studies of the area. Velocity versus depth models determined from the data analyzed in this report are, therefore, compared with results from island arc systems other than the Mariana. A brief description of the Mariana system follows.

TECTONIC SETTING

The Mariana island arc system is located in the northwest Pacific, separating the Philippine Sea from the Pacific ocean proper. Its surface expression is the Mariana Islands located south of the Bonin and Volcano Islands on Figure 1. Figure 2 shows the tectonic elements of the Mariana system in detail. A cross-section of a typical island arc system with the terminology used in this paper is shown in Figure 3.

The Pacific plate just east of the Mariana trench is thought to contain some of the oldest material in the Pacific basin. Lack of magnetic anomalies here places the age of this crust in one of the Mesozoic quiet zones. Extrapolation backward from magnetic anomaly lineations nearby indicates a Jurassic age for most of the Mariana basin. Parts of the basin, however, may be as young as upper Cretaceous in age from DSDP drill site results and a more complex early development of the Pacific plate (Hilde et al., 1977). Structure here is complicated by the presence of a seamount province. A significant problem in this area is determining the crustal thickness and velocity structure of old sea floor crust.

The Mariana trench, where the Pacific plate is being subducted under the Philippine plate, is defined on Figure 2 by the 6 km depth contour, but is over 11 km deep at its deepest point (Fisher and Hess, 1963, page 418). Earthquake epicenters indicate that it dips at an angle of 40° to 60° from the surface to a depth of 200 to

Fig. 1. Location of the Mariana Islands.

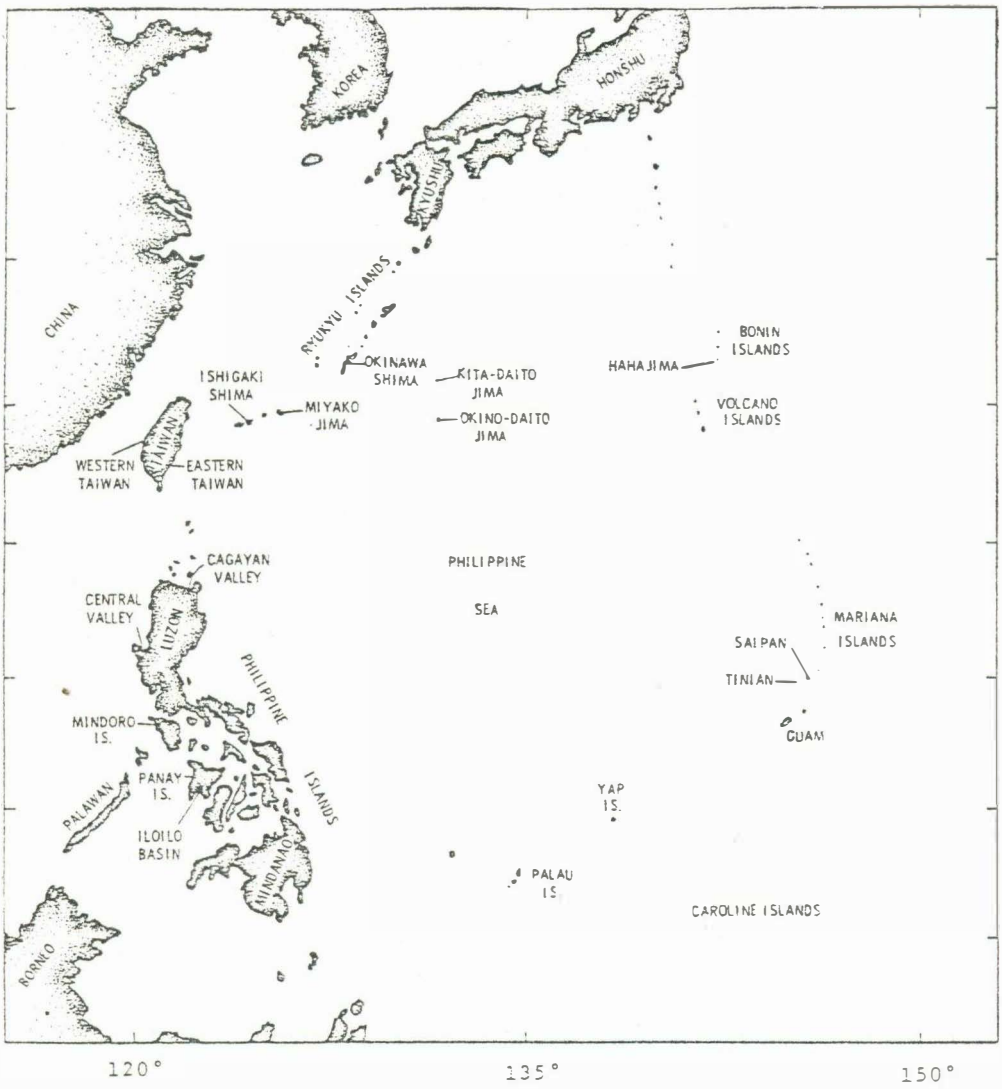
KOREA
HONSHU
SHIKOKU
CHINA
RYUKYU ISLANDS
OKINAWA SHIMA
KITA-DAITO JIMA
OKINO-DAITO JIMA
HAHAJIMA
BONIN ISLANDS
VOLCANO ISLANDS
ISHIGAKI SHIMA
MIYAKO JIMA
TAIWAN
WESTERN TAIWAN
EASTERN TAIWAN
CAGAYAN VALLEY
CENTRAL VALLEY
LUZON
PHILIPPINE SEA
PHILIPPINE ISLANDS
MARIANA ISLANDS
SAIPAN
TINIAN
GUAM
MINDORO IS.
PANAY IS.
PALAWAN
ILOILO BASIN
MINDANAO
YAP IS.
PALAU IS.
CAROLINE ISLANDS
BORNEO
35° N
25° N
15° N
5° N
120°
135°
150°

Fig. 2. Major tectonic features of the Mariana island arc system outlined by generalized depth contours in kilometers. An approximation of the track line along which the data for this study were collected (dashed line) is shown along with DSDP drill sites closest to the study region. The starred pattern indicates the approximate position of the mid-slope basement high between the frontal arc and the trench, and triangles mark the positions of recent andesitic volcanoes (adapted from Karig, 1971a).

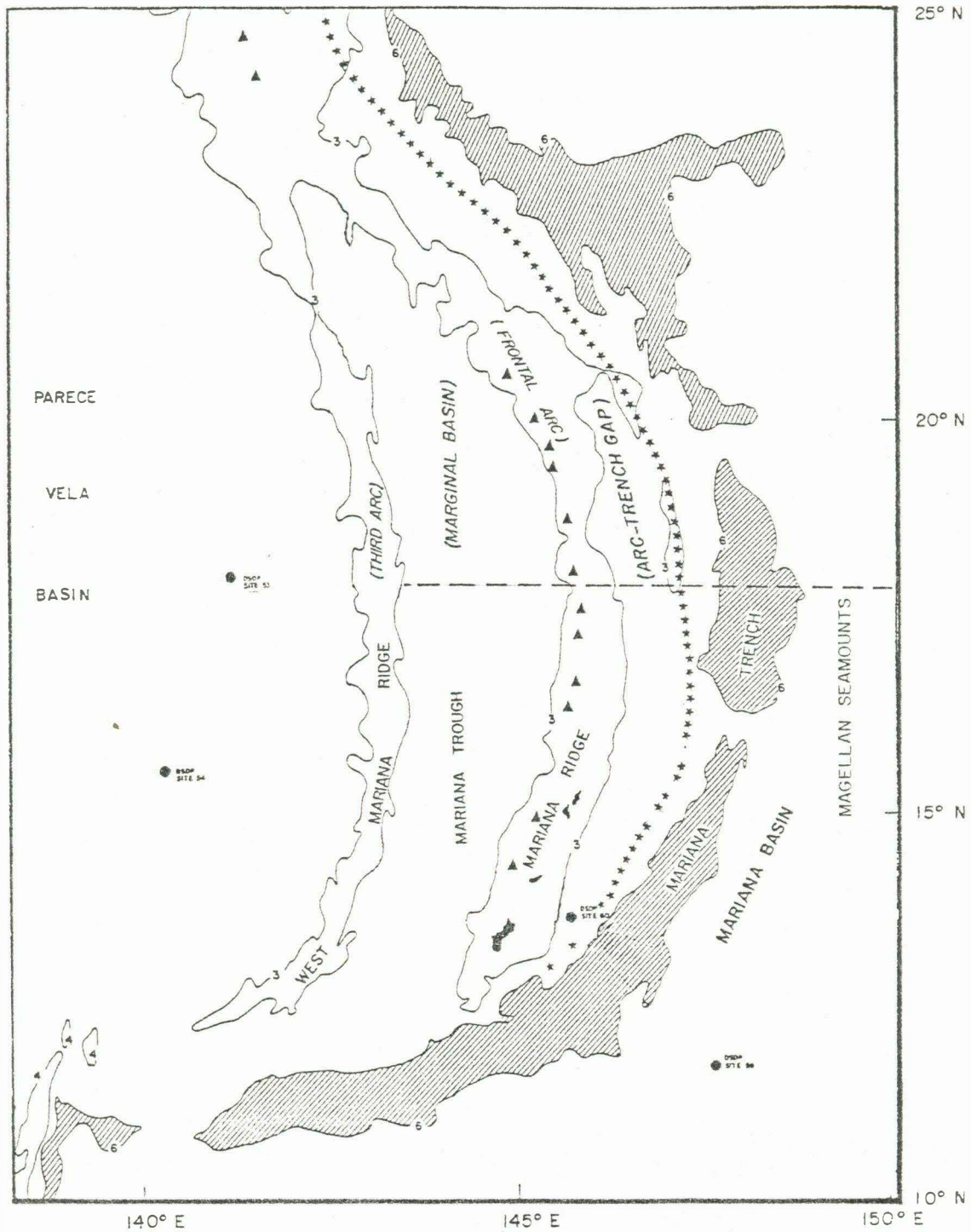
25° N
20° N
15° N
10° N
140° E
145° E
150° E
PARECE
VELA
BASIN
(THIRD ARC)
RIDGE
(MARGINAL BASIN)
FRONTAL ARC
(ARC-TRENCH GAP)
MARIANA TROUGH
MARIANA RIDGE
TRENCH
MAGELLAN SEAMOUNTS
MARIANA BASIN
WEST MARIANA
DSDP SITE 53
DSDP SITE 54
DSDP SITE 60
DSDP SITE 59

Fig. 3. Cross section of a typical island arc system, showing tectonic units and terminology used in this paper (adapted from Karig and Sharman, 1975).

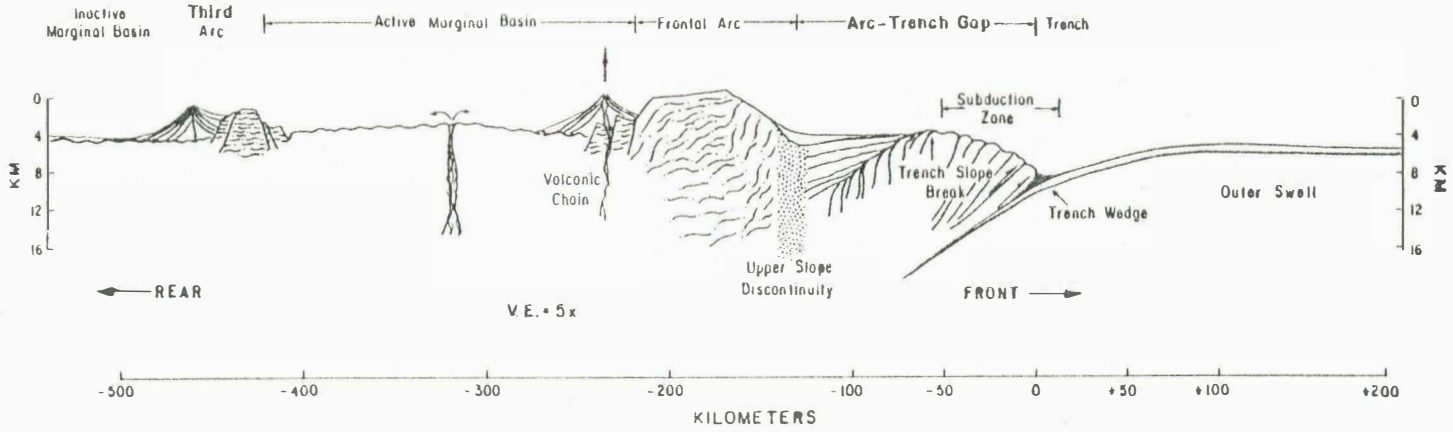
Inactive Marginal Basin
Third Arc
Active Marginal Basin
Frontal Arc
Arc-Trench Gap
Trench
Subduction Zone
Volcanic Chain
Trench Slope Break
Trench Wedge
Outer Swell
Upper Slope Discontinuity
REAR
FRONT
V.E. = 5x
KM
0
4
8
12
16
-500
-400
-300
-200
-100
-50
0
+50
+100
+200
KILOMETERS

300 km. From there the dip becomes steeper until it is nearly vertical at 700 km depth (Isack et al., 1968; Katsumata and Sykes, 1969; Mogi, 1973). This configuration may be due to the subducted plate actually sinking and exerting an extensional force on the plate at the surface (Mogi, 1973; Moberly, 1972), or simply to rapid subduction (Katsumata and Sykes, 1969). However, rapid subduction also occurs at the Peru-Chile trench and the seismic zone there dips only 10^{o} to 35^{o} (Hussong et al., 1976). The steepening of the Mariana seismic zone could be attributed to the recent (10 m.y. ago) beginning of the Philippine trench just east of the Philippine Islands (see Figure 1). This trench subducts the Philippine plate and, in effect, pulls the island arc system westward, but the lower part of the slab subducting in the Mariana trench sticks in the deeper mantle, causing its dip angle to increase (Sclater, 1972).

The arc-trench gap, consisting of the area between the Mariana ridge and trench, which Karig terms the accretionary prism, is made up of sediments from either the island arc vulcanism, scrapings off the subducting plate or a mixture of both. Karig and Sharman (1975) describe the buildup of material in the arc-trench gap as the accretion of the sediment and some of the igneous crust from the downgoing plate in the form of thrust slices or sheared-off slabs. The upper, more horizontal part of the arc-trench gap (Figure 3) contains volcanic ash, pumice and other pyroclastics ranging in age from Miocene to Recent in layered deposits (Shipboard Scientific

Party, 1974; Fryer, 1977). Seismic data may show which of these processes is more important in the Mariana system.

The Mariana ridge (frontal arc), the shallowest element of the island arc system, in outlined in Figure 2 by the 3 km depth contour. It ranges in width from over 250 km where it joins the Bonin ridge to the north to less than 40 km wide near the survey area at 18° north. The ridge contains the Mariana islands as well as active submarine volcanoes. The structure of the ridge is not well known. Evidence from other frontal arcs indicates that it is not simply a constructional pile of volcanics. Mafic schists, with serpentinite and peridotite bodies similar to those described under other frontal arcs may occur beneath the volcanic rocks and calcareous rock of the raised limestone islands (Karig, 1971a). On the other hand, it could be built upon material from an old north-south fracture zone along which it is postulated by Hilde et al. (1977) the original Mariana trench subduction was initiated shortly after 45 m.y. ago. Determining crustal thickness under the ridge might help resolve its origin. Andesitic volcanoes located along the ridge's western edge almost entirely bury the sharp fault scarp dividing this ridge from the Mariana trough. This scarp is postulated (Karig, 1971a) to have been split away from the West Mariana ridge (third arc) during a cycle of back-arc spreading.

Sea floor spreading similar to that at mid-ocean ridges is thought to have generated the marginal basins or troughs behind island arcs, including the Mariana trough. Several hypotheses have

been put forth describing the mechanism of this spreading. Moberly (1972) suggests that the sinking slab causes an extensional region to form behind the island arc and trench, and that warm asthenosphere pushed aside by the sinking slab simply moves upward to fill in this extensional region. Karig (1971b), on the other hand, postulates that shear-heated mantle material in the form of diapirs wells up and causes the extension while building new crust. There is considerable evidence for crustal extension in the trough, including (1) steep normal fault zones bounding the basin, (2) thick sediment covers on the outer flanks of the frontal arc and third arc which bound the basin, and an almost sediment-free area in the basin interior, (3) similarities in structure, morphology and sediment distribution between the Mariana trough and the basin to the west, which are successively older (Karig, 1971a). A ridge and trough topography roughly parallel to the strike of the island arc dominates the surface structure. The central part of the trough (the axial high) is about 1 km shallower than the average basin depth. Heat flow measurement show high values on and near the axial high with abnormally low values away from the axis, possibly due to hydrothermal circulation (Anderson, 1975). Surface and body wave attenuation studies may indicate the presence of a zone of low velocity material in the upper mantle under the trough (Seekins and Teng, 1977; Barazangi and Isacks, 1971; Aggarwal and Barazangi, 1972). Dredge hauls from the axial high have all contained fresh

and very recent basalts (Karig, 1971a; Hart et al., 1972; Fryer, 1977). Trace element analysis of such basalts by Hart et al. (1972) indicate that they are similar to basalts dredged from mid-ocean ridges.

Very little refraction data have been collected in active marginal basins, almost none in the Mariana trough. In the area of the Philippine Sea, Murauchi et al. (1968) ran 28 refraction profiles across the Philippine and Parce Vela basins, and the Nansei Shoto, Oki-Daito, Kyushu-Palau and Honshu-Mariana ridges. These authors found velocities similar to oceanic crust beneath the basins with a layer of 3.5 km/sec velocity material controlling the characteristically rough topography. Under the ridges they found crustal thickening associated mainly with the thickening of the 3.5 km/sec layer and a thick section of material with a velocity of 5.5 to 6.0 km/sec. Extreme crustal diversity was found in refraction studies in the marginal basins of the Melanesian Borderland (the area between Australia on the west and New Zealand and Tonga on the east). In the Lau-Havre trough, an active marginal basin like the Mariana trough, crustal thinning toward the center was found (Shor et al., 1971). Interesting problems in the trough include determining crustal thickness, locating the center or centers of spreading and working out the age of the trough.

DATA COLLECTION

In February, 1976, as a part of an IPOD reconnaissance survey (KK76-01-03 Leg 2) a series of refraction profiles were shot for 500 km across the Mariana trough, ridge and trench, and an additional 235 km series of profiles were shot out onto the Mariana basin (Pacific plate). Using the R. V. Kana Keoki, single ship refraction shooting techniques were employed. The line started at 17°48.825'N, 143°26.429'E with the deployment of the first receiver, and ended at 17°55.437'N, 150°49.270'E with the last shot. The location of the line is shown on Figure 2. Figure 4 shows detailed bathymetry and the ship's track for the shot line.

Three tethered ocean bottom seismometers (TOBS), four pop-up ocean bottom seismometers (POBS) and 32 U. S. Navy SSQ-41A sonobuoys were used as receivers. The sonobuoy data are analyzed in this paper.

The refraction shoot was continuous for 47 hours. Sonobuoys were deployed an average of one every 90 minutes. The sonobuoy positions are shown on the track line (Figure 4). Sources were 765 explosive charges made of Tovex Extra, ranging in weight from 1 to 240 pounds. The first 600 shots were spaced three minutes apart, the remainder were spaced five minutes apart.

Sonobuoy data were telemetered by VHF radio to the Kana Keoki and received by U. S. Navy sonobuoy receivers. Signals were divided and filtered in four separate frequency ranges and recorded on four channels of visual recorder.

Fig. 4. Detailed bathymetry of the survey area showing the ship track for the refraction shoot as well as sonobuoy launch positions.

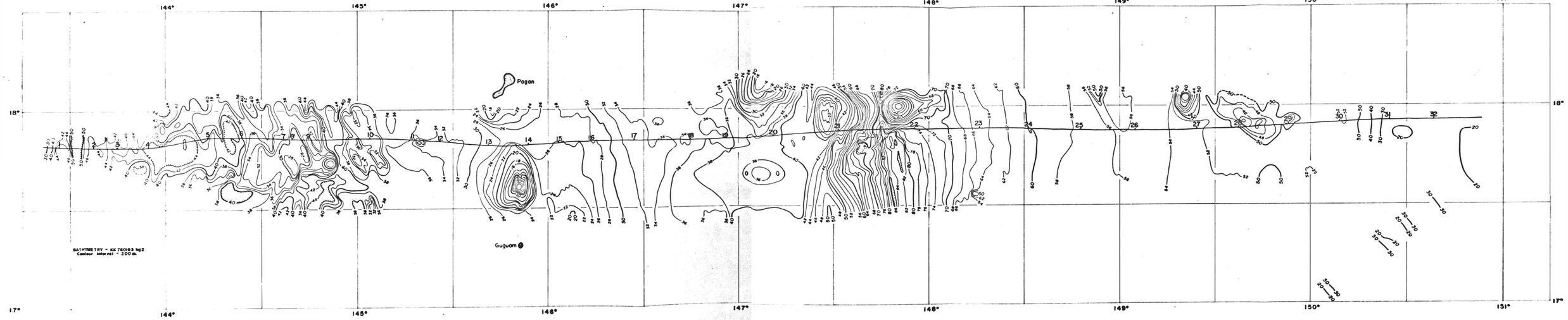
144°
145°
146°
147°
148°
149°
150°
151°
18°
17°
Pagan
Guguan
BATHYMETRY - KK 760603 leg 2
Contour interval - 200 m.

Bathymetry, gravity and magnetics were recorded continuously for the whole leg and reflection records were obtained on all but the shooting track. The profile of bathymetry and gravity along the shooting track and magnetics along a parallel line is shown in Figure 5. All navigation was satellite controlled. Positions were interpolated between satellite fixes from continuously recorded ship's heading and speed through the water.

Fig. 5. Profile of bathymetry and gravity along the shooting track and magnetics along a parallel track.

DATA ANALYSIS

Processing of Sonobuoy Data. The sonobuoy paper record contains three sets of data channels with four channels each, for a total of twelve data channels (see Figure 6 for a sample record). Each set of data channels records one sonobuoy at four different filter settings. Direct water wave and first reflection travel times are picked most often from the high frequency channel since they are less attenuated. Additional channels record the shot detonation time from the towed hydrophone array (Eel), one second tic marks, binary-coded decimal reference time code (datum time), Universal time (station JJY) and the 3.5 KHz echo sounder.

When each sonobuoy is launched, its signal is recorded on the first channels until the signal becomes weak or noisy, or until the average useful limiting range of these sonobuoys is reached, whichever occurs first. Then its signals are switched to the second set of four channels and the newly launched sonobuoy is recorded on the first set. In this way, up to three sonobuoys are recorded simultaneously for each shot. In practice, the third sonobuoy was often beyond its useful range, so channels 9-12 often duplicated channels 5-8. From the paper record of each shot, the following times are picked:

(1) the shot break (detonation) time is read to the nearest 0.01 second off the datum time channel.

(2) the direct (water wave) arrival time is picked as the time difference in seconds between the shot detonation

Fig. 6. Sample sonobuoy record showing data recorded on each channel.

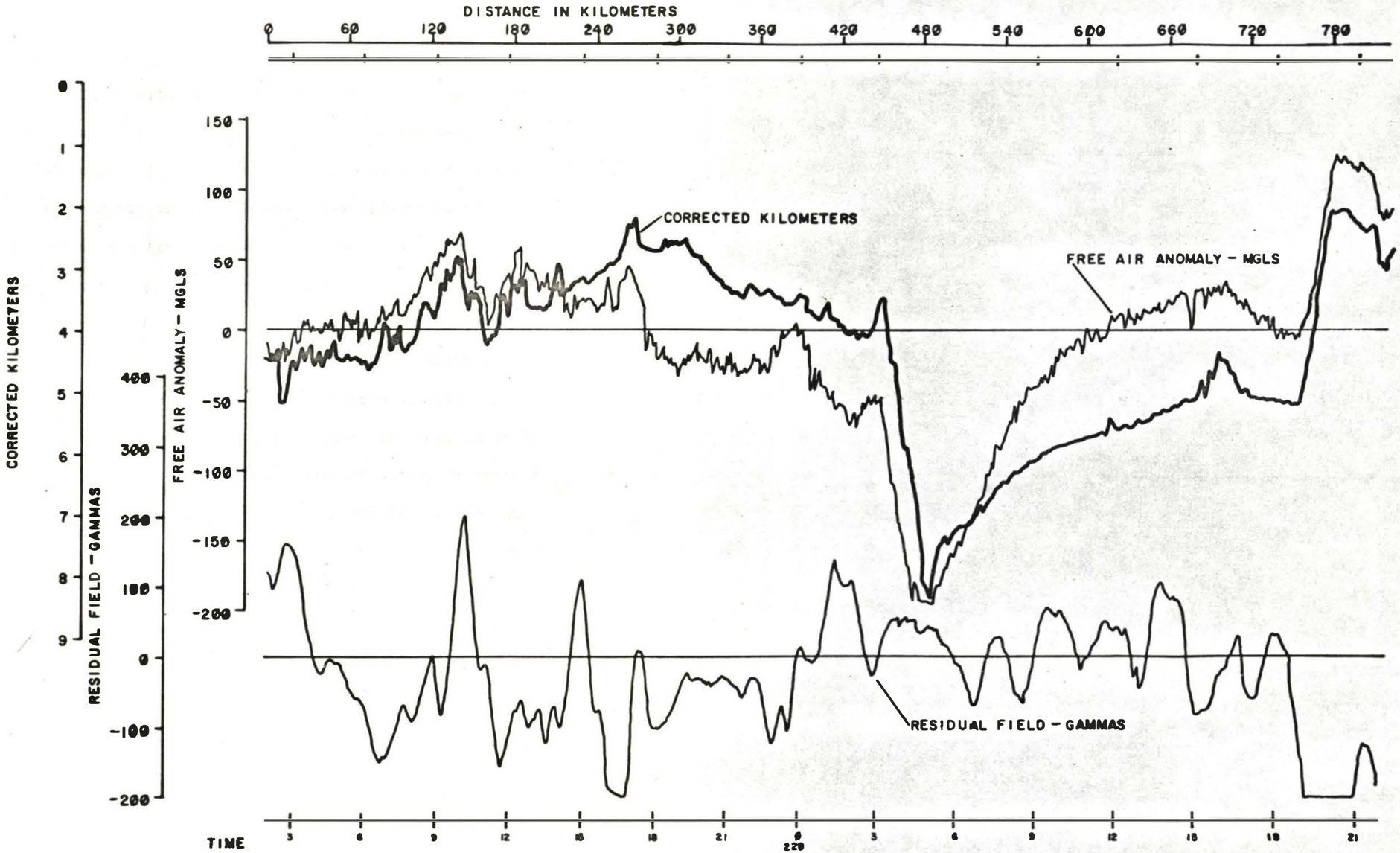

BATHYMETRY, GRAVITY AND MAGNETICS
MARIANA TROUGH TO MARIANA BASIN

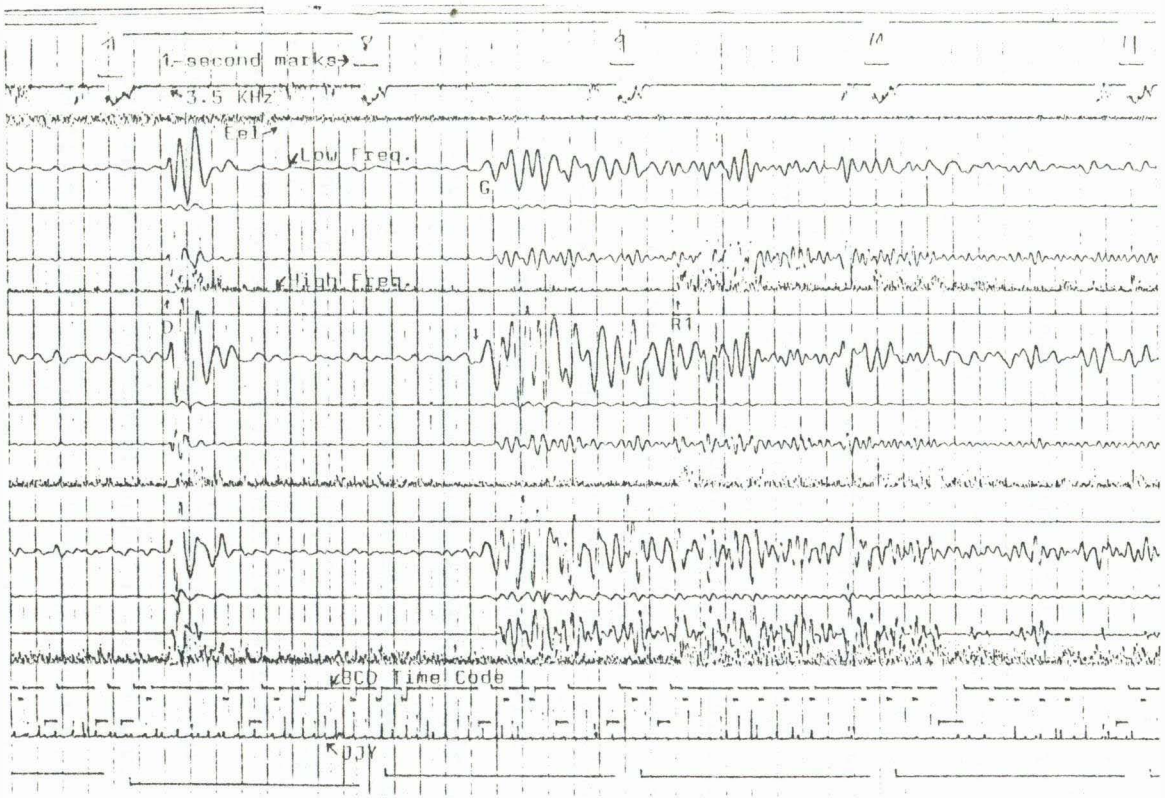
1-second marks
3.5 KHz
Low Freq.
High Freq.
BCD Time Code
P
R1
G

time and the arrival time to the nearest 0.01 second.

(3) in the same manner, arrival times for the first reflected arrival and one or more refracted arrivals are picked.

While these travel times are being picked, the reflection and refraction arrival times are plotted versus water wave travel time to obtain an initial velocity model.

Records were picked a minimum of three times. My system of recording picked arrival times included a subjective evaluation of the pick--good or questionable--depending on signal strength, continuity of waveform from shot to shot, background noise level, shot size and distance from the receiver. These evaluations were reflected in the plots and gave more, or less, weight to each point.

Limitations of Sonobuoy Data. The data for this study were collected along single-ended refraction lines. Thus, the magnitude and direction of any dip in the refracting layer cannot be calculated as it can using a reversed or split profile, although it can be inferred from depth differences in a refracting layer from adjacent stations. Inverse slopes of the travel time curves will give apparent velocities which are too high if the shots are up-dip from the receiving position or too low if the shots are down-dip (Ewing, 1963). This limitation could be especially severe in the area of the arc-trench gap where its structure may be that of an accretionary prism (large, high angle thrust fault slices) postulated by Karig and Sharman (1975).

Applying Corrections and Replotting. Several types of corrections were applied to the refraction data. These include (a) a burn time correction which corrects the shot detonation time, (b) shot and receiver depth corrections which correct both shot and receiver to the ocean's surface, (c) receiver drift correction which corrects for the moderate westward current encountered along much of the shooting leg, (d) shot and receiver bathymetry corrections which correct for variations between a sloping "datum" line and the actual sea floor topography. FORTRAN programs were developed which calculate these corrections as well as performing shot and receiver location and bathymetry lookup functions. A description of the corrections and theory used to generate them are included in Appendix A.

These corrections were applied to the travel times and shot to receiver distance, the times were replotted and a revised velocity and intercept interpretation obtained. Final plots appear in Appendix B.

Tracing Record Sections. In order to aid in the interpretation, shots to one or more sonobuoys in each structural province were traced onto a record section. Travel time and distance corrections have been applied as well as a reducing velocity of 6.0 km/sec. These record sections were then interpreted for velocities and intercepts using "best fit" straight lines. These lines were fitted by eye through the data. Velocities were computed using the relationship:

$$V = \frac{D_i}{(T_i + Di/RV) - T_o}$$

where V = apparent velocity

D_i = distance for T_i

RV = reducing velocity

T_o = intercept time @ D = ϕ

T_i = arrival time @ D_i

Inversion of Travel Time Data and Development of Structure Sections. Inversion of apparent velocity and intercept data to layer velocity versus depth models was done using ray tracing in a spherically stratified earth. The computer program SERIT (Spherical Earth Refraction Inversion Technique, Odegard, 1975) inverts single-ended seismic refraction data using a spherical earth coordinate system, assuming that arrivals are head waves due to velocity discontinuities at various depths. Given the intercepts and apparent velocities, the program uses a bisection method of successive approximations to iterate to the correct solution for each layer velocity and depth. The output includes depth to layer, layer thickness, velocity and critical distance.

A spherical earth ray tracing program (Gettrust, 1977, Geophysical and Polar Research Center, University of Wisconsin) was used to confirm the seismic model arrived at above. This program numerically integrates through a velocity-depth function and produces a table of p, X, T, dp/dΔ, and estimated amplitudes. Up to 200 ray arrivals are plotted versus distance scaled to the user's original

record section. Then the actual water depth and sediment thickness from reflection records were added to the model, along with an assumed sediment velocity. Layer depths were modified and velocity gradients introduced so that the ray arrival times matched the travel times picked on the record sections. In this manner, seismic velocity sections were obtained.

RESULTS

The data presented here can only approximate the actual structure of the survey area. First, because inversion of seismic data is non-unique, the layer velocities and depths shown for each sonobuoy are but one of several possible solutions. In addition to this, the Pacific plate, the simplest structure sampled along the refraction line, is complicated by secondary vulcanism from the Magellan seamount province (Figure 2) as well as crustal deformation caused by the subduction of the plate. From this structurally "simple" region, the analysis extends behind the trench to an even more complex structural province for which the basic assumptions for interpretation--planar, homogeneous isovelocity layers--certainly are only a rough approximation. Even so, consistent trends in velocities and thicknesses of layers allow a generalized interpretation of the Mariana island arc structure to emerge.

Of the thirty-two stations at which data were collected, twenty-six are analyzed in this paper. Stations were numbered sequentially from west to east, but will be discussed in reverse order. A plot of picked and corrected travel times versus distance and the inverted velocity-depth model is included in Appendix B for each buoy, along with seven interpreted record sections for stations 2, 3, 9, 10, 16 and 25. In the following discussion of results by structural province, reference will be made to oceanic layers 2A, 2B, 3A and 3B. The velocity and layer thickness ranges defining these layers are listed in Table 2. A summary of the velocity-depth

models obtained in this study superimposed on a bathymetry plot is shown in Figure 7. Table 1 contains the corresponding tabulated values of velocities, thicknesses and depth to mantle (where determined), as well as station locations. To aid interpretation of the crustal structure, the velocities on Figure 7 were contoured at one km/sec intervals (Figure 8). Also, mean values of velocity and layer thickness for each structural province are summarized in Table 3.

Table 1: Seismic Stations - Mariana Trough to Mariana Basin

Station	Position	Water Depth at Receiver (km)	Velocity (km/sec)							Datum Water Depth (km)[c]	Thickness (km)						Total Depth To Mantle (km)
			1	2	3	4	5	6	7		1	2	3	4	5	6	
1	17°48.8'N 143°26.4'E	4.50	2.44	3.28	3.78	7.77				4.65	0.85	0.90	4.20				10.60
2	17°48.6' 143°37.4'	4.62	2.00[a]	2.8[b]	4.70	6.50	8.06			4.50	0.20	0.54	1.17	3.95			10.36
3	17°48.5' 143°45.3'	4.60	"	3.2[b]	4.30	6.49	8.08			4.53	0.25	0.52	1.57	1.95			8.82
4	17°48.6' 143°55.0'	4.53	"	4.85	5.82	7.49				4.53	0.30	2.29	2.26				9.38
5	17°51.5' 144°13.2'	4.06	-	3.44	5.64	8.18				4.20	-	1.64	2.38				8.23
6	17°51.6' 144°23.1'	4.23	-	3.60[b]	5.12	6.85				3.75	-	2.14	0.45				
8	17°51.2' 144°38.4'	3.05	-	4.51	6.95					3.30	-	3.85					
9	17°51.0' 144°43.6'	3.50	-	3.07	4.35	5.73				4.23	-	1.62	0.19				
10	17°51.2' 145°03.8'	3.42	2.00[a]	3.38	5.55	6.91				3.55	0.46	1.05	2.11				
11	17°50.8' 145°16.9'	3.63	"	2.85	3.69	4.38				3.25	0.53	1.34	1.85				
12	17°50.2' 145°25.6'	3.30	"	2.96	4.75	6.53				3.10	1.12	1.75	1.50				

Table 1: (continued) Seismic Stations - Mariana Trough to Mariana Basin

Station	Position	Water Depth at Receiver (km)	Velocity (km/sec)							Datum Water Depth (km)[c]	Thickness (km)						Total Depth To Mantle (km)
			1	2	3	4	5	6	7		1	2	3	4	5	6	
13	17°49.0' 145°41.0'	2.97	2.56[b]	3.13	4.61	6.54				2.60	1.36	0.96	1.15				
14	17°49.3' 145°54.2'	2.72	2.00[a]	3.31	4.61	5.94				2.68	1.03	1.37	1.48				
15	17°49.9' 146°03.3'	2.69	"	3.63	4.73	6.32	7.22			2.85	0.80	1.58	1.15	1.77			
16	17°50.3' 146°12.8'	2.78	"	3.83	4.61	6.55				3.07	0.49	1.35	2.04				
17	17°50.4' 146°26.7'	3.32	"	3.94	5.80	6.39				3.37	1.00	2.22	1.13				
18	17°50.6' 146°44.6'	3.43	"	4.29	6.15					3.52	0.40	2.93					
19	17°50.8' 146°55.6'	3.45	"	4.00	4.68	6.10				3.71	0.29	1.44	1.99				
20	17°51.4' 147°10.7'	3.88	"	4.14	5.32	6.50				4.00	0.60	1.53	1.79				
23	17°53.2' 148°16.1'	6.49	"	4.11	5.39	6.92	8.20			6.25	0.25	1.65	1.53	1.28			10.96
24	17°52.9' 148°31.7'	6.01	"	3.50[a]	5.39	6.60	7.91			5.89	0.30	1.09	0.90	2.04			10.22

Table 1: (continued) Seismic Stations - Mariana Trough to Mariana Basin

Station	Position	Water Depth at Receiver (km)	Velocity (km/sec)							Datum Water Depth (km)[c]	Thickness (km)						Total Depth To Mantle (km)
			1	2	3	4	5	6	7		1	2	3	4	5	6	
25	17°52.4' 148°48.0'	5.77	"	3.06[b]	4.11	5.89	6.54	7.38	8.20	5.61	0.15	0.49	1.13	0.92	1.20	2.90	12.40
26	17°52.5' 149°04.9'	5.56	"	4.00[a]	5.88	6.85	8.03			5.40	0.19	2.17	0.91	1.83			10.50
27	17°52.7' 149°24.1'	5.22	3.12[b]	4.25	5.40	6.53				5.00	0.78	0.55	1.63				
28	17°52.7' 149°37.3'	4.85	-	3.26	5.30	7.18				4.58	-	2.31	1.97				
29	17°53.9' 149°53.2'	4.98	2.00[a]	4.29	5.86	7.86				5.08	0.15	2.40	2.20				

[a]Assumed velocity

[b]Average velocity - a gradient, not a discrete layer

[c]Averaged along the datum for each station

Table 2: Oceanic Layer Velocities and Thicknesses

Oceanic Layer	Oceanic Velocity* (km/sec)	Thickness* (km)
2A	2.5-3.8	0.5-1.5
2B	4.0-6.0	0.5-1.5
3A	6.5-6.8	2.0-3.0
3B	7.0-7.7	2.0-5.0
Mantle	8.1-8.3	---

*After Clague and Straley, 1976, Table 1, page 135.

Fig. 7. Summary of velocity-depth models determined in this study.

BATHYMETRY PROFILE WITH VELOCITY/DEPTH MODELS

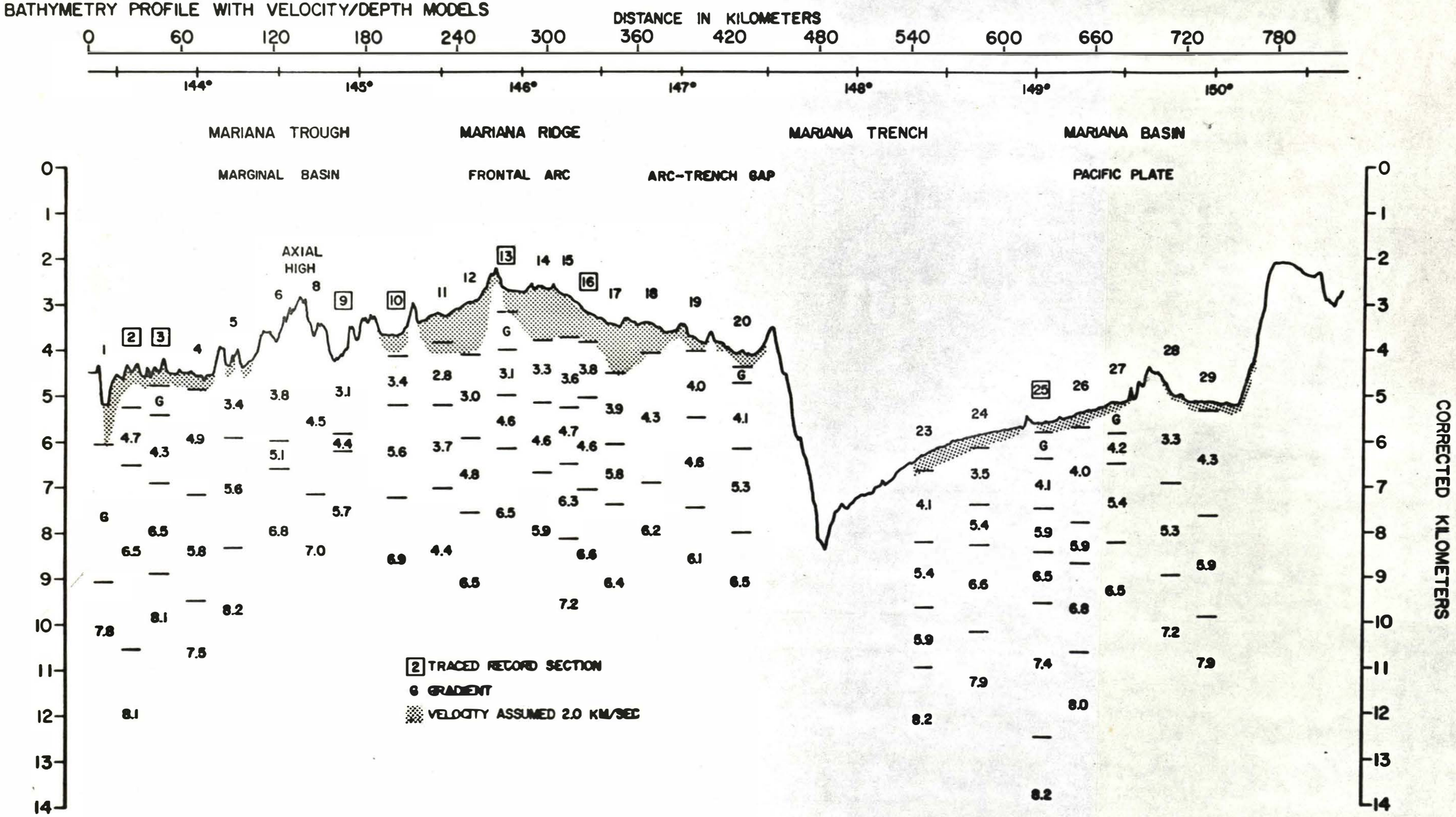

Fig. 8. Velocities contoured at 1-km intervals from the models on Figure 7.

BATHYMETRY PROFILE WITH CONTOURED VELOCITIES

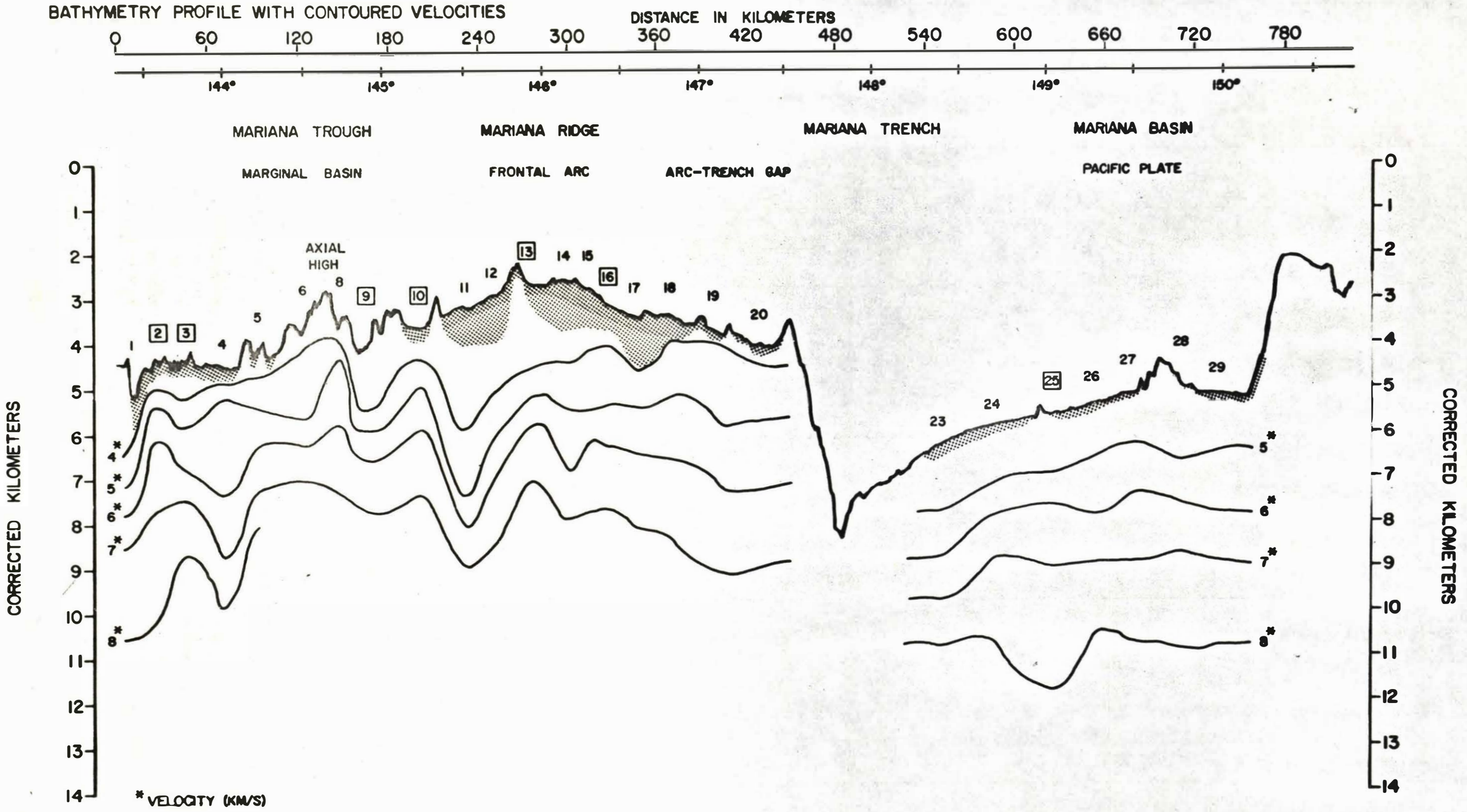

Table 3. Mean Layer Velocity and Thickness by Structural Province for Mariana Island Arc System

Structural Province	Layer Velocity - km/sec[a] ( ) = standard deviation							Layer Thickness - km ( ) = standard deviation						Crustal Thickness km[b]	Depth to Mantle km
	0[c]	1[d]	2A	2B	3A	3B	4	0	1	2A	2B	3A	3B		
Marginal Basin															
Stations 1-5	1.5	2.0	3.3	4.6	6.3	--	7.9	4.5	0.4	0.9	2.3	2.7		5.0	9.5
			(.24)	(1.10)	(.52)	--	(.51)	(.25)	(.45)	(.85)	(1.73)	(1.42)			
Stations 6-11	1.5	2.0	3.3	4.9	6.9	--	--	3.6	0.5	1.6	1.6			--	--
			(.64)	(1.29)	(.07)	--	--	(.67)	(.05)	(.72)	(2.66)				
Frontal Arc															
Stations 12-15	1.5	2.0	3.3	4.7	6.3	7.2[e]	--	2.8	1.1	1.4	1.3	1.8		--	--
			(.42)	(.13)	(.40)	--	--	(.34)	(.33)	(.50)	(.34)	--			
Arc-trench Gap															
Stations 16-20	1.5	2.0	3.9	4.7	6.3	--	--	3.5	0.6	1.8	2.6	--			
			(.08)	(1.43)	(.38)	--	--	(.58)	(.44)	(.62)	(1.76)	--			
Old Pacific Plate															
Stations 23-29 and 29	1.5	2.0	3.3	4.1	5.7	6.7	7.4[e]	8.0	5.6	0.2	0.8	1.8	1.3	1.6	2.9[e]	5.2	10.8
			(.31)	(.16)	(.53)	(.31)	--	(.29)	(.76)	(.12)	(.42)	(.89)	(1.02)	(.70)	--		

[a] Velocities grouped according to oceanic layer velocities (Table 2).

NOTE: Standard deviation = $\left[\frac{1}{n} \sum_{i=1}^{n} (X_i - \bar{X})^2 \right]^{1/2}$

[b] Average crustal thickness = Depth to mantle minus average water depth.

[c] Water velocity assumed.

[d] Sediment velocity assumed.

[e] Not an average - only 1 value.

DISCUSSION OF RESULTS

Pacific Plate. The Pacific plate just east of the Mariana trench is thought to be Mesozoic in age, formed in either the Jurassic or upper Cretaceous. Thus, the expected depth of water would be between 5.5 and 6 km (Sclater and Francheteau, 1970). Average depth is 5.4 km in this study. Oceanic crust has been observed to increase in thickness with age (Woollard, 1975) and this has been attributed to thickening of layer 3 (Goslin et al., 1972; Clague and Straley, 1977; Epp and Suyenaga, 1978). The expected crustal thickness of Pacific plate older than 70 m.y. would be equal to or greater than that of average models for the Pacific. In this study the average crustal thickness is 5 km (using the average of all seven stations). This is quite thin compared to other Pacific crustal sections (see Figure 9). However, depth to Moho is best determined at station 25 (Figures 22 and 23). Crustal thickness there is 6.8 km which is about the same as thicknesses in the Woollard 3- and 4-layer models and only 0.3 km less than the Hussong 4-layer model (Figure 9). However, instead of a thick layer 3, layers 2A and 2B determined here are thicker than those shown in other Pacific plate models. This could be due to deformation of the crust during subduction. However, the deformation would not be expected to be important over 150 km from the trench. The effect on apparent velocities due to down-dip shooting would be to increase those velocities slightly, so this does not account for the comparatively low velocities. There is evidence from several sonobuoy

Fig 9. Average two-, three-, and four-layer oceanic crustal sections determined by seismic refraction compared with the crustal section found at station 25 and an average of the sections found at stations 23 through 29 in this study. (Adapted from Clague and Straley, 1976 and Hussong et al., 1976).

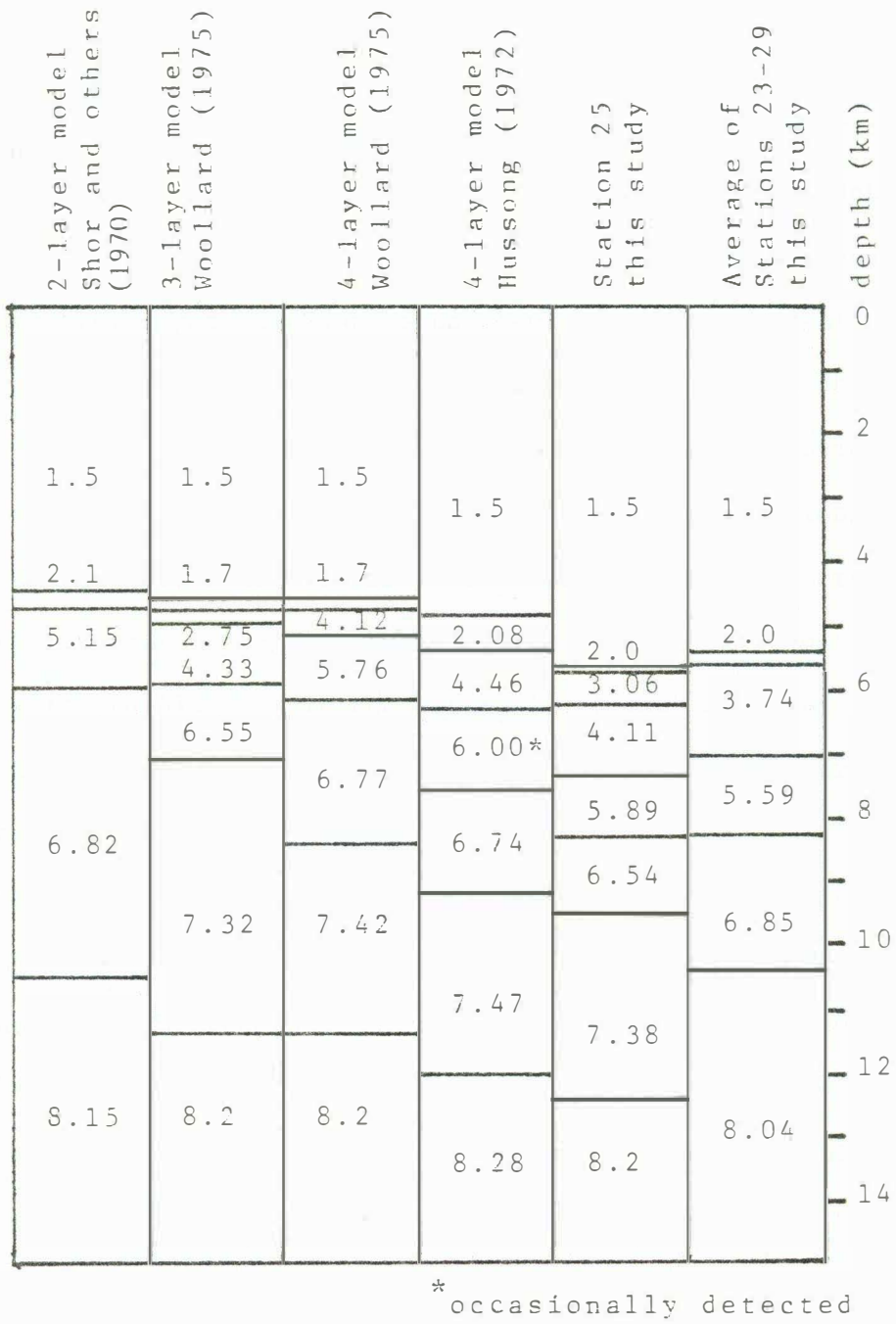
2-layer model
Shor and others
(1970)
3-layer model
Woollard (1975)
4-layer model
Woollard (1975)
4-layer model
Hussong (1972)
Station 25
this study
Average of
Stations 23-29
this study
depth (km)
0
2
4
6
8
10
12
14
1.5
2.1
5.15
6.82
8.15
1.5
1.7
2.75
4.33
6.55
7.32
8.2
1.5
1.7
4.12
5.76
6.77
7.42
8.2
1.5
2.08
4.46
6.00*
6.74
7.47
8.28
1.5
2.0
3.06
4.11
5.89
6.54
7.38
8.2
1.5
2.0
3.74
5.59
6.85
8.04
*occasionally detected

refraction studies that the thickness of layer 2A in Pacific crust older than 110 m.y. is greater than its thickness in crust from 30-110 m.y. old (Houtz and Ewing, 1976). These studies exclude areas of seamount volcanism. In addition, volcanic aprons around seamounts have the same seismic velocity as layer 2A and this velocity does not increase with age, apparently due to the lack of fracturing which prevents hydrothermal alteration (Houtz, 1976). Thus the thick layer 2A found in this study could be due to a combination of consolidated sediment and seamount volcanics. Other possible interpretations on Pacific plate are that a low velocity zone exists within the crust, lowering the apparent velocity; or that thrust faults exist over 100 km out onto the plate as in the Peru-Chile trench model by Hussong et al. (1976). The data in this study supports neither of these interpretations.

Arc-Trench Gap. The arc-trench gap is a region of fairly shallow crust and low seismic velocities (refer to Table 3 and Figures 7 and 8). The record section for station 16 (Figure 30) is characteristic of this region. It has thick (1.5-3 km) sequences of layer 2A material (4.0-6.0 km/sec). A few layer 3A determinations were made as well as one layer with a velocity of 7.22 km/sec at a depth of 8.1 km. No Moho velocities were found, so total crustal thickness could not be determined here. In general, the thickness of the uppermost sediments decreased while that of all other layers increased as the trench was approached. The velocity contours on Figure 8 show this trend well. The velocities determined in this

study were low relative to those presented by Murauchi et al. (1968, station 7) as representative of the arc-trench gap in the Bonin arc at 23.5°N, but thickness trends agree. Velocities in this study are similar to those obtained behind the New Hebrides trench by Shor et al. (1971). Looking at the individual sonobuoys' velocity-depth models for the arc-trench gap on Figure 7, it can be seen that the layers of a given velocity jump in depth from buoy to buoy. This may support large scale vertical faulting as seen in unpublished multichannel seismic observations (Donald Hussong, personal communication, 1978). Karig's model of accretionary building up of the arc-trench gap for the Mariana area includes sheared-off slabs of sediment and basement successively tucked under the inner wall of the trench (Karig and Sharman, 1975). If refractors could be seen, they might be expected to have anomalously high velocities due to the steep dip of these slabs. On the other hand, deformation in such an accretionary prism might make discrete layers impossible to see. Neither of these indications is present in the data analyzed here. Perhaps the refraction data presented here is not on as fine a scale as is needed to detect evidence of accretion. In any case, there is no evidence from this study that material from the Pacific plate is being accreted to the arc-trench gap region.

Mariana ridge. In general, velocities across the ridge are very similar to those found in the arc-trench gap (refer to Table 3 and Figures 7 and 8). Depth to 6-6.5 km/sec material is fairly constant at about 4 km. Layer 2B (4.0-6.0 km/sec) seems to be represented across both the ridge and arc-trench gap with thicknesses ranging from 1 to 2 km. The layer 2A (2.5-3.8 km/sec)

generally increases in velocity from the ridge to the trench. This is to be expected if it represents mainly pyroclastic sediments which become more consolidated further from the source at the volcanic arc. The thickness of layer 2A remains fairly constant at about 1.5 km. The ridge velocity structure determined here is grossly similar to that across the Honshu-Mariana ridge at 23.5°N (Murauchi et al., 1968). On the traced record section for station 13 (Figure 34), notice the anomalously early arrival times of refractions on shots 286-290 marked by the dotted line on the figure. If these arrivals are used to determine a layer, its velocity would be 8.4 km/sec and its depth 6.8 km. This seems unreasonable and does not agree with refraction profiles at other stations on the ridge or with those of other ridges (Murauchi et al., 1968 and Shor et al., 1975) where the mantle is anomalously deep. The fact that these shots are up-dip from the receiver will have the effect of increasing the apparent velocity somewhat, but not enough to fully explain these arrivals. One possible cause of these anomalous arrivals could be a high velocity body at a shallow depth, which would speed up rays passing through a lower velocity layer. For example, if there is a body of 6.5 km/sec material within the 3.1 km/sec layer, it would cause the negative delay times shown in Table 4. Using these and the velocity contrast, a crude estimate of the size (assuming a depth of less than 5 km) of the body can be made (see Figure 10). In this crude model the body could be shaped like a volcanic plug or solidified magma chamber, or it could be a

Table 4. Delay times for anomalous body under station 13.

Shot no.	Distance from Receiver (km)	Delay time* (sec)	Calculated width of body** (km)
286	13.8	- .98	3.4
287	14.6	-1.14	3.9
288	15.5	-1.32	4.5
289	16.4	-1.48	5.1
290	17.2	-1.68	5.8

* Difference in arrival times between the 3.1 km/sec layer and the 8.4 km/sec arrivals on the record section, Fig. 34.

**Assuming the ray traveled the entire shot-receiver distance in the 3.1 km/sec layer and the anomalous high-velocity layer.

Fig. 10. Sketches of anomalous body under frontal arc. Top models body as a sill, bottom as a volcanic plug.

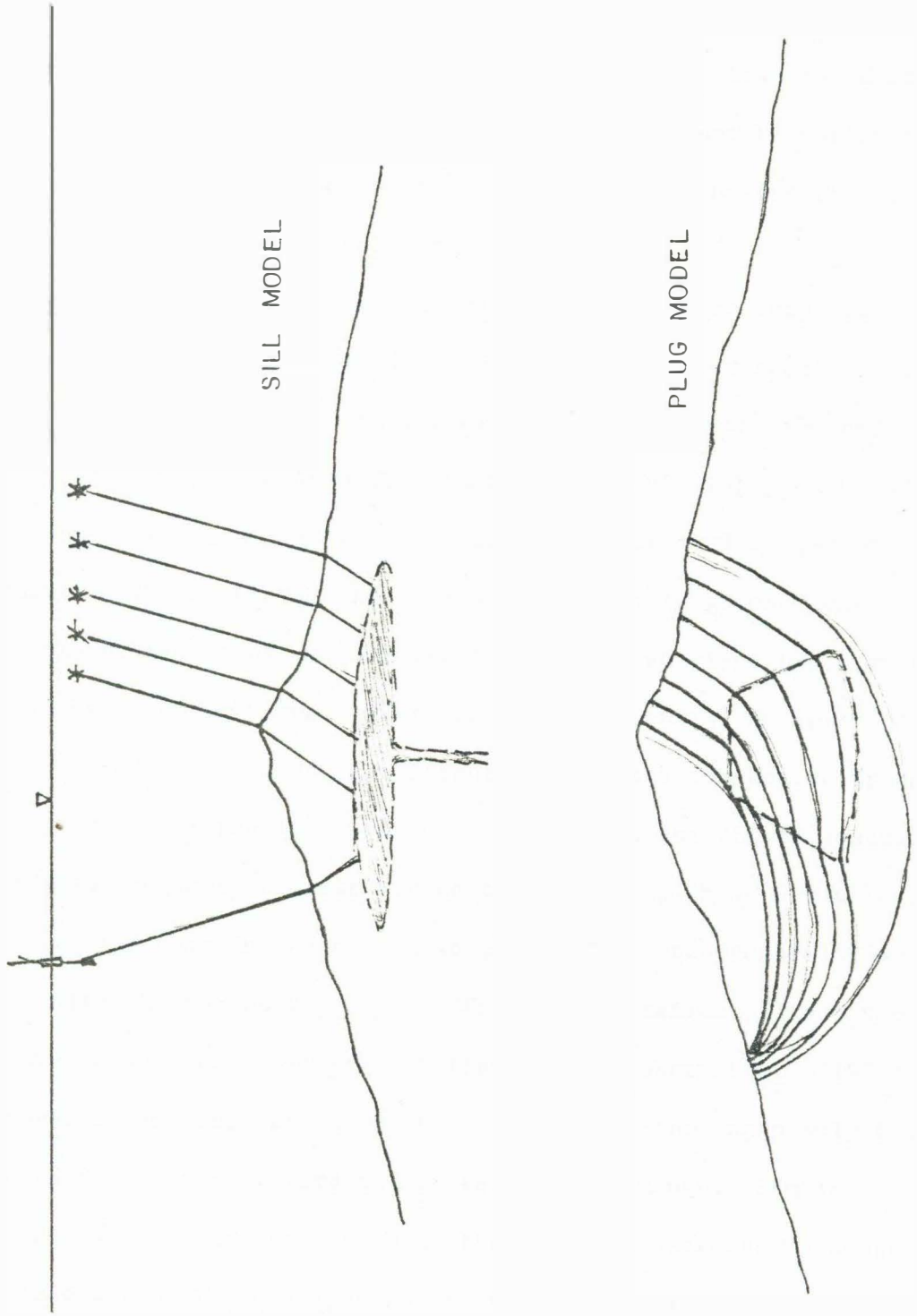
SILL MODEL
PLUG MODEL

thin layer of high velocity material such as a sill. The free air anomaly plotted with bathymetry in Figure 5 follows the depth rather closely. However, a body this size would not be expected to cause much of an anomaly. More information is needed to better define the cause of this velocity anomaly.

Mariana trough. The trough represents the most complicated structural region encountered in this study. Record sections for stations 2 and 3 (Figures 48 and 46) represent the western side of the trough, while sections for stations 9 and 10 (Figures 40 and 38) are just east of the axial high. Looking at the velocity-depth structure across the Mariana trough as a whole (Figures 7 and 8), the interpretation of its formation by mid-ocean ridge type crustal spreading is not obvious. There is a fairly consistent layer 3A (6.5-6.8 km/sec) at a depth of about 7 km across the entire trough. The thickness of the lower velocity layers, 2A and 2B, in general, increases from west to east across the trough, with very little 2A material found in the western most part. These two generalities agree with the Murauchi et al. (1968) interpretation, although no comparable data was collected in that study. Shor et al. (1971) presents an interpretation of the Havre trough showing nearly 6 km of crustal thinning toward the center of the trough. Similar evidence in the Mariana trough is the apparent decrease in depth of mantle between stations 1 and 5 in the western part of the trough (Figure 7 and Table 1). The mantle velocity and depth at station 5 (Figure 44) are poorly determined. Contoured velocities on

Figure 8, however, do support about 1 km of crustal thinning toward the center of the trough. In Table 3 crustal sections for stations 1 through 5 are averaged, and the average of crustal thicknesses is 5 km. This is much thinner than average Pacific crust as shown in the models of Figure 9. A comparison of two averaged crustal sections in the trough from this study with other sections in active and inactive marginal basins is shown in Figure 11. The Mariana trough crust is seen to be similar in structure to these basins.

Some other comparisons of marginal basin and oceanic crust involve heat flow versus depth and age versus depth relationships. Refer to Figures 12 and 13 for the following discussion. Active mid-ocean ridges have a characteristic age versus depth relationship discussed by Sclater et al. (1972) and shown on Figure 12. Two JOIDES drill sites from the Parce Vela basin, an inactive marginal basin (Karig, 1971b), plotted on this curve plot too deep for their age when compared to mid-ocean ridges. The Mariana trough is thought to be less than 5 m.y. old (Karig, 1971a) and it also plots too deep for its age. Even if its age was 10 m.y., this relationship would remain valid. Mid-ocean ridges also exhibit a heat flow versus depth relationship which is shown on Figure 13. Heat flow versus depth (mean elevation) for marginal basins of the northwestern Pacific, including the Mariana trough, plotted on this figure show that these basins are too hot for their depths compared to the same data for mid-ocean ridges. The data for the Mariana trough is an average of 9 heat flow readings on the

Fig. 11. Comparative crustal sections in marginal basins of the Pacific showing two averaged Mariana trough sections. While velocities compare with the Lau - Havre trough, the only other active marginal basin in the western Pacific, layer thicknesses and slopes are not directly comparable. (Modified after Karig, 1971b).

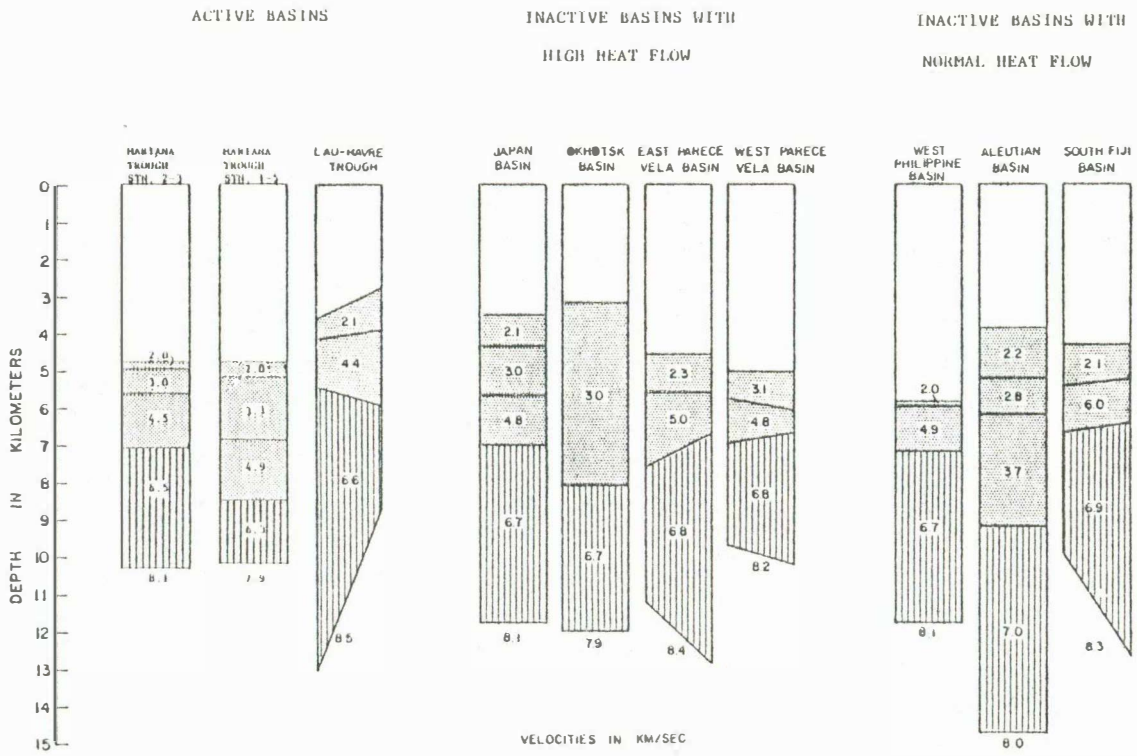
ACTIVE BASINS
INACTIVE BASINS WITH HIGH HEAT FLOW
INACTIVE BASINS WITH NORMAL HEAT FLOW
MARIANA TROUGH STH. 2-3
MARIANA TROUGH STH. 1-2
LAU-HAVRE TROUGH
JAPAN BASIN
OKHOTSK BASIN
EAST PARECE VELA BASIN
WEST PARECE VELA BASIN
WEST PHILIPPINE BASIN
ALEUTIAN BASIN
SOUTH FIJI BASIN
DEPTH IN KILOMETERS
0
1
2
3
4
5
6
7
8
9
10
11
12
13
14
15
2.0
1.0
4.5
6.5
8.1
2.0
1.0
3.1
4.9
6.3
7.9
2.1
4.4
6.6
8.5
2.1
3.0
4.8
6.7
8.1
3.0
6.7
7.9
2.3
5.0
6.8
8.4
3.1
4.8
6.8
8.2
2.0
4.9
6.7
8.1
2.2
2.8
3.7
7.0
8.0
2.1
6.0
6.9
8.3
VELOCITIES IN KM/SEC

Fig. 12. Depth versus age of crust for Mariana trough (open square) and two JOIDES sites compared with empirical depth versus age for the active mid-ocean ridges. All active ridges except in the North Atlantic close to Iceland fall within +500 or -300 meters of the empirical curve (the shaded area).

Fig. 13. Mean elevations of the marginal basins in the northwestern Pacific versus mean heat flow. The bars represent standard error. The following symbols have been used: solid circle, Okinawa trough; solid triangle, (1) Yamato basin, (2) Northern Japan abyssal plain, (3) southern Japan abyssal plain; solid diamond, eastern Skikoku basin, open diamond, western Shikoku basin; asterisk, Sea of Okhotsk; solid square, Parce Vela basin; star, Sulu basin; open circle, Celebes basin; open triangle, western Philippine basin; circled cross, northwestern Pacific; open square, Mariana trough. For a normal mid-ocean ridge, a plot of mean heat flow against mean depth should fall within curves 2-5. (Revised after Sclater et al., 1972). Note: standard error for the Mariana figure is $\pm$2.5 due to large scatter.

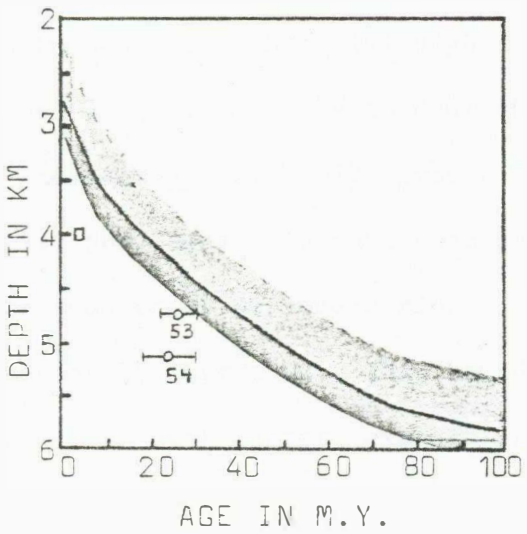
DEPTH IN KM
AGE IN M.Y.
2
3
4
5
6
0
20
40
60
80
100
53
54

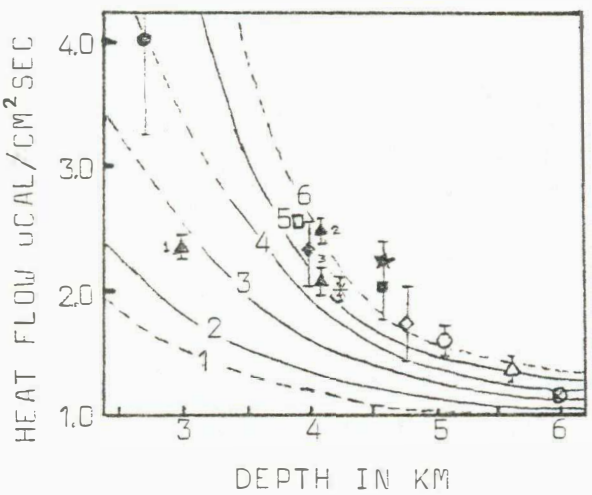
HEAT FLOW uCAL/CM²SEC
DEPTH IN KM
4.0
3.0
2.0
1.0
3
4
5
6
1
2
3
4
5
6

axial high (Anderson, 1975, page 4044, stations 5 through 13). These values were used, rather than an overall average, because crust less than 10 km away from the axial high cooled to an abnormally low mean value, which may be due to hydrothermal circulation (Anderson, 1975). Sclater et al. (1972) proposed that the best explanation for these phenomena with data then available was a thinner lithosphere than under mid-ocean ridges, allowing for much faster loss of the heat of intrusion. This rapid cooling also causes the young crust to sink faster, explaining anomalously deep marginal basin elevations.

Data from this study lends support to this thin crustal model for marginal basins.

SUMMARY OF CONCLUSIONS

1. The Pacific plate east of the Mariana trench is of similar total thickness as average Pacific crust (6.8 km), but contains thicker low velocity layers. Seamount volcanism introduces more low velocity material onto the crust, and this combined with consolidated sediments could explain the thicker low velocity layers. The best data, from station 25, gives a structure very similar to recent 4-layer models by Woollard and Hussong. Depth of the crust below the ocean surface agrees with depth-age relationships developed by Sclater.
2. The structure of the arc-trench gap is not very successfully modeled by flat lying layers. The fact that no mantle velocites (and only one higher than 7.0 km/sec) were seen may be due to structure or an anomalously deep mantle here. Data from this study supports the interpretation of large-scale vertical faulting across this province. There is no evidence from this study supporting an accretionary prism for the Mariana arc-trench gap.
3. No mantle velocities were determined on the Mariana ridge. This could mean that the mantle here is very deep and cannot be resolved with the limited range of sonobuoys in rough terrain. An anomalously high apparent velocity found at shallow depths (less than 7 km) under station 13 could be caused by a volcanic plug or other high velocity body. This needs further investigation.

4. The data from the trough support some crustal thinning toward the center of the trough, but not as much as other authors have found in other marginal basins. Crustal thickness as determined in the western part of the trough is less than that of average Pacific ocean crust. The trough is deeper for its age and has higher heat flow for its depth than do mid-ocean ridges. These data support Sclater's idea of a modified mid-ocean ridge type of crustal formation. The marginal basin mechanism of spreading produces thinner crust which:

    (1) Makes for higher heat flow over the spreading center itself,

    (2) Allows for faster cooling of the newly-formed crust which, in turn,

    (3) Produces a faster sinking crust and thus average depths greater than would be expected for young crust.

APPENDIX A

FORTRAN PROGRAMS FOR TRAVEL TIME CORRECTIONS

The following is a brief description of the theory and methods used to calculate refraction corrections in the group of Fortran programs called REFRAC. These corrections are divided into two types, the burn time correction and the travel time and range corrections. The burn time correction corrects the reference time of the shot detonation and is not affected by changes in crustal structure or water depth. The remaining corrections, however, do vary with water depth and crustal structure, and are different for each shot-receiver combination and each refracted ray.

Burn Time Correction. In marine explosion refraction surveys shots are dropped off the after deck of the ship and explode some seconds later at some depth which varies according to shot size and fuse length. The shot detonation time (shot break time) recorded by the hydrophones towed behind the ship (called the eel) is therefore some fractions of a second later that the actual detonation time, which is needed as a reference for all seismic arrivals at the sonobuoy or ocean bottom seismometer (OBS). Thus a time correction must be made which is termed the burn time correction (BTC). The burn time correction is made as follows: (refer to Fig. 14).

The BTC is the slant path from the shot to the end of the eel ($\overline{SE}$ in Fig. 14) in seconds of travel time. To find this we determine the shot depth ($\overline{SD}$) and the shot to eel distance along the surface

Fig. 14. Illustration of burn time correction calculation.

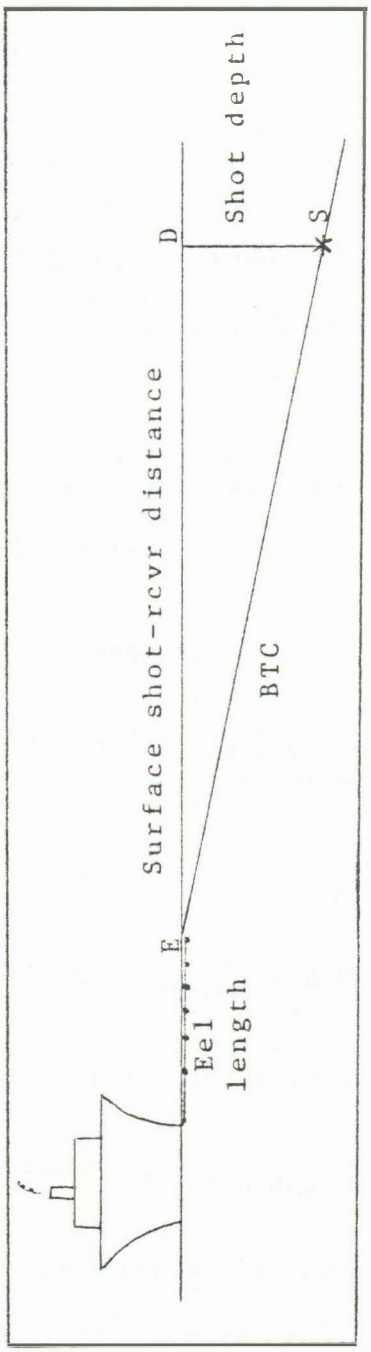
Surface shot-rcvr distance
D
Shot depth
S
E
Eel
length
BTC

($\overline{DE}$) and use the pythagorean theorem. First, the shot depth is calculated using a standard sinking rate for Tovex (Hussong, personal communication, 1977) 1.19 meters per second, and burn time (BT) which is recorded in the shot log.

$$SD(\text{meters}) + BT(\text{seconds}) * 1.19\ (\text{m/sec})$$

Then, the surface shot to eel distance is calculated from the eel length in meters, the ship's speed (SS) in knots and the burn time.

$$DIST. = BT(\text{sec}) * SS/3600\ (\text{n.m./sec}) * 1852\ (\text{m/n.m.}) - \text{eel length(meters)}$$

The burn time correction then is:

$$BTC = [(SD)^2 + (DIST)^2]^{\frac{1}{2}}/\text{surface water velocity in meters/sec}$$

The actual shot break time is then:

$$SBT_{actual} = SBT_{recorded} - BTC$$

Or, to correct a travel time, apply BTC as follows:

$$TT = \text{Arrival time} - SBT_{recorded} + BTC$$

Travel Time and Range Corrections. In order to simplify the inversion of travel time data from our marine seismic refraction work, the programs used to make corrections are based on the layer

solution method. This method assumes the following about the nature of the velocity model (Ewing et al., 1939 and Ewing, 1963):

1. Velocities in successive layers increase as the depth increases.
2. Velocities are constant throughout each layer.
3. Each layer is bounded top and bottom by planes.
4. Layers are thick compared to the seismic wavelength.
5. At the interface between two layers, the path of the seismic wave is bent according to Snell's law, which, in a rectangular coordinate system is $\sin \theta_1 / \sin \theta_2 = V_1 / V_2$. (Refer to Fig. 15).
6. A wave traveling in any layer with a velocity V, and incident upon the surface of the layer above at an angle α with the normal, has an apparent velocity (phase velocity) $V/\sin\alpha$ along the surface. (Fig. 16)
7. Any travel time will be unchanged if shot point and recording point are interchanged.

The model is actually two-dimensional since data is collected along "lines" and lateral homogeneity is assumed.

The program assumes a velocity structure of four (or less) layers--water plus three sloping layers, usually termed sediment, basement and refractors. Figure 17 shows the ray path and slopes, incident and refracted angles of each layer.

AL1, AL2 and AL3 are the relative slopes (slope relative to the layer above) of the sediment, basement and refractor, respectively.

Fig. 15. Ray path for refracted seismic wave showing incident and refracted angle.

Fig. 16. Incident angle used for apparent velocity calculation.

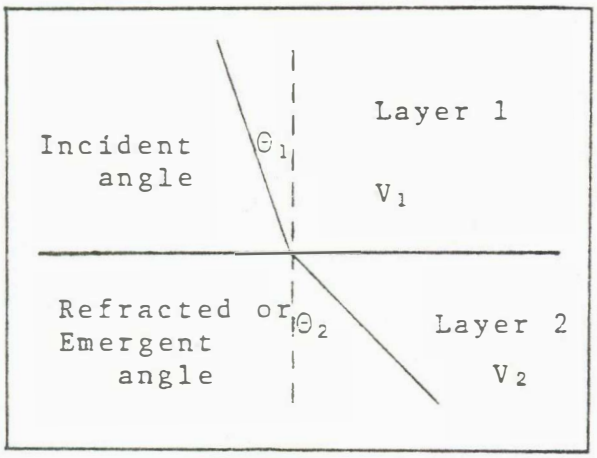
Incident
angle
Θ_1
Layer 1
V_1
Refracted or
Emergent
angle
Θ_2
Layer 2
V_2

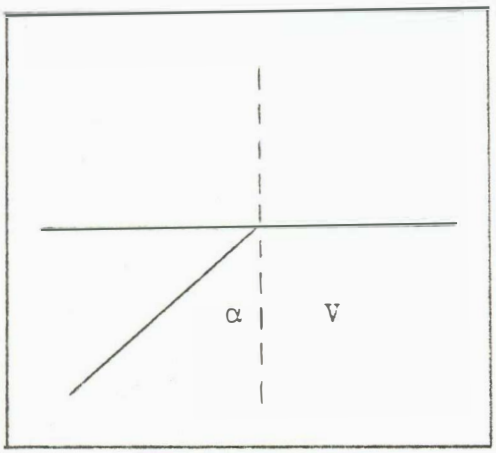
α
V

Fig. 17. Sloping layer model with dips and angles identified.

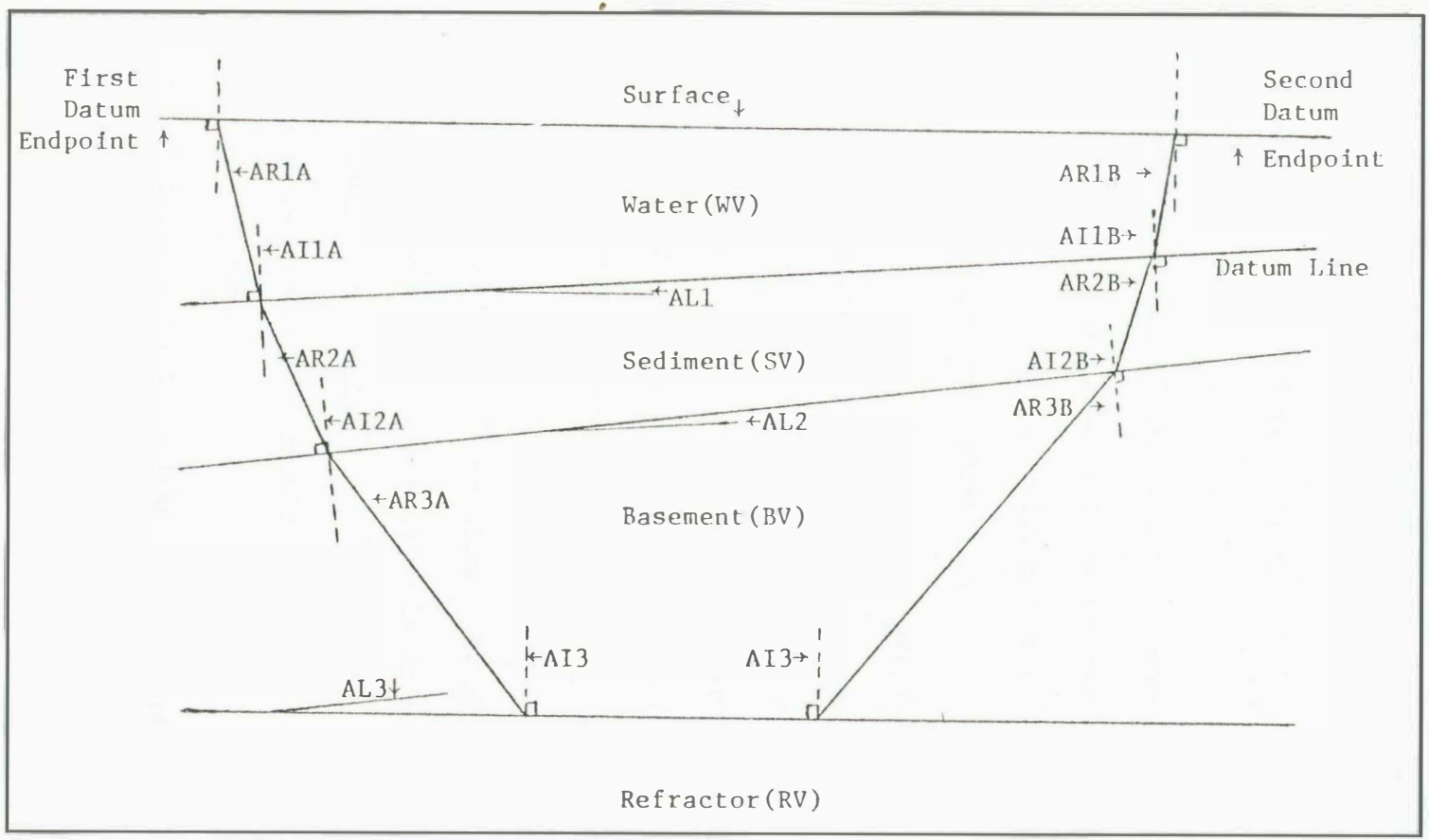
First
Datum
Endpoint
Surface
Second
Datum
Endpoint
AR1A
Water(WV)
AR1B
AI1A
AI1B
Datum Line
AR2B
AL1
AR2A
Sediment(SV)
AI2B
AI2A
AL2
AR3B
AR3A
Basement(BV)
AI3
AI3
AL3
Refractor(RV)

Notice that we have assumed a horizontal refractor so that its relative slope is -(AL1 + AL2). Thus, since $V_{apparent} = V_{actual}/\sin\alpha$, where α is the emergent angle, the true velocity is always less than or equal to the apparent velocity and so velocities are always corrected downward in this model.

AI1A & B, AI2A & B and AI3 are incident angles while AR1A & B, AR2A & B and AR3A & B are emergent or refracted angles. Since the wave is critically refracted at the refractor layer, the ray enters and leaves this layer at the same angle AI3.

The types of corrections we want to make are these:

(1) Correcting the shot and the receiver to the same elevation, i.e., to the surface of the ocean in this case,

(2) the consequent correction in shot to receiver distance, and

(3) correcting for deviations of the sediment layer (or ocean bottom of whatever type) from a plane surface, which we will call the datum line, at the ray entry and exit points. This is called the bathymetry correction. It also includes path length differences due to a sloping layer model rather than a horizontal layer model.

It is this latter correction that requires the bulk of the program system to calculate.

The data is organized by datum line, receiver number and shot number. For each group of shots and receivers a datum is chosen which best approximates the bottom slope. For each shot-receiver pair, the refracted ray path is determined by calculating all the

angles from (1) known slopes and (2) assumed layer velocities. Once the ray path is known, the point where the ray enters the sea floor (on the datum line) is known. We call this point, or more accurately its image on the surface of the ocean, the migrated point. The ray path length (in time) from the surface to the migrated point plus the path through the sediments is calculated for both the shot and the receiver end of the ray. Then the real bathymetry at the migrated point is looked up. The "real" sea floor and sediment layer are modeled at this point as horizontal layers. The modeled "real" ray path length through water and sediment is then calculated. The correction factor is the difference between this and the "datum" ray path length.

Correction of shot and receiver to the surface, and shot to receiver distance are determined using simple trigonometry once the ray path has been determined.

APPENDIX B

TRAVEL TIME PLOTS AND VELOCITY/DEPTH MODELS

Interpreted travel time graphs for stations 1 through 29 in reverse order, that is from east to west. The top part of each figure is a plot of arrival time versus distance for the first reflection and for the refractions. Slopes and intercepts of the layer interpretations are given on the right side of each figure. Bathymetry along the datum line is also shown. The bottom part of each figure shows the inverted velocity - depth structure with each layer beginning at its computed critical distance. Velocity of the unconsolidated sediments is assumed to be 2.00 km/sec and thicknesses of these sediments are determined from reflection profiles. Figures 25-31 are for the Pacific plate, Figures 32-36 are for the Arc-trench gap, Figures 37-40 are for the Mariana ridge, and Figures 41-50 are for the Mariana trough.

Fig. 18. Interpreted travel time plot with bathymetry and velocity/depth model for Station 29.

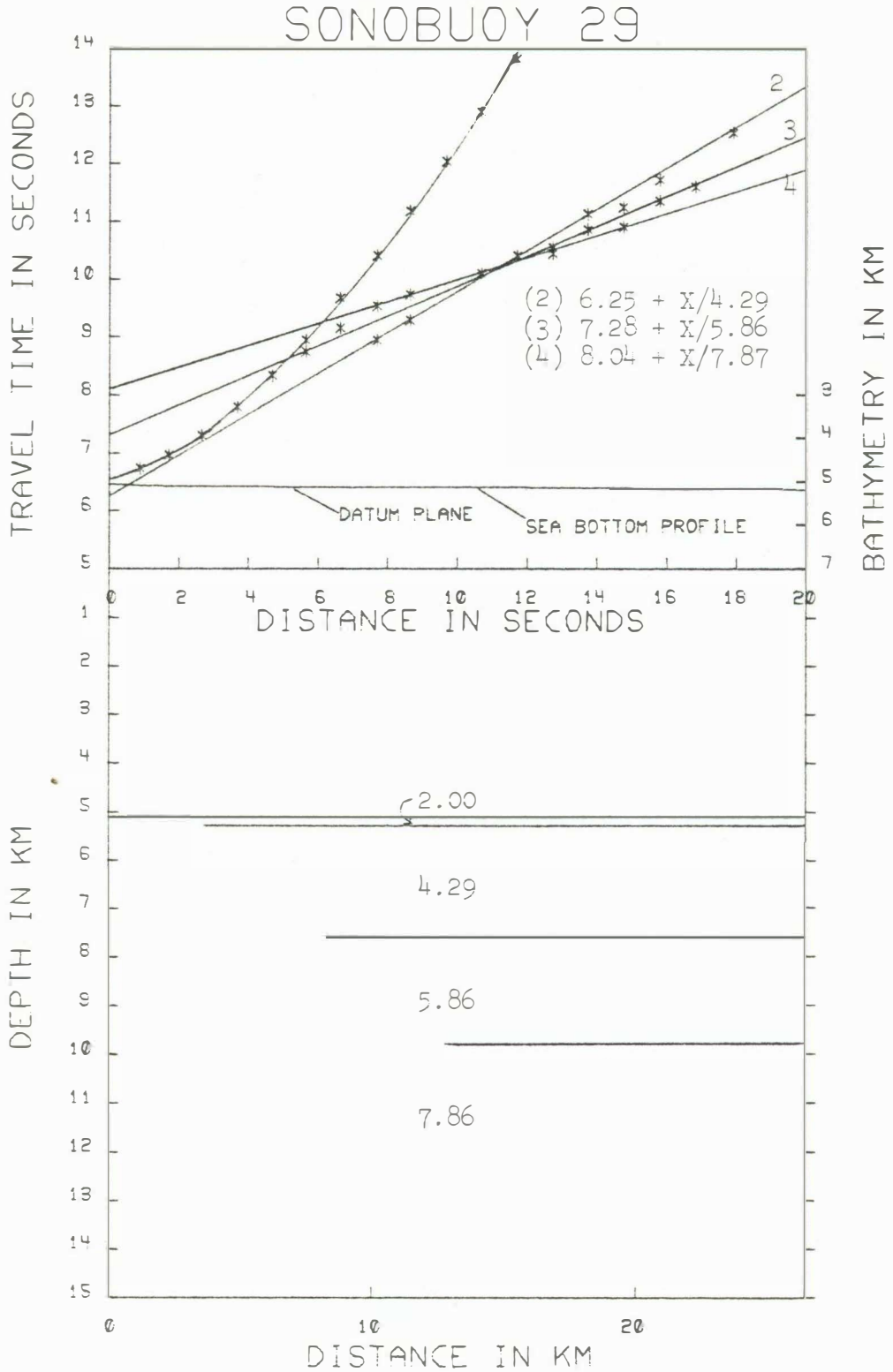
SONOBUOY 29
TRAVEL TIME IN SECONDS
BATHYMETRY IN KM
DISTANCE IN SECONDS
(2) 6.25 + X/4.29
(3) 7.28 + X/5.86
(4) 8.04 + X/7.87
DATUM PLANE
SEA BOTTOM PROFILE
DEPTH IN KM
2.00
4.29
5.86
7.86
DISTANCE IN KM

Fig. 19. Interpreted travel time plot with bathymetry and velocity/depth model for Station 28. Layer 1 velocity is too low.

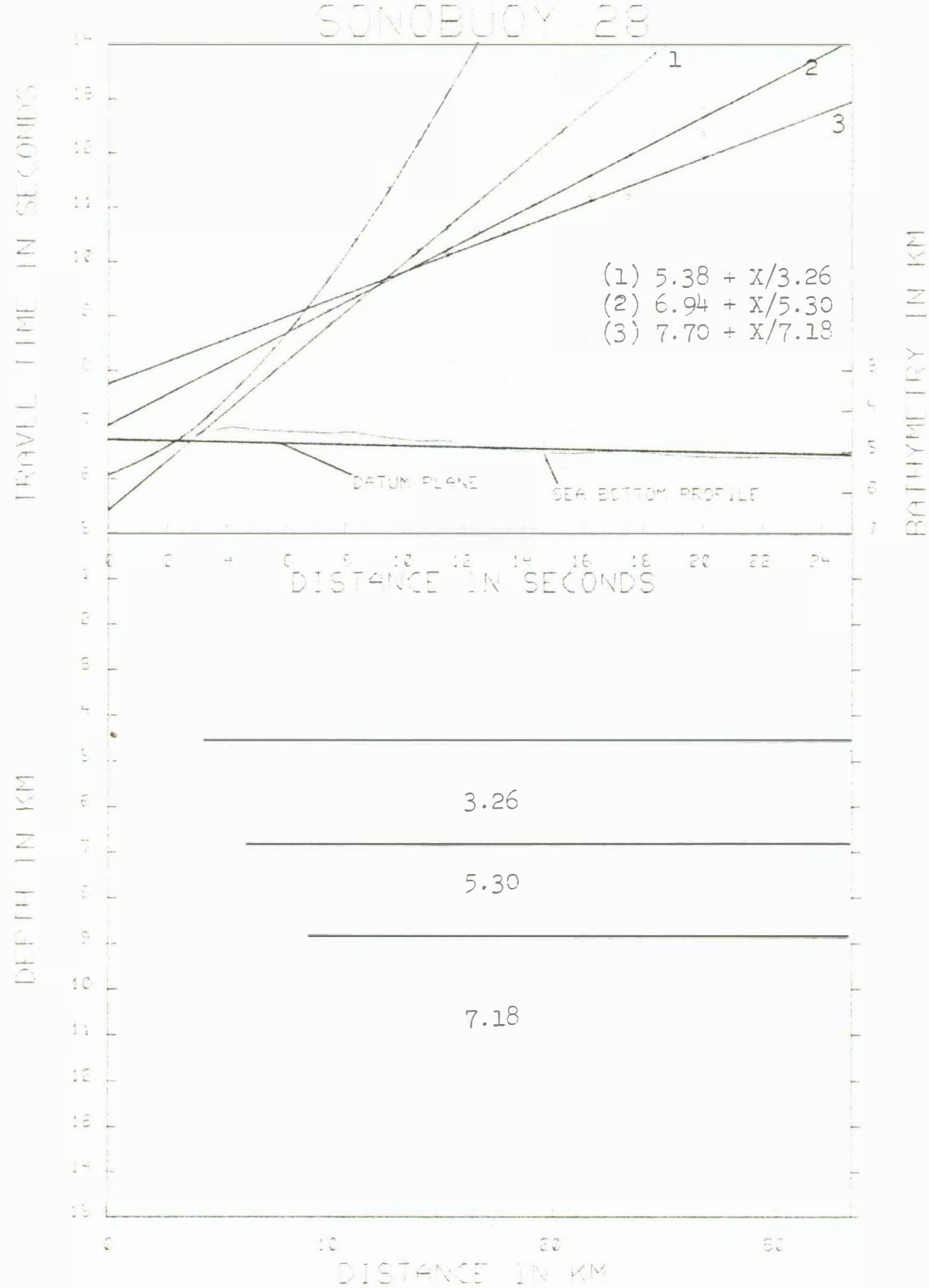
SONOBUOY 28
1
2
3
(1) 5.38 + X/3.26
(2) 6.94 + X/5.30
(3) 7.70 + X/7.18
DATUM PLANE
SEA BOTTOM PROFILE
TRAVEL TIME IN SECONDS
BATHYMETRY IN KM
DISTANCE IN SECONDS
3.26
5.30
7.18
DEPTH IN KM
DISTANCE IN KM

Fig. 20. Interpreted travel time plot with bathymetry and velocity/depth model for Station 27. The first layer is assumed to grade from 2.0 to 4.25 km/sec as only 0.20 sec of unconsolidated sediment is present according to reflection records.

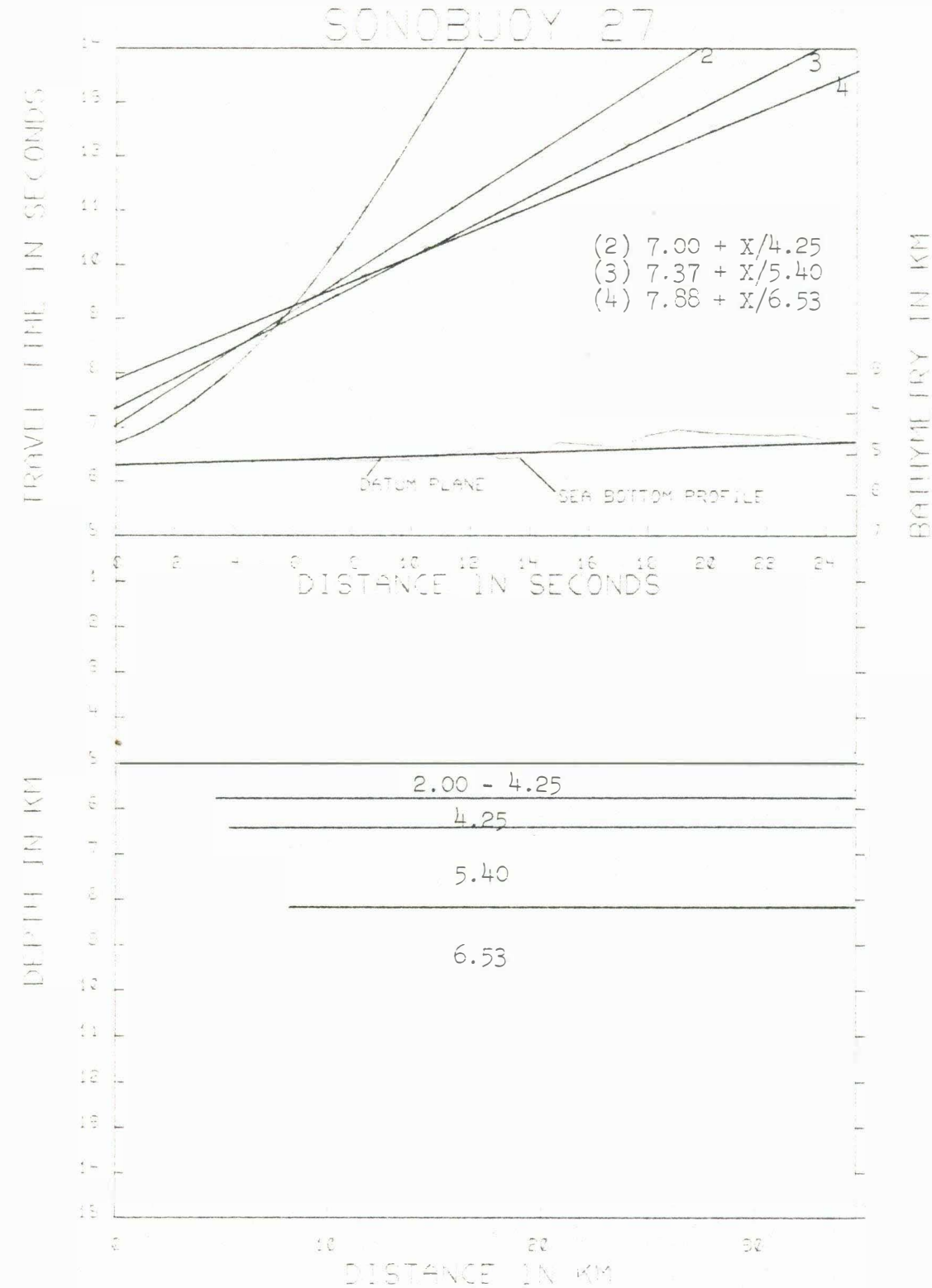
SONOBUOY 27
2
3
4
(2) 7.00 + X/4.25
(3) 7.37 + X/5.40
(4) 7.88 + X/6.53
DATUM PLANE
SEA BOTTOM PROFILE
TRAVEL TIME IN SECONDS
BATHYMETRY IN KM
DISTANCE IN SECONDS
2.00 - 4.25
4.25
5.40
6.53
DEPTH IN KM
DISTANCE IN KM

Fig. 21. Interpreted travel time plot with bathymetry and velocity/depth model for Station 26.

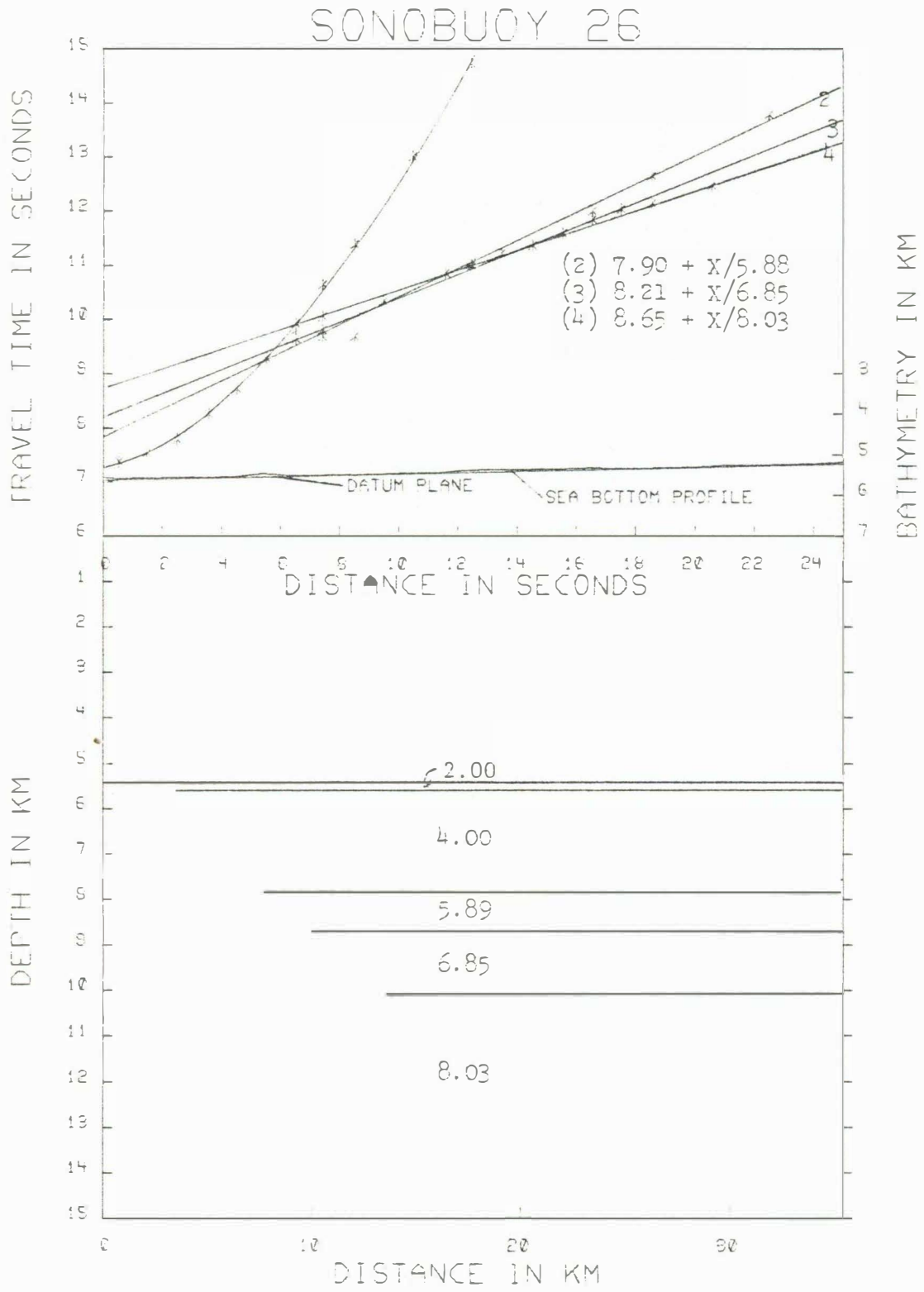
SONOBUOY 26
TRAVEL TIME IN SECONDS
BATHYMETRY IN KM
(2) 7.90 + X/5.88
(3) 8.21 + X/6.85
(4) 8.65 + X/8.03
DATUM PLANE
SEA BOTTOM PROFILE
DISTANCE IN SECONDS
DEPTH IN KM
2.00
4.00
5.89
6.85
8.03
DISTANCE IN KM

Fig. 22. Record section for Station 25.

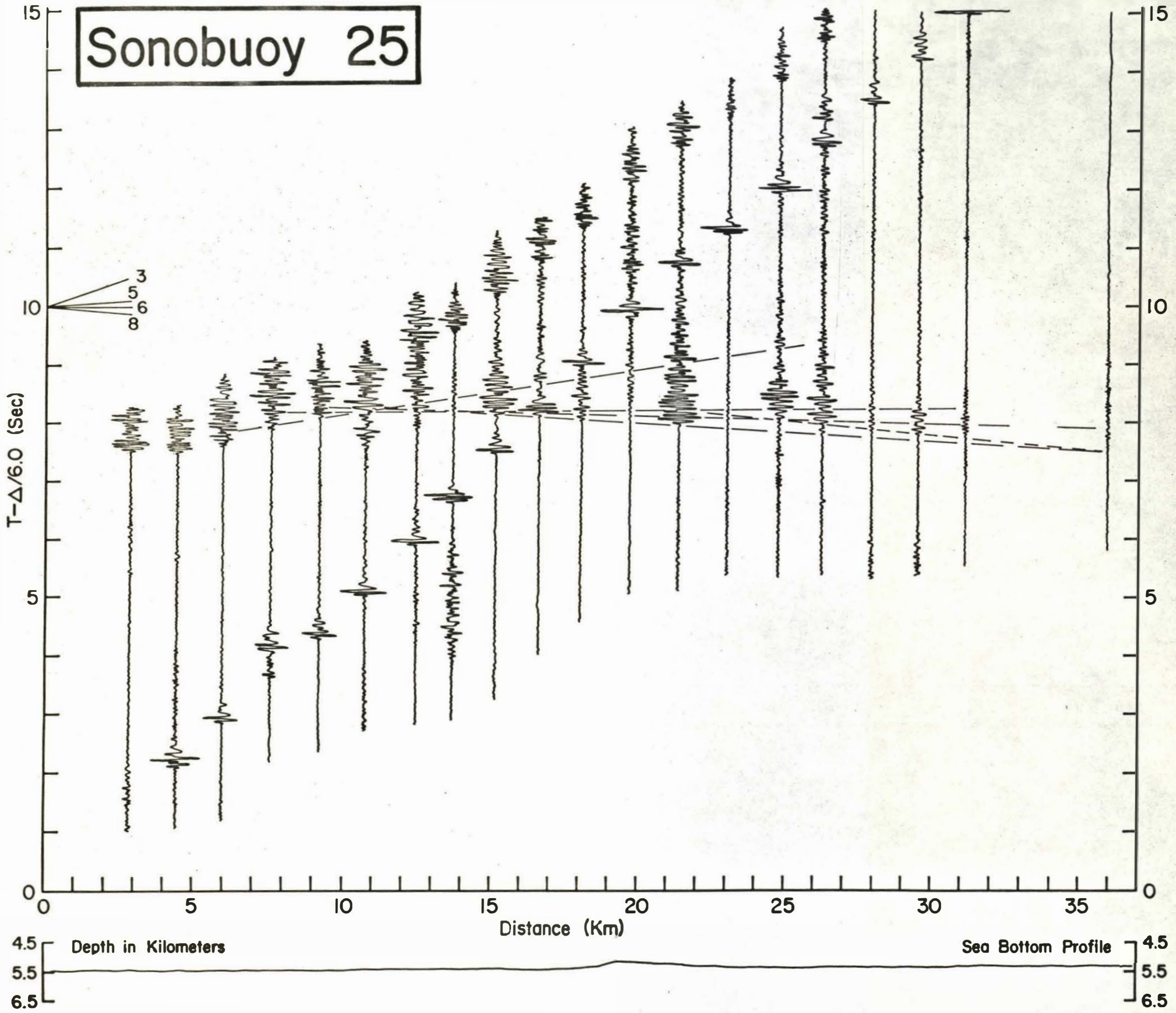
Sonobuoy 25
T-Δ/6.0 (Sec)
15
10
5
0
3
5
6
8
0
5
10
15
20
25
30
35
Distance (Km)
Depth in Kilometers
4.5
5.5
6.5
Sea Bottom Profile

Fig. 23. Interpreted travel time plot with bathymetry and velocity/depth model for Station 25. The 2.00 layer thickness is based on reflection records.

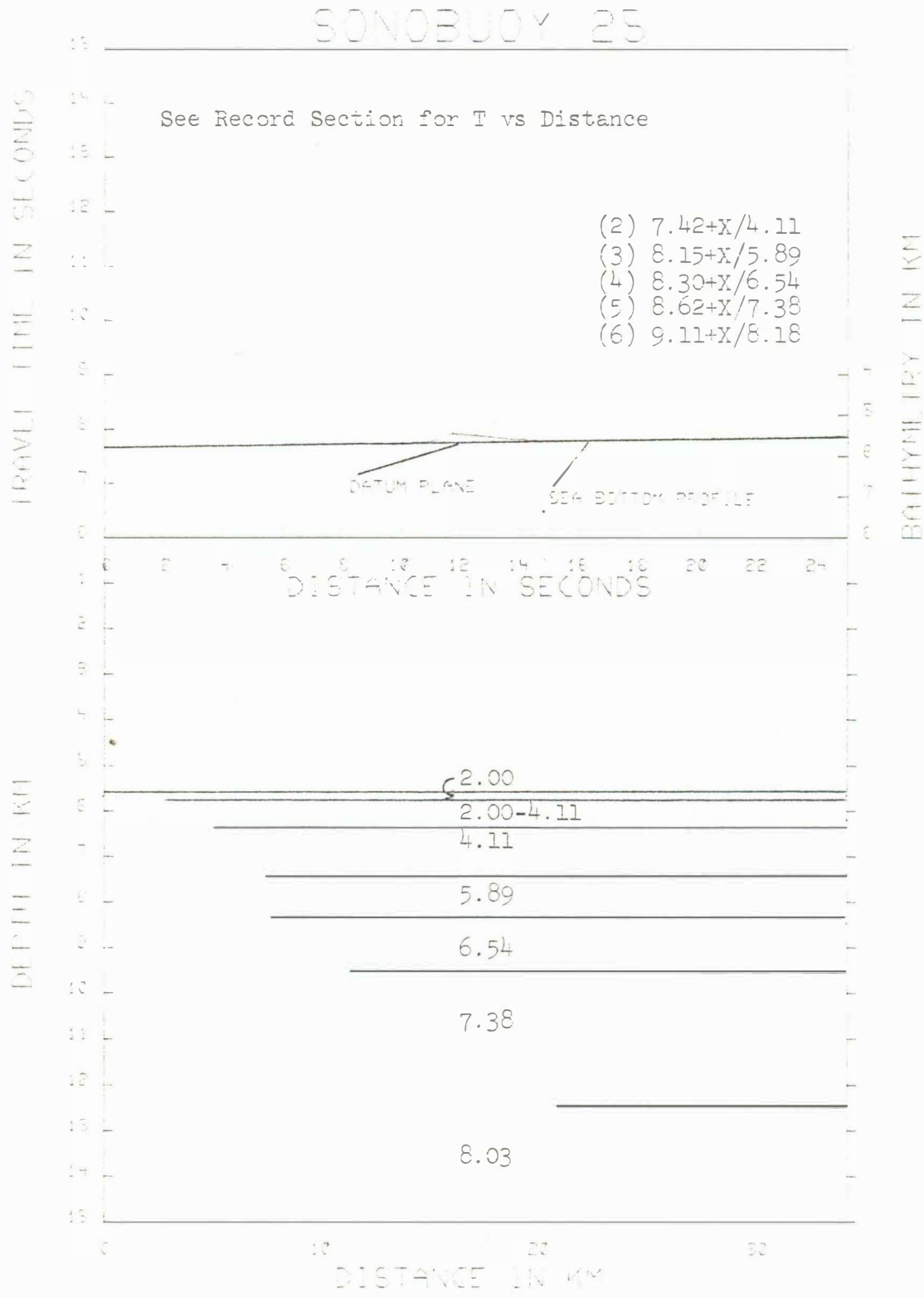
SONOBUOY 25
See Record Section for T vs Distance
(2) 7.42+X/4.11
(3) 8.15+X/5.89
(4) 8.30+X/6.54
(5) 8.62+X/7.38
(6) 9.11+X/8.18
DATUM PLANE
SEA BOTTOM PROFILE
DISTANCE IN SECONDS
TRAVEL TIME IN SECONDS
BATHYMETRY IN KM
DEPTH IN KM
2.00
2.00-4.11
4.11
5.89
6.54
7.38
8.03
DISTANCE IN KM

Fig. 24. Interpreted travel time plot with bathymetry and velocity/depth model for Station 24. The second layer velocity range was assumed. Sediment thickness is based on reflection records.

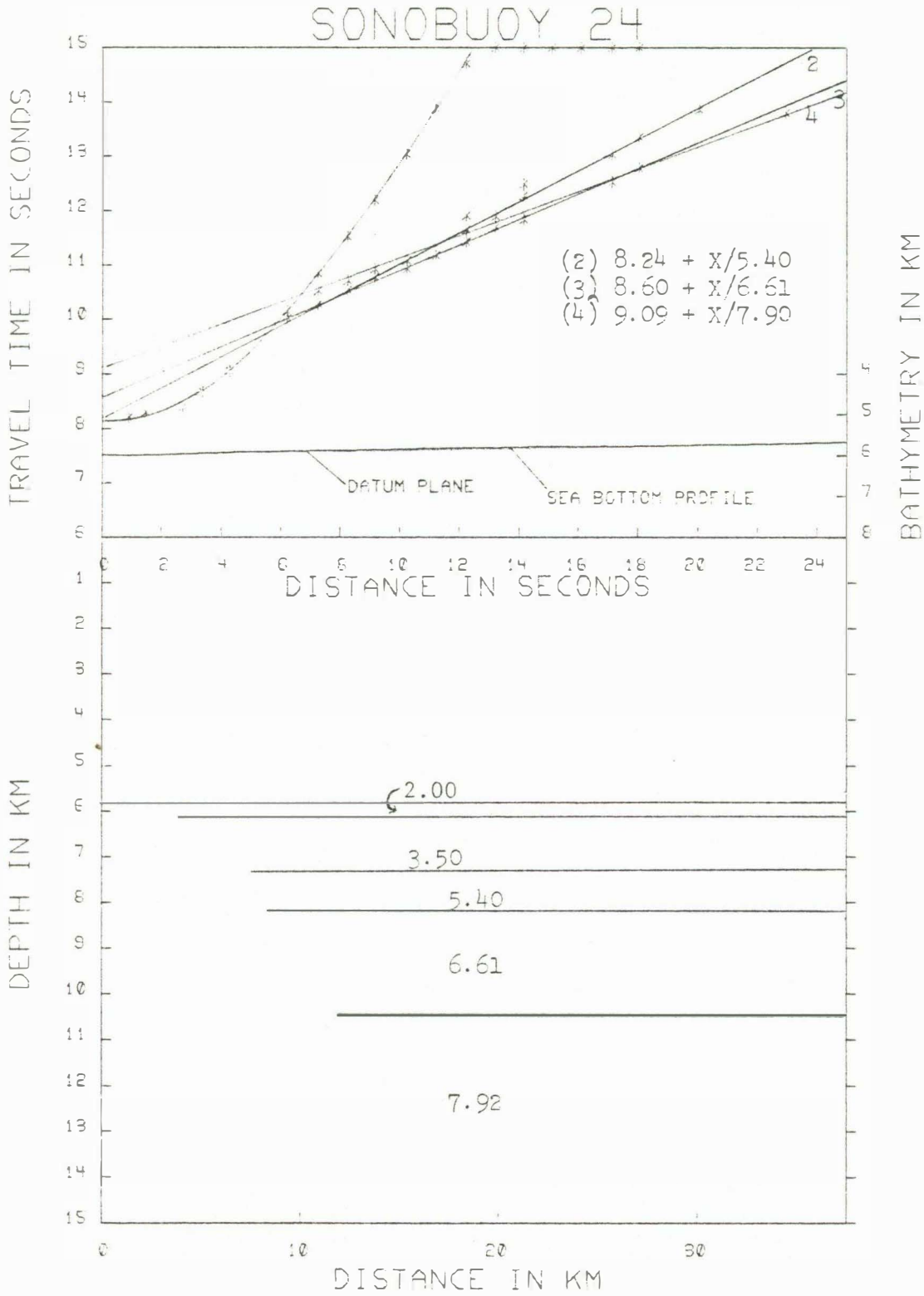
SONOBUOY 24
TRAVEL TIME IN SECONDS
BATHYMETRY IN KM
(2) 8.24 + X/5.40
(3) 8.60 + X/6.61
(4) 9.09 + X/7.90
DATUM PLANE
SEA BOTTOM PROFILE
DISTANCE IN SECONDS
DEPTH IN KM
2.00
3.50
5.40
6.61
7.92
DISTANCE IN KM

Fig. 25. Interpreted travel time plot with bathymetry and velocity/depth model for Station 23.

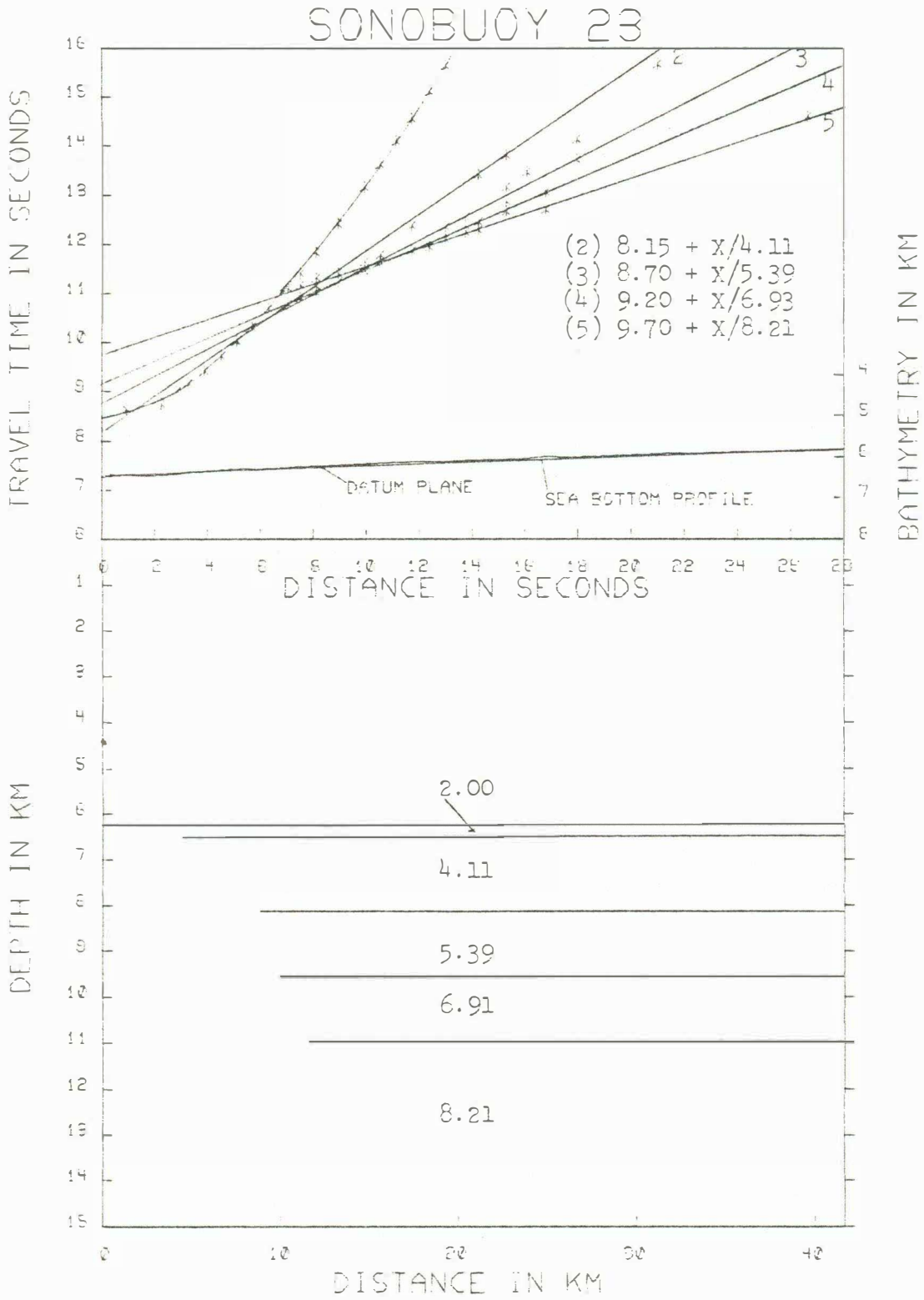
SONOBUOY 23
TRAVEL TIME IN SECONDS
BATHYMETRY IN KM
(2) 8.15 + X/4.11
(3) 8.70 + X/5.39
(4) 9.20 + X/6.93
(5) 9.70 + X/8.21
DATUM PLANE
SEA BOTTOM PROFILE
DISTANCE IN SECONDS
DEPTH IN KM
2.00
4.11
5.39
6.91
8.21
DISTANCE IN KM

Fig. 26. Interpreted travel time plot with bathymetry and velocity/depth model for Station 20.

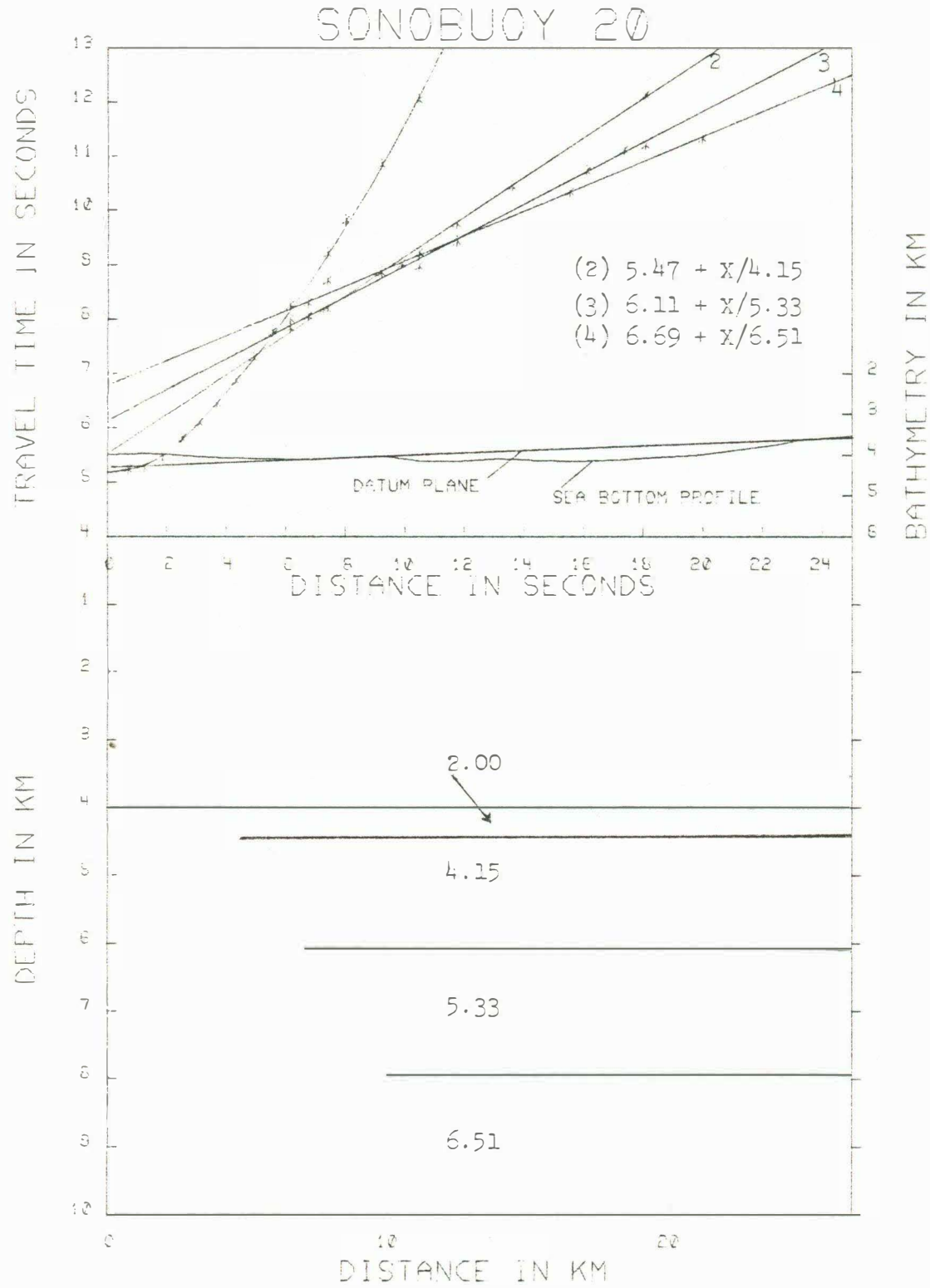
SONOBUOY 20
TRAVEL TIME IN SECONDS
BATHYMETRY IN KM
(2) 5.47 + X/4.15
(3) 6.11 + X/5.33
(4) 6.69 + X/6.51
DATUM PLANE
SEA BOTTOM PROFILE
DISTANCE IN SECONDS
DEPTH IN KM
2.00
4.15
5.33
6.51
DISTANCE IN KM

Fig. 27. Interpreted travel time plot with bathymetry and velocity/depth model for Station 19.

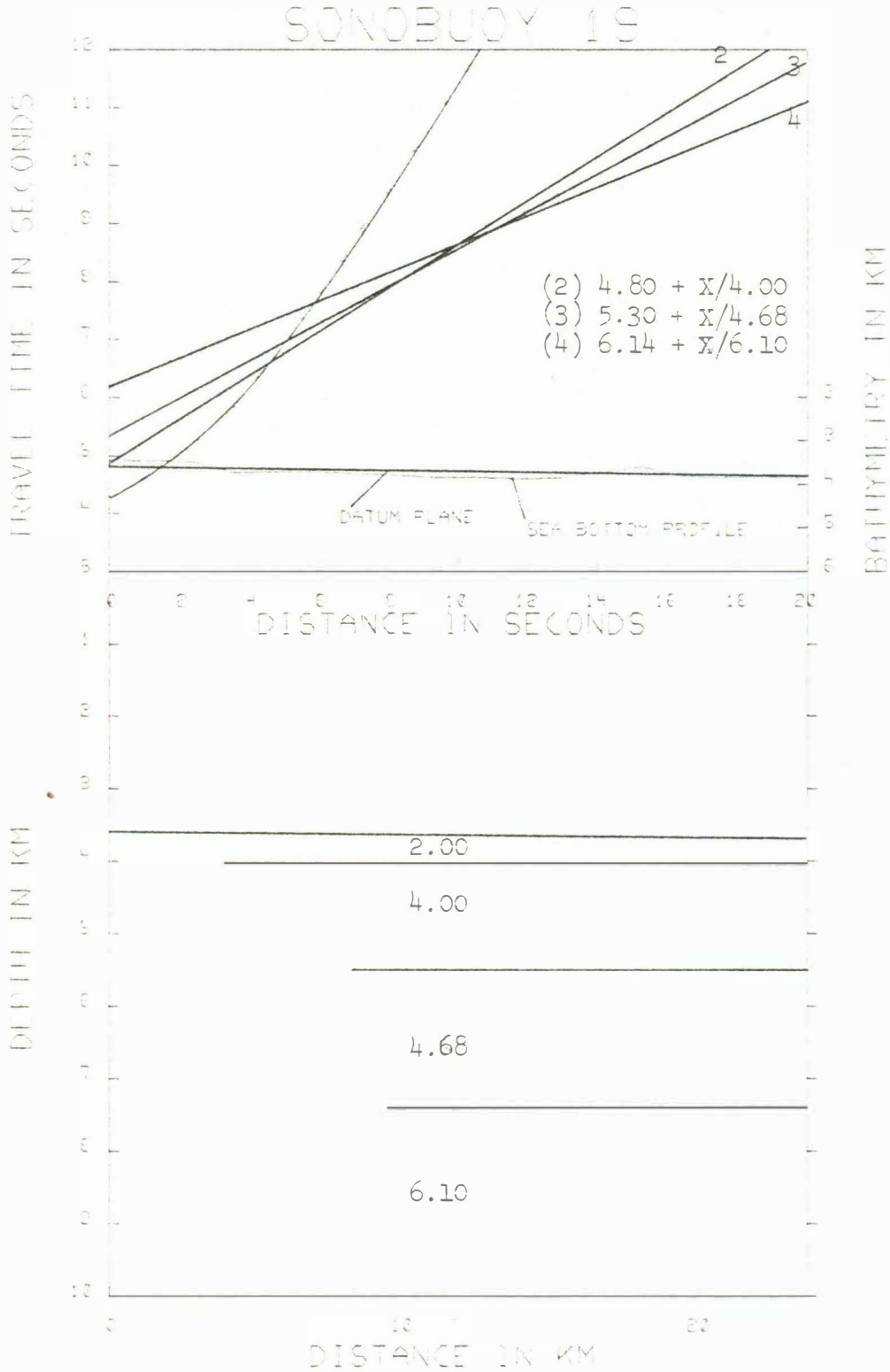
SONOBUOY 19
TRAVEL TIME IN SECONDS
BATHYMETRY IN KM
(2) 4.80 + X/4.00
(3) 5.30 + X/4.68
(4) 6.14 + X/6.10
DATUM PLANE
SEA BOTTOM PROFILE
DISTANCE IN SECONDS
DEPTH IN KM
2.00
4.00
4.68
6.10
DISTANCE IN KM

Fig. 28. Interpreted travel time plot with bathymetry and velocity/depth model for Station 18.

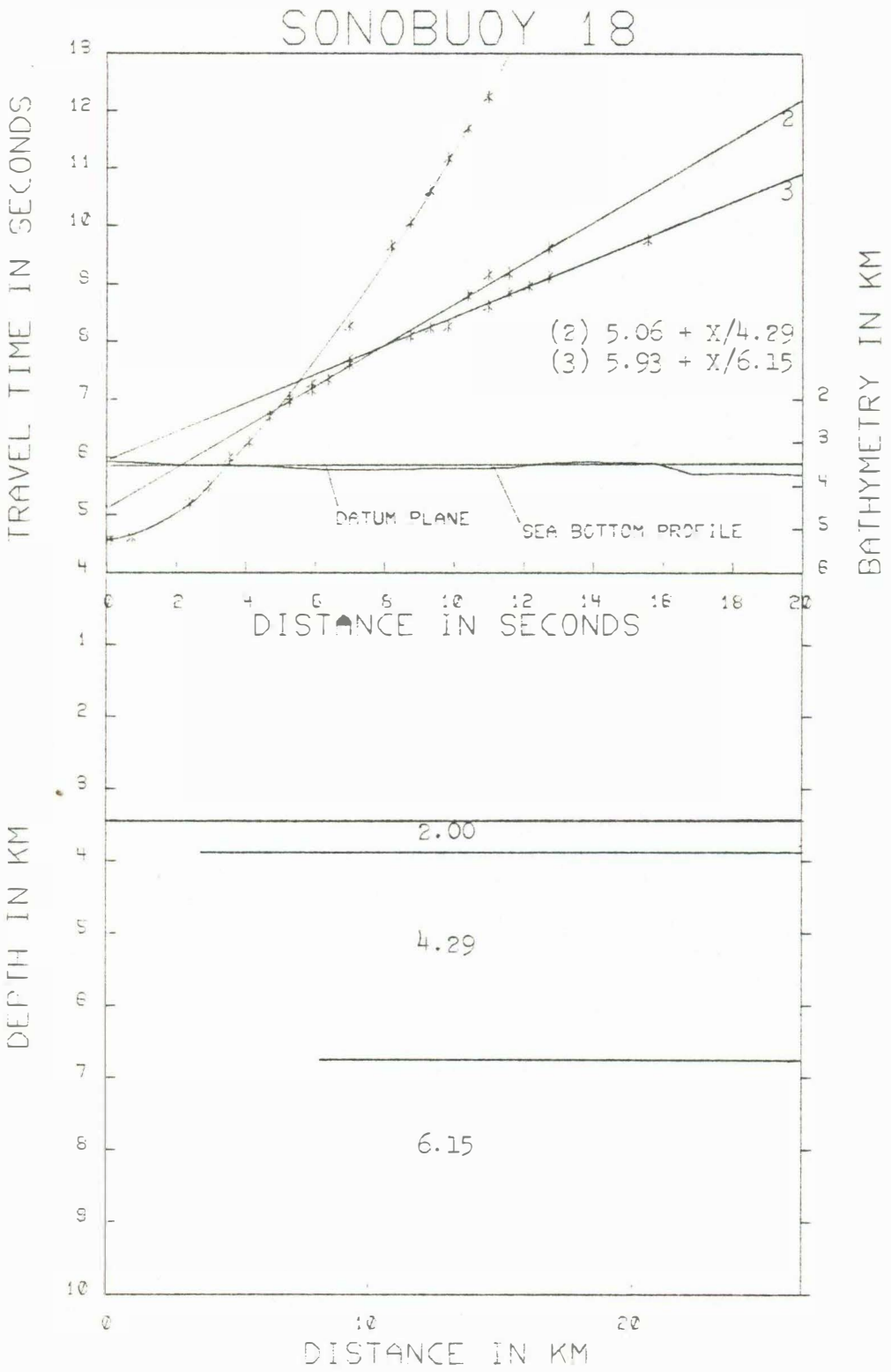
SONOBUOY 18
TRAVEL TIME IN SECONDS
BATHYMETRY IN KM
(2) 5.06 + X/4.29
(3) 5.93 + X/6.15
DATUM PLANE
SEA BOTTOM PROFILE
DISTANCE IN SECONDS
DEPTH IN KM
2.00
4.29
6.15
DISTANCE IN KM

Fig. 29. Interpreted travel time plot with bathymetry and velocity/depth model for Station 17.

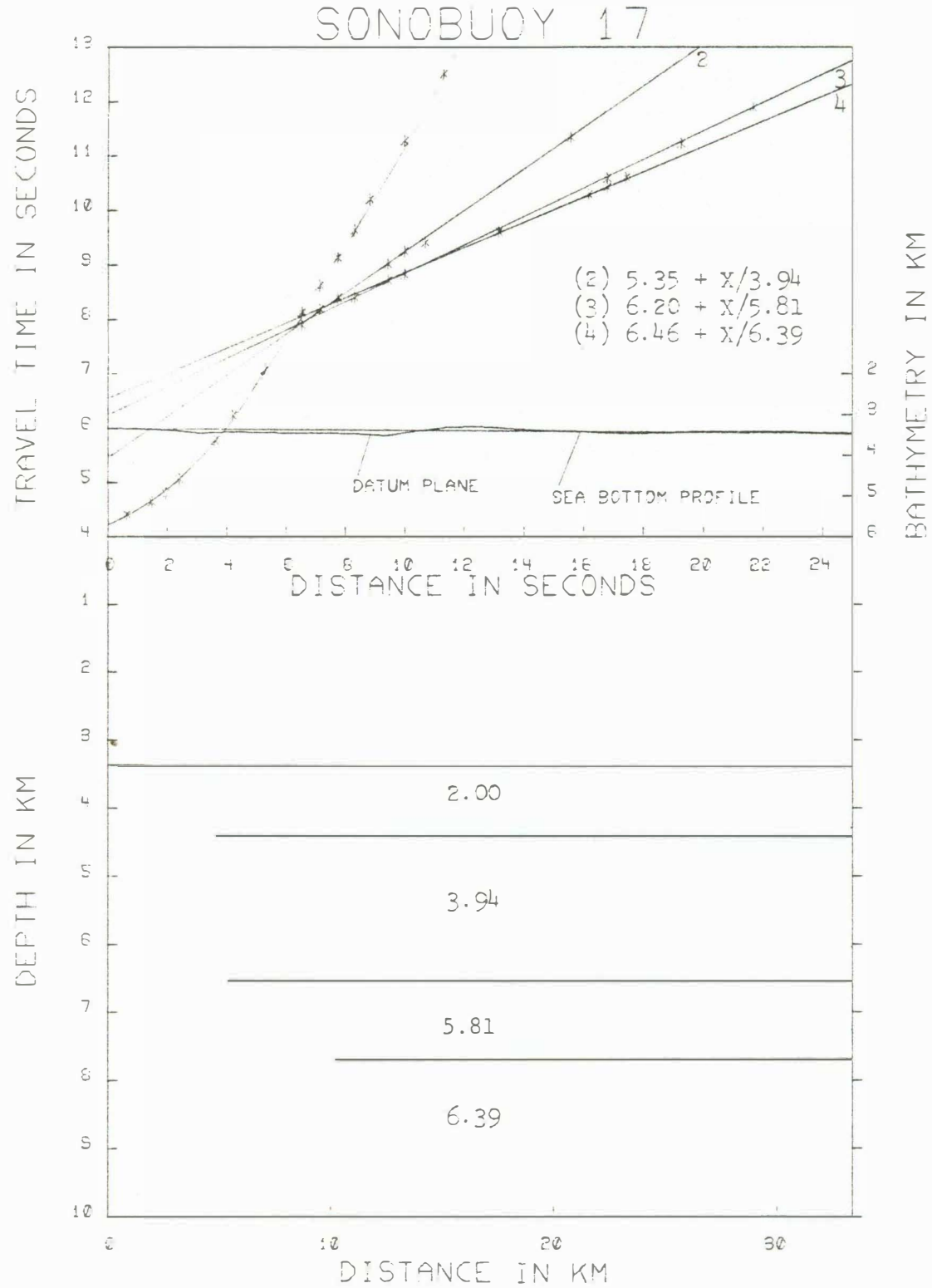
SONOBUOY 17
TRAVEL TIME IN SECONDS
(2) 5.35 + X/3.94
(3) 6.20 + X/5.81
(4) 6.46 + X/6.39
DATUM PLANE
SEA BOTTOM PROFILE
BATHYMETRY IN KM
DISTANCE IN SECONDS
DEPTH IN KM
2.00
3.94
5.81
6.39
DISTANCE IN KM

Fig. 30. Record section for Station 16.

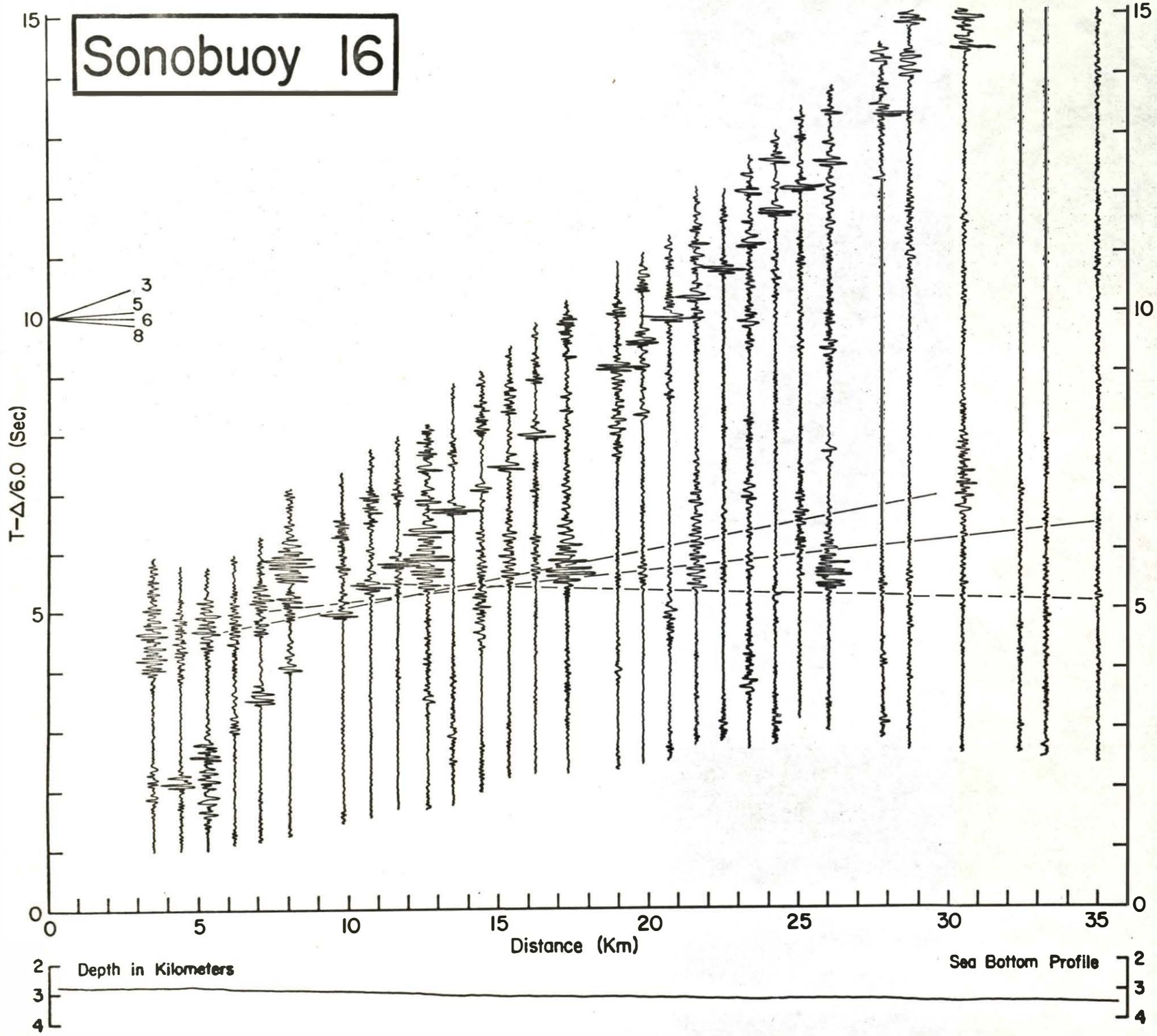
Sonobuoy 16
T-Δ/6.0 (Sec)
15
10
5
0
3
5
6
8
0
5
10
15
20
25
30
35
Distance (Km)
Depth in Kilometers
2
3
4
Sea Bottom Profile

Fig. 31. Interpreted travel time plot with bathymetry and velocity/depth model for Station 16.

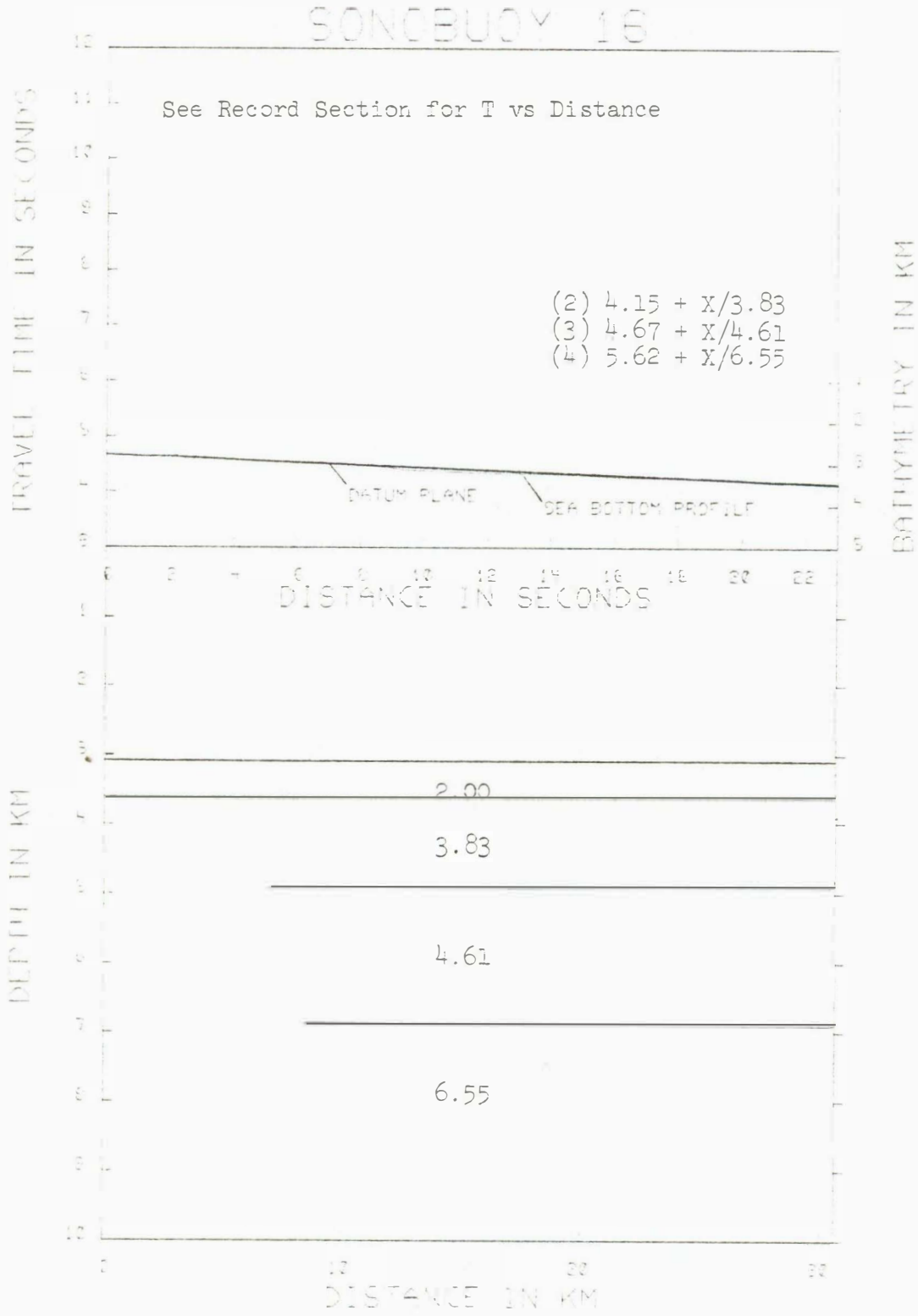
SONOBUOY 16
See Record Section for T vs Distance
(2) 4.15 + X/3.83
(3) 4.67 + X/4.61
(4) 5.62 + X/6.55
DATUM PLANE
SEA BOTTOM PROFILE
TRAVEL TIME IN SECONDS
BATHYMETRY IN KM
DISTANCE IN SECONDS
DEPTH IN KM
2.00
3.83
4.61
6.55
DISTANCE IN KM

Fig. 32. Interpreted travel time plot with bathymetry and velocity/depth model for Station 15.

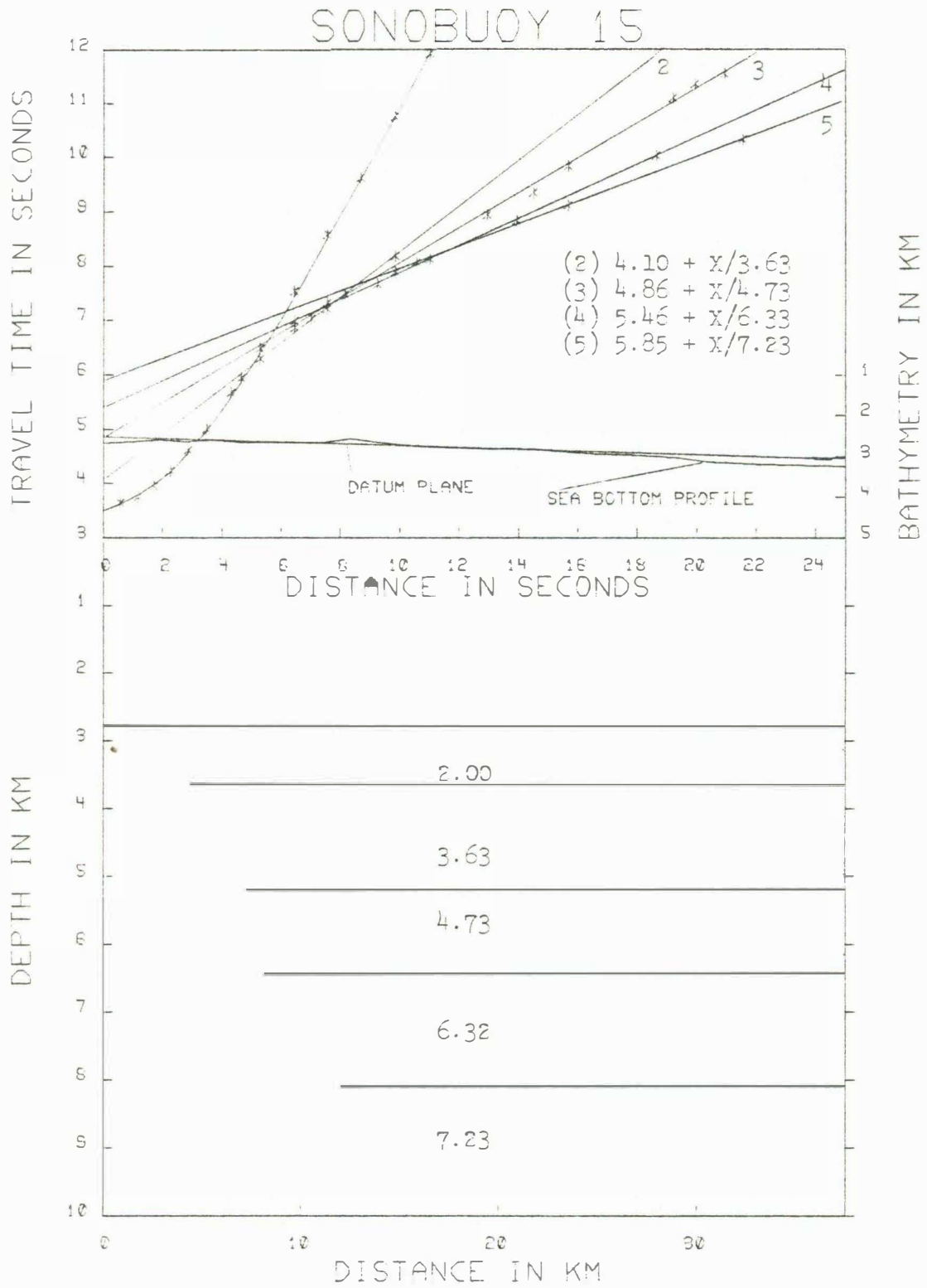
SONOBUOY 15
TRAVEL TIME IN SECONDS
BATHYMETRY IN KM
(2) 4.10 + X/3.63
(3) 4.86 + X/4.73
(4) 5.46 + X/6.33
(5) 5.85 + X/7.23
DATUM PLANE
SEA BOTTOM PROFILE
DISTANCE IN SECONDS
DEPTH IN KM
2.00
3.63
4.73
6.32
7.23
DISTANCE IN KM

Fig. 33. Interpreted travel time plot with bathymetry and velocity/depth model for Station 14.

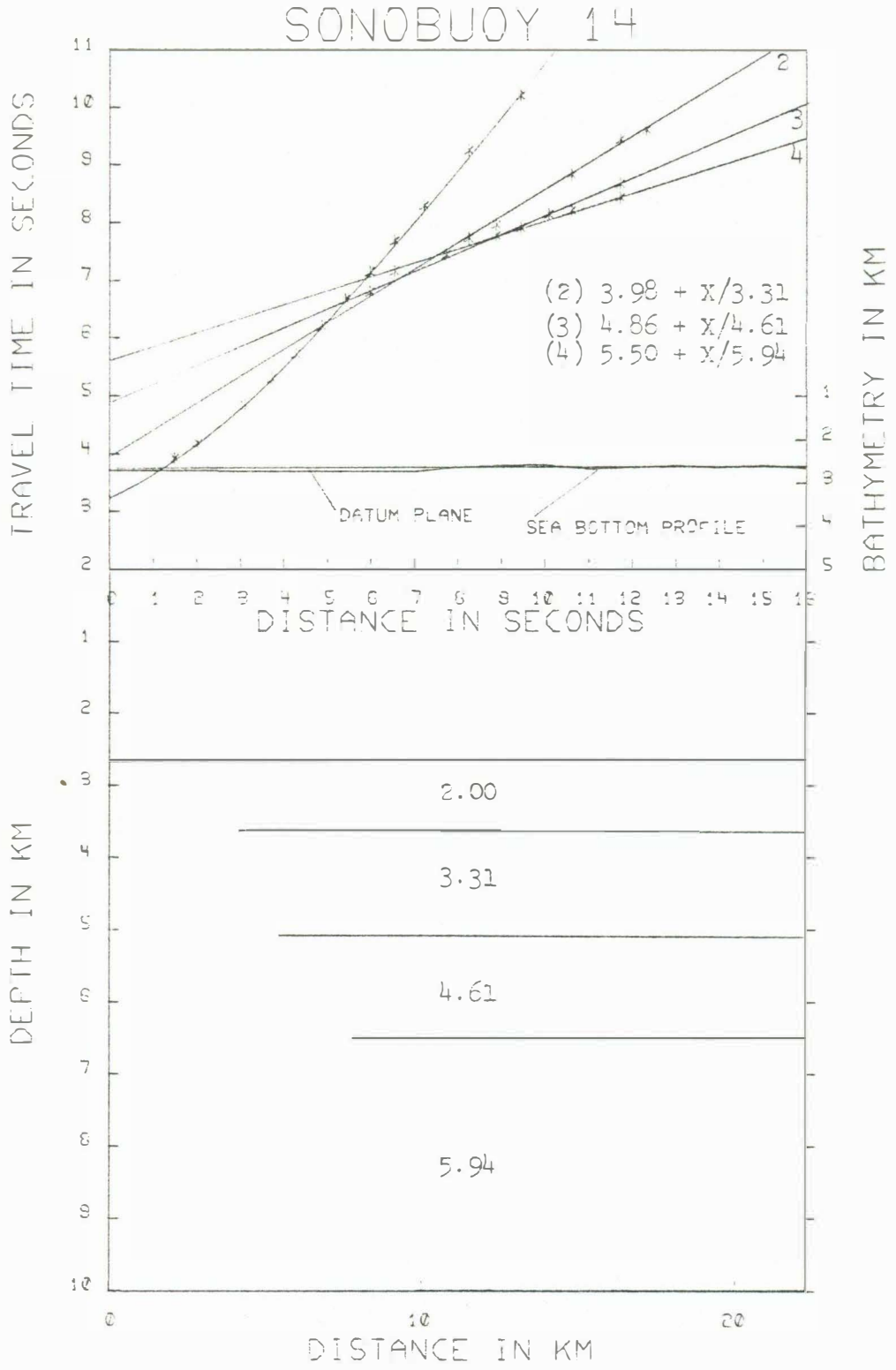
SONOBUOY 14
TRAVEL TIME IN SECONDS
(2) 3.98 + X/3.31
(3) 4.86 + X/4.61
(4) 5.50 + X/5.94
DATUM PLANE
SEA BOTTOM PROFILE
DISTANCE IN SECONDS
BATHYMETRY IN KM
DEPTH IN KM
2.00
3.31
4.61
5.94
DISTANCE IN KM

Fig. 34. Record section for Station 13.

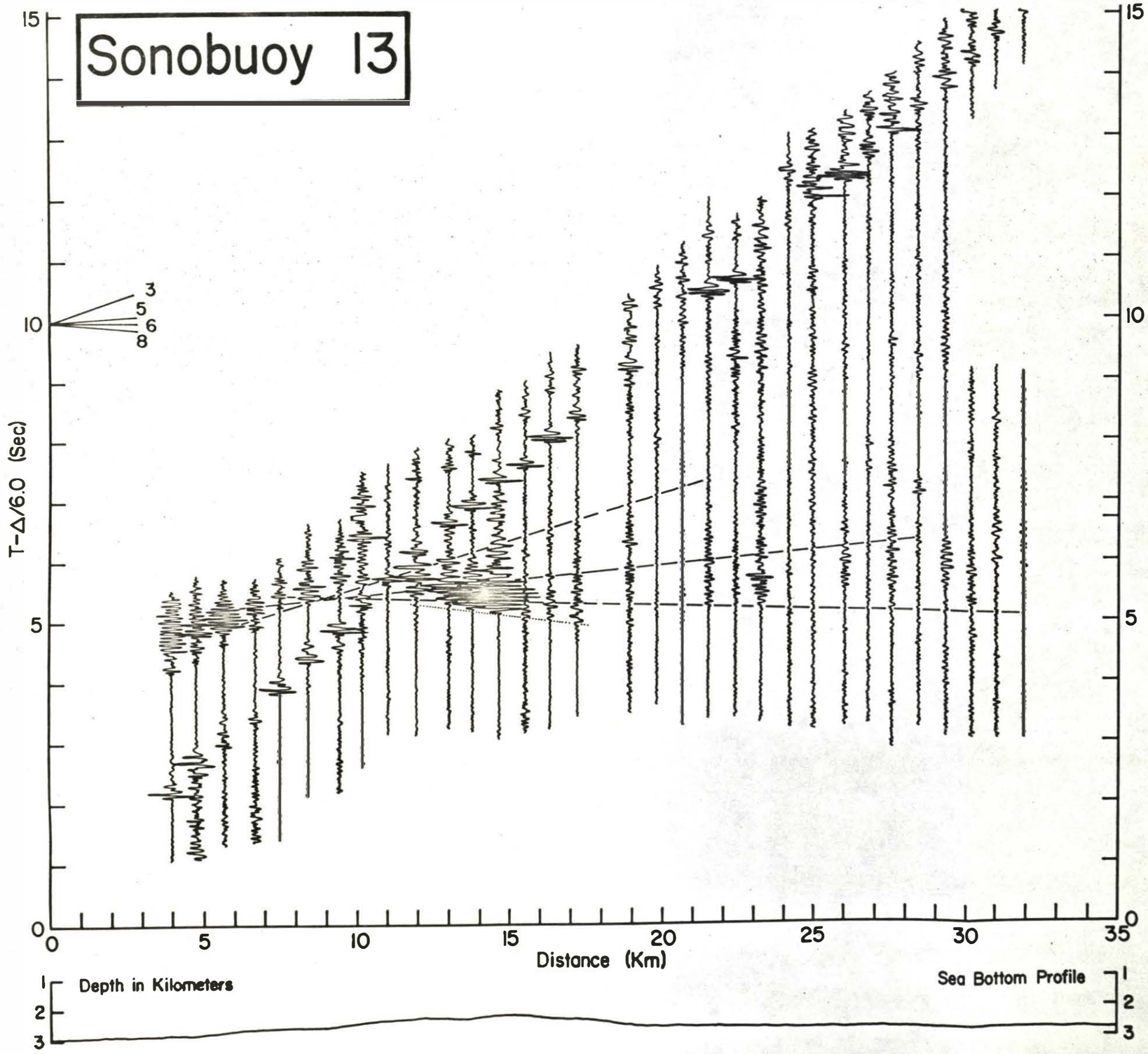
Sonobuoy 13
T-Δ/6.0 (Sec)
15
10
5
0
3
5
6
8
0
5
10
15
20
25
30
35
Distance (Km)
Depth in Kilometers
1
2
3
Sea Bottom Profile

Fig. 35. Interpreted travel time plot with bathymetry and velocity/depth model for Station 13.

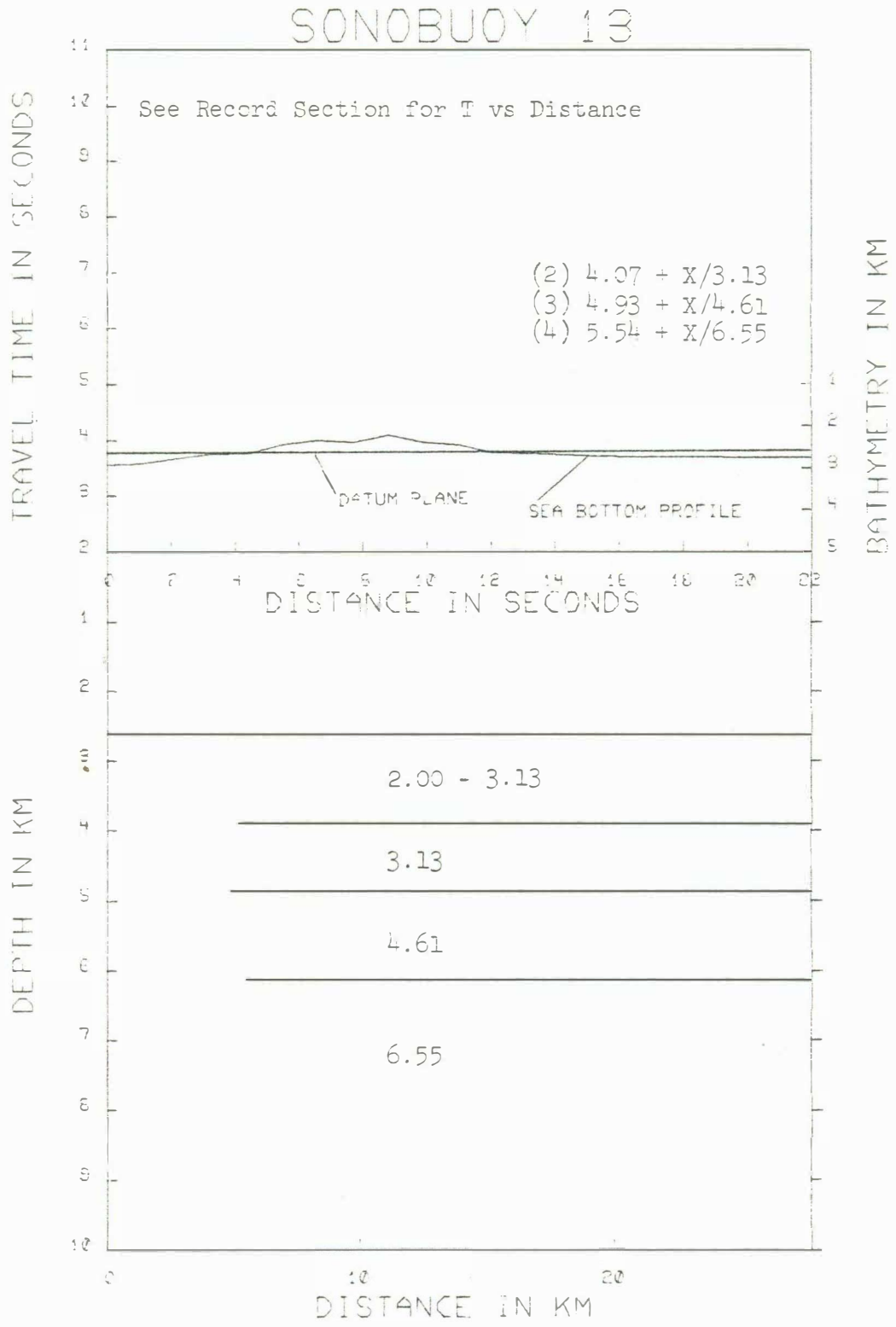
SONOBUOY 13
See Record Section for T vs Distance
(2) 4.07 + X/3.13
(3) 4.93 + X/4.61
(4) 5.54 + X/6.55
DATUM PLANE
SEA BOTTOM PROFILE
TRAVEL TIME IN SECONDS
BATHYMETRY IN KM
DISTANCE IN SECONDS
2.00 - 3.13
3.13
4.61
6.55
DEPTH IN KM
DISTANCE IN KM

Fig. 36. Interpreted travel time plot with bathymetry and velocity/depth model for Station 12.

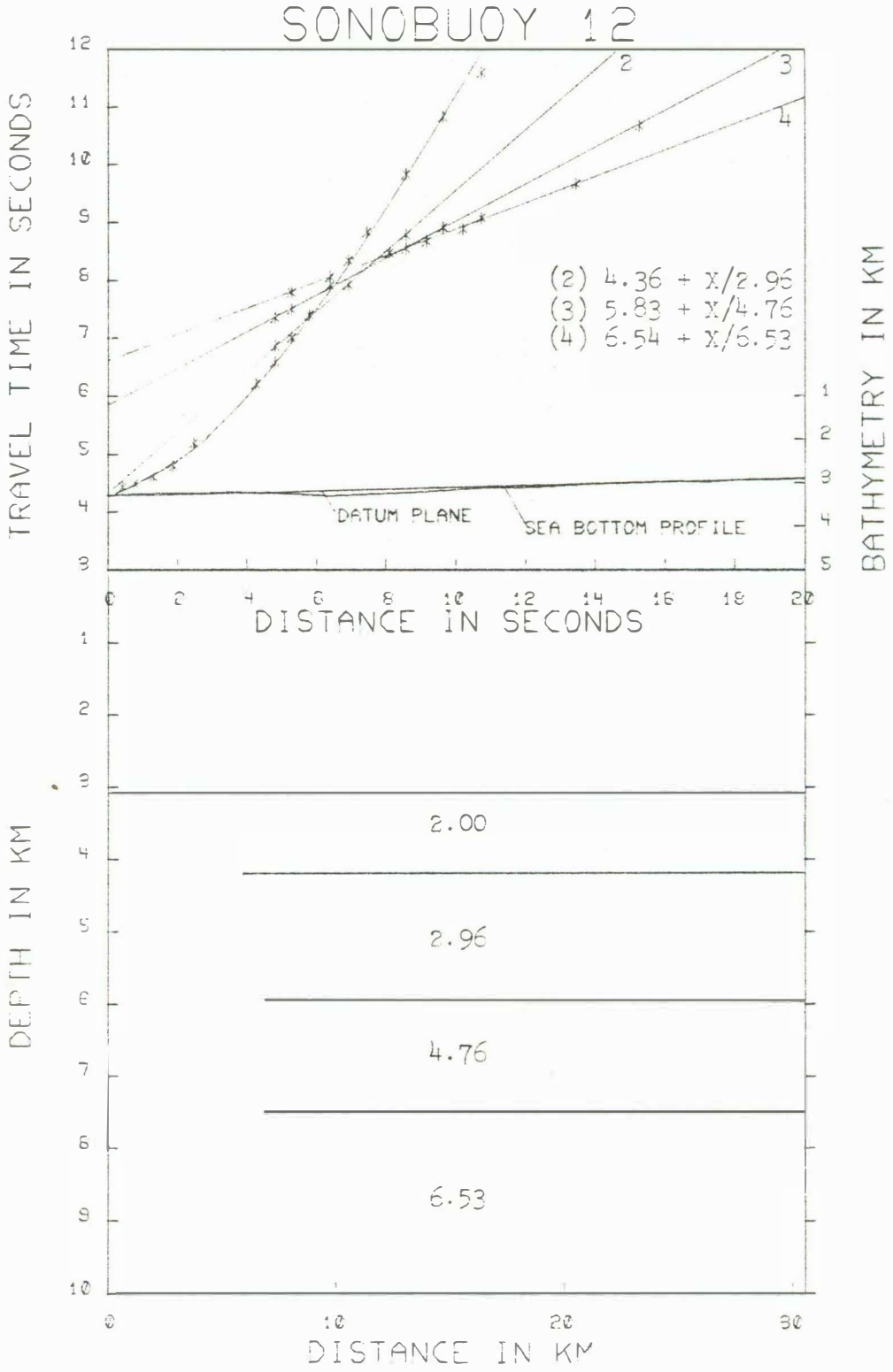
SONOBUOY 12
TRAVEL TIME IN SECONDS
BATHYMETRY IN KM
(2) 4.36 + X/2.96
(3) 5.83 + X/4.76
(4) 6.54 + X/6.53
DATUM PLANE
SEA BOTTOM PROFILE
DISTANCE IN SECONDS
DEPTH IN KM
2.00
2.96
4.76
6.53
DISTANCE IN KM

Fig. 37. Interpreted travel time plot with bathymetry and velocity/depth model for Station 11.

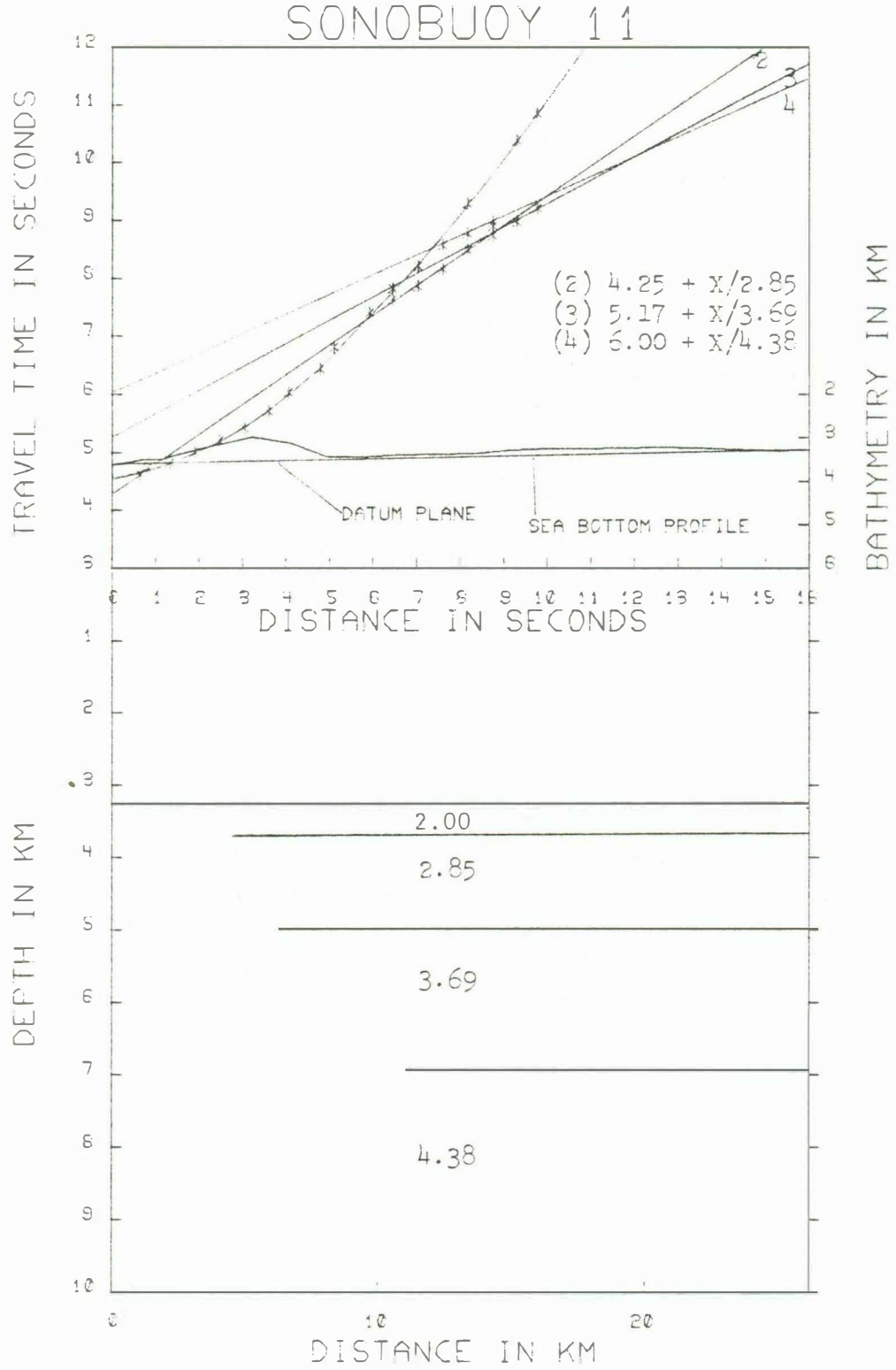
SONOBUOY 11
TRAVEL TIME IN SECONDS
BATHYMETRY IN KM
(2) 4.25 + X/2.85
(3) 5.17 + X/3.69
(4) 6.00 + X/4.38
DATUM PLANE
SEA BOTTOM PROFILE
DISTANCE IN SECONDS
DEPTH IN KM
2.00
2.85
3.69
4.38
DISTANCE IN KM

Fig. 38. Record section for Station 10.

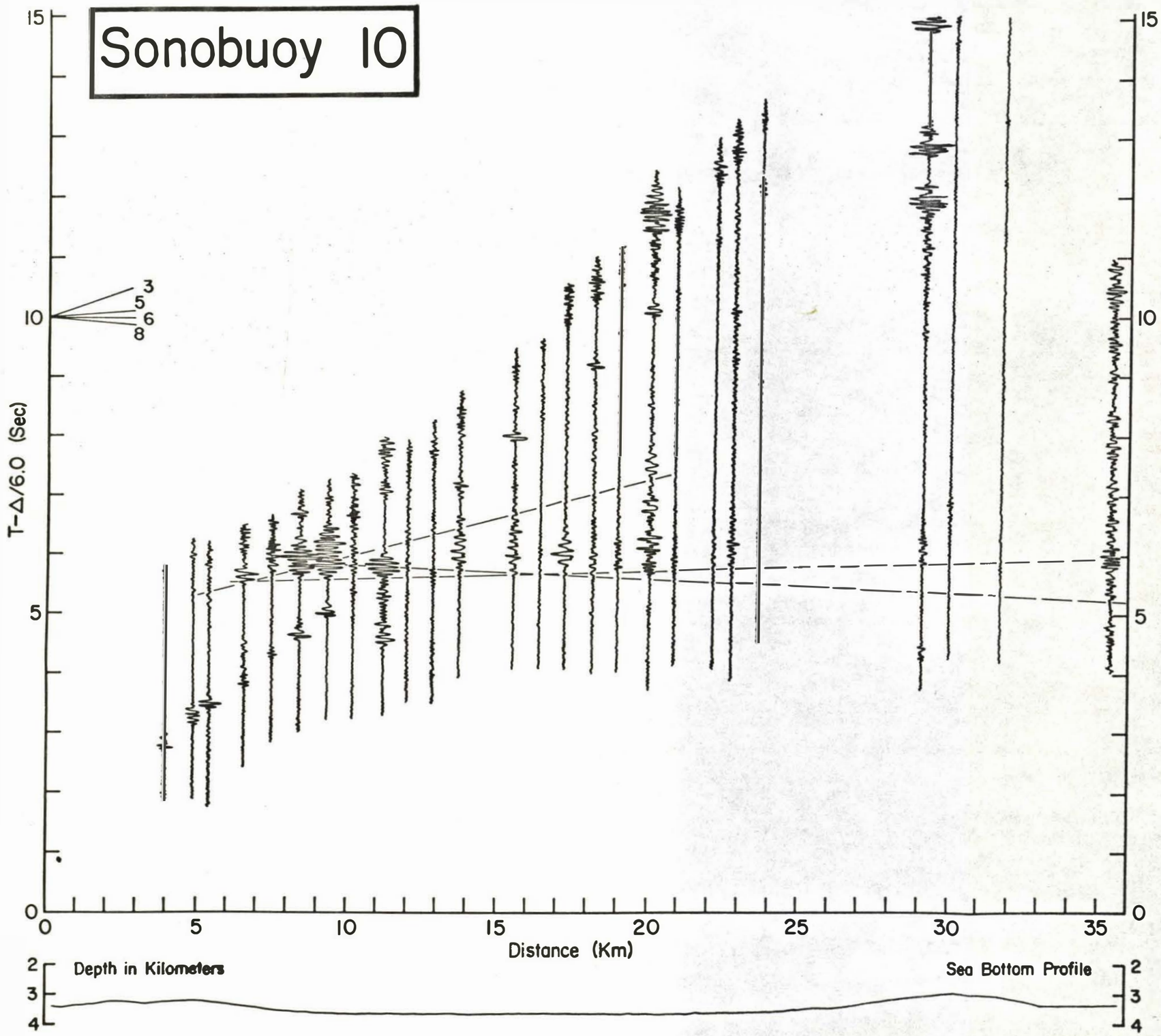
Sonobuoy 10
T-Δ/6.0 (Sec)
15
10
5
0
3
5
6
8
0
5
10
15
20
25
30
35
Distance (Km)
Depth in Kilometers
Sea Bottom Profile
2
3
4

Fig. 39. Interpreted travel time plot with bathymetry and velocity/depth model for Station 10.

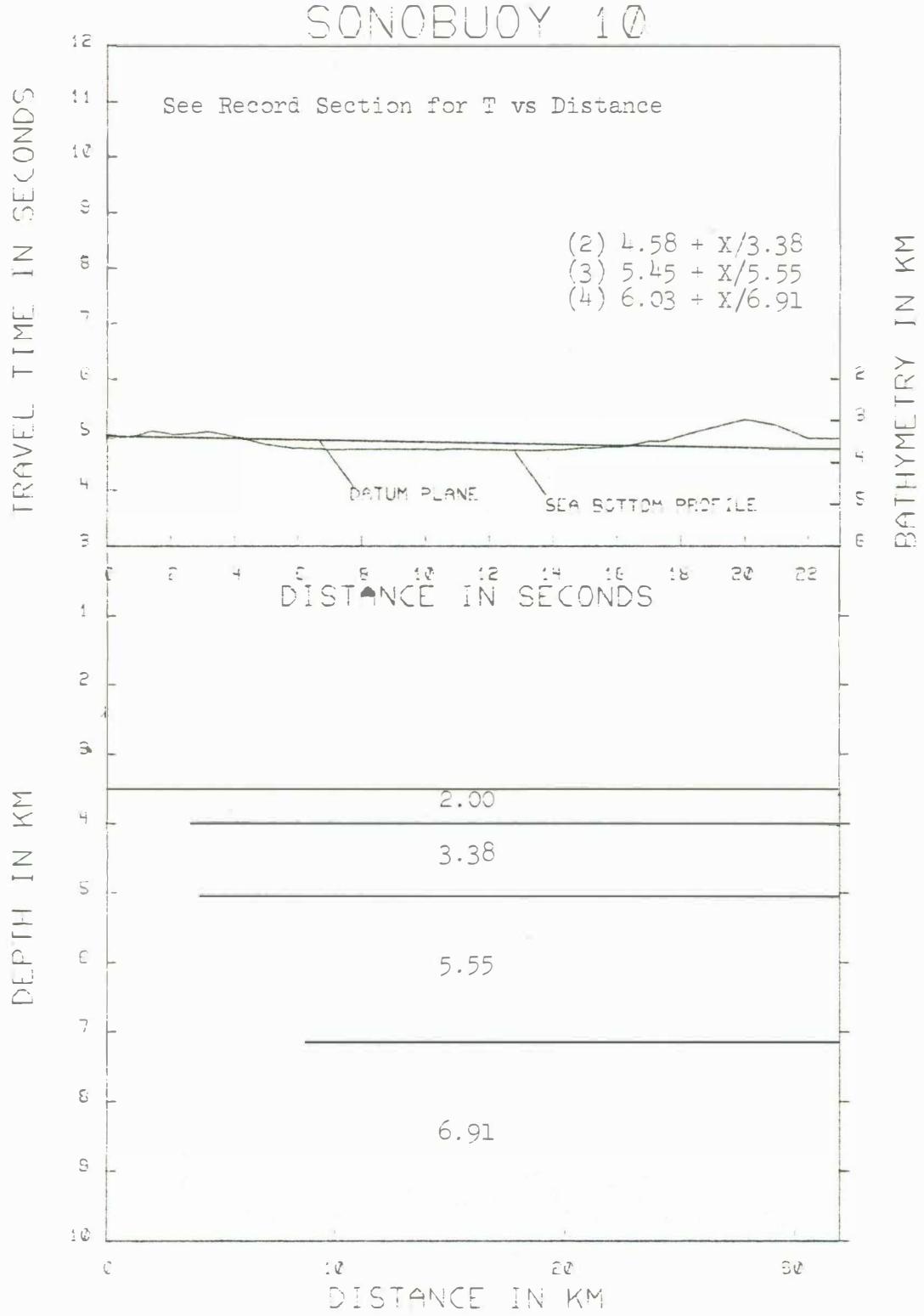
SONOBUOY 10
See Record Section for T vs Distance
(2) 4.58 + X/3.38
(3) 5.45 + X/5.55
(4) 6.03 + X/6.91
DATUM PLANE
SEA BOTTOM PROFILE
TRAVEL TIME IN SECONDS
BATHYMETRY IN KM
DISTANCE IN SECONDS
2.00
3.38
5.55
6.91
DEPTH IN KM
DISTANCE IN KM

Fig. 40. Record section for Station 9.

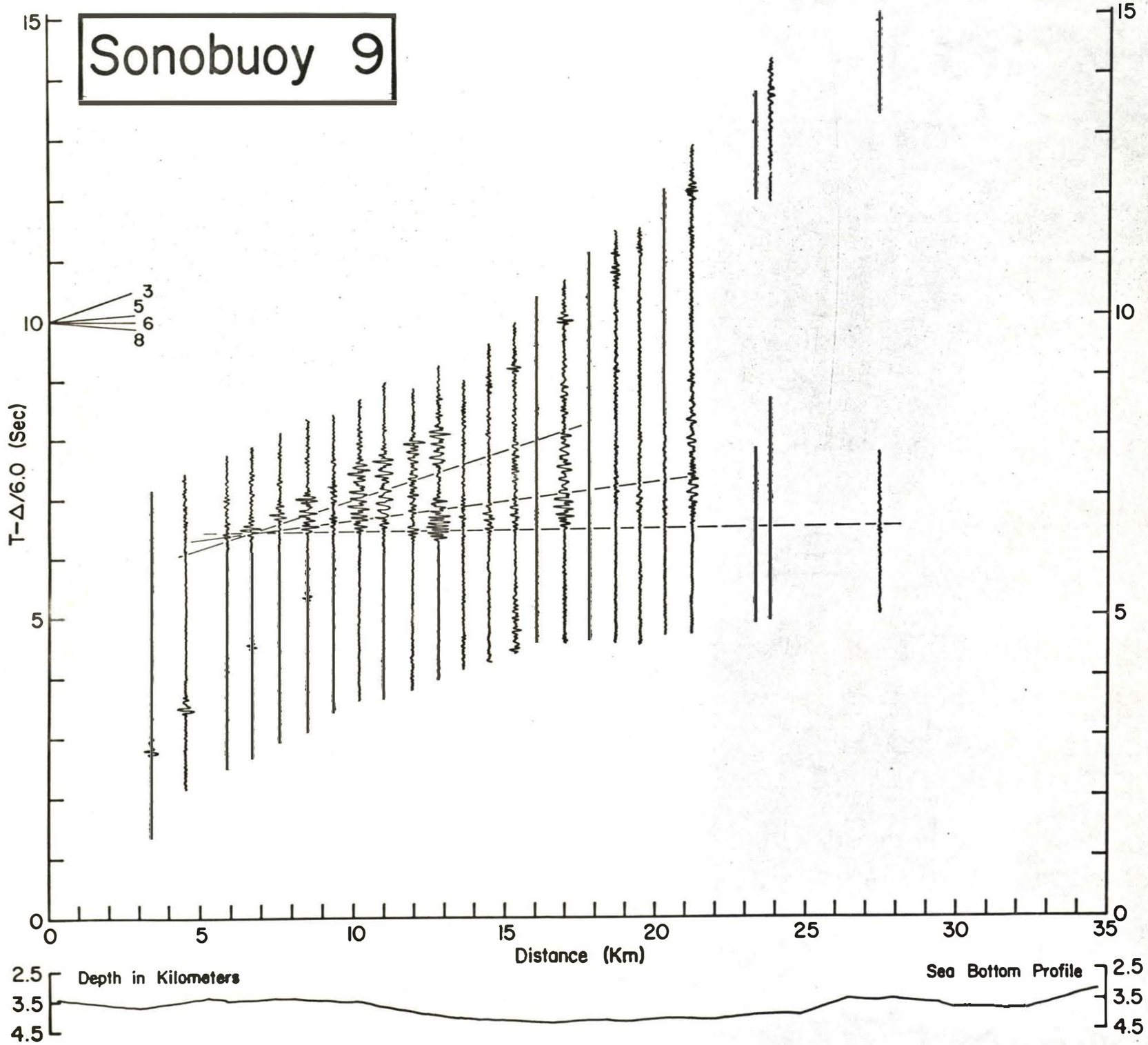
Sonobuoy 9
T-Δ/6.0 (Sec)
15
10
5
0
3
5
6
8
0
5
10
15
20
25
30
35
Distance (Km)
Depth in Kilometers
2.5
3.5
4.5
Sea Bottom Profile

Fig. 41. Interpreted travel time plot with bathymetry and velocity/depth model for Station 9.

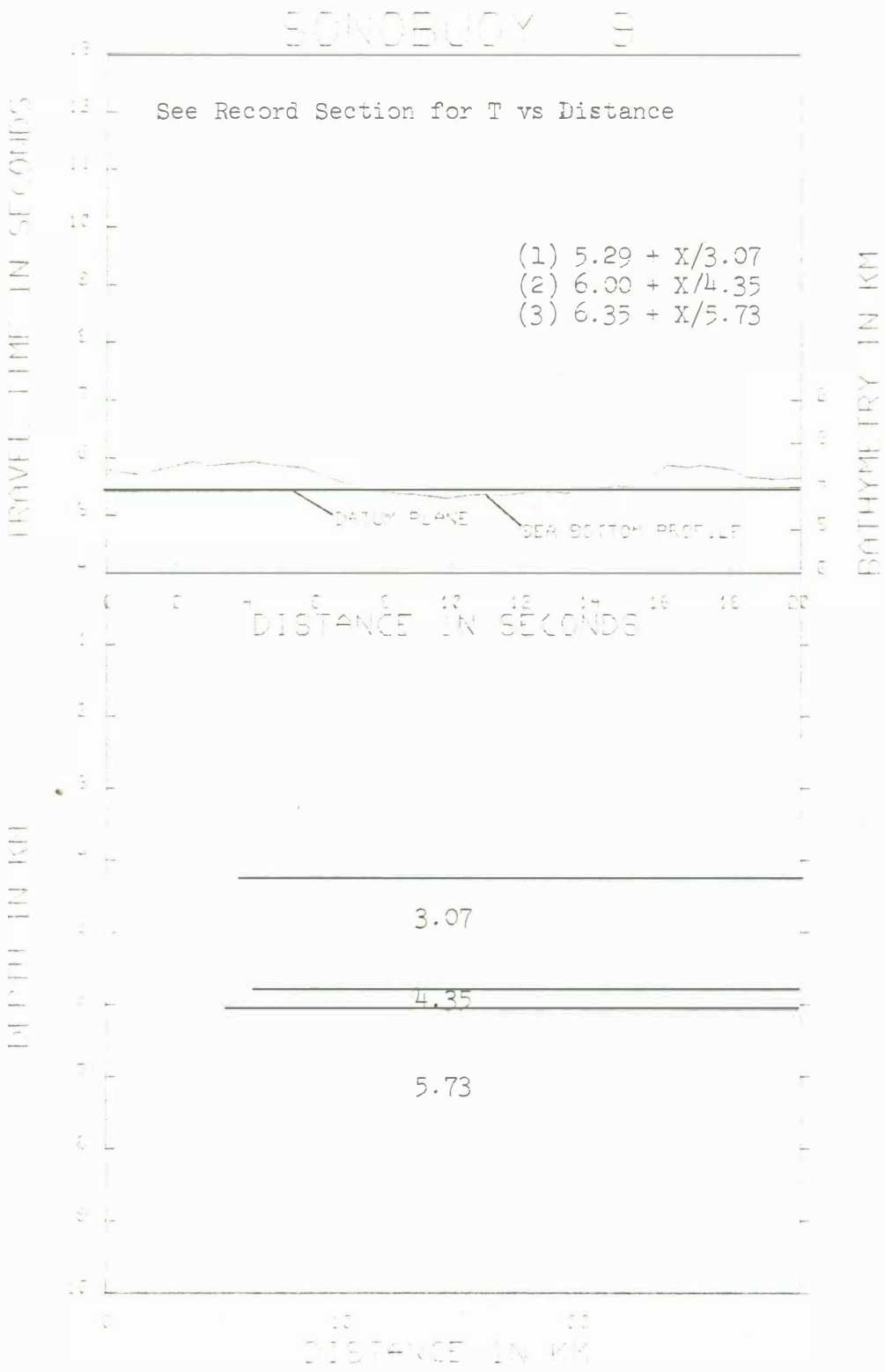
SONOBUOY 9
See Record Section for T vs Distance
(1) 5.29 + X/3.07
(2) 6.00 + X/4.35
(3) 6.35 + X/5.73
DATUM PLANE
SEA BOTTOM PROFILE
TRAVEL TIME IN SECONDS
BATHYMETRY IN KM
DISTANCE IN SECONDS
DEPTH IN KM
3.07
4.35
5.73
DISTANCE IN KM

Fig. 42. Interpreted travel time plot with bathymetry and velocity/depth model for Station 8.

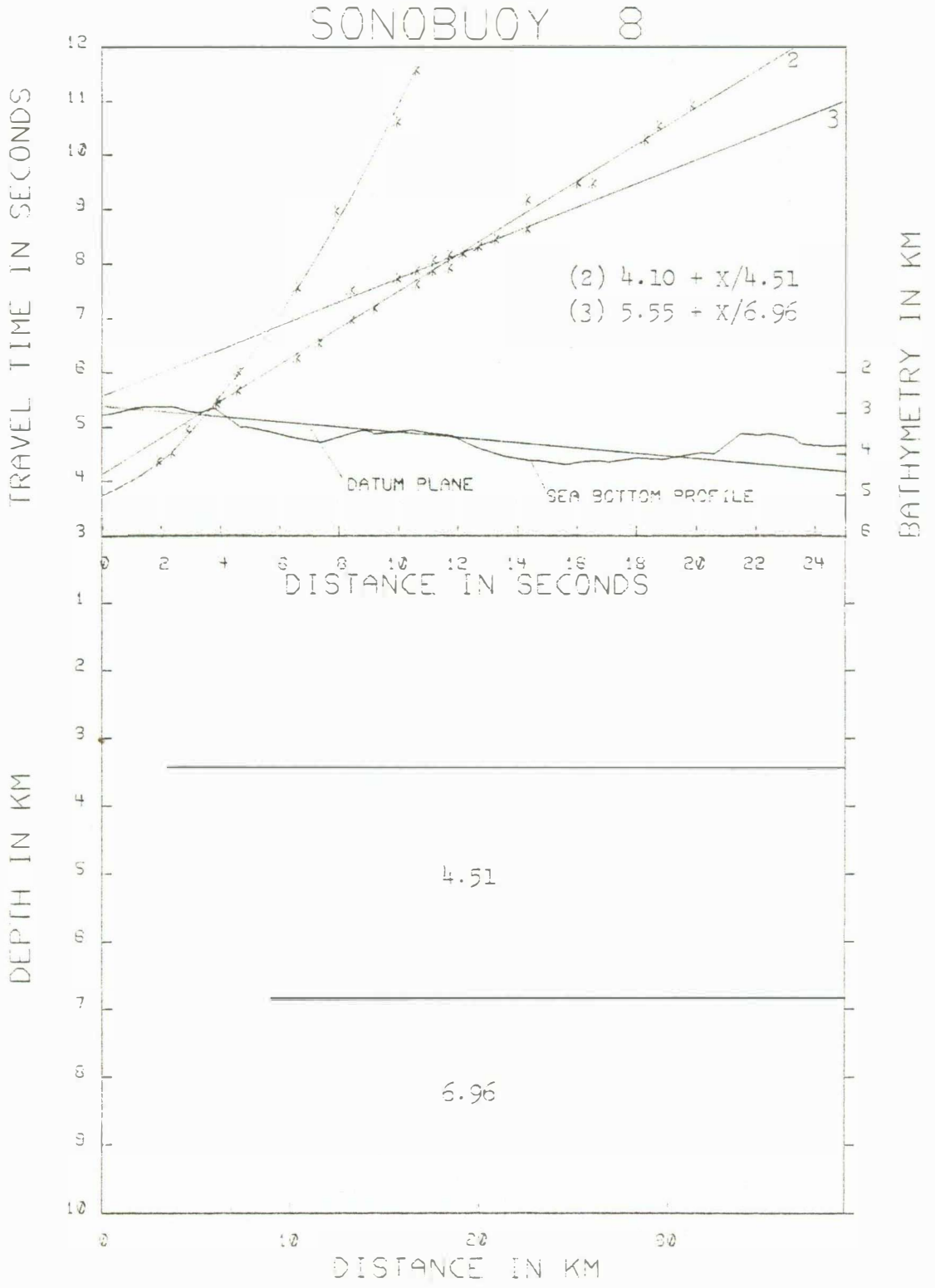
SONOBUOY 8
TRAVEL TIME IN SECONDS
BATHYMETRY IN KM
(2) 4.10 + X/4.51
(3) 5.55 + X/6.96
DATUM PLANE
SEA BOTTOM PROFILE
DISTANCE IN SECONDS
DEPTH IN KM
4.51
6.96
DISTANCE IN KM

Fig. 43. Interpreted travel time plot with bathymetry and velocity/depth model for Station 6.

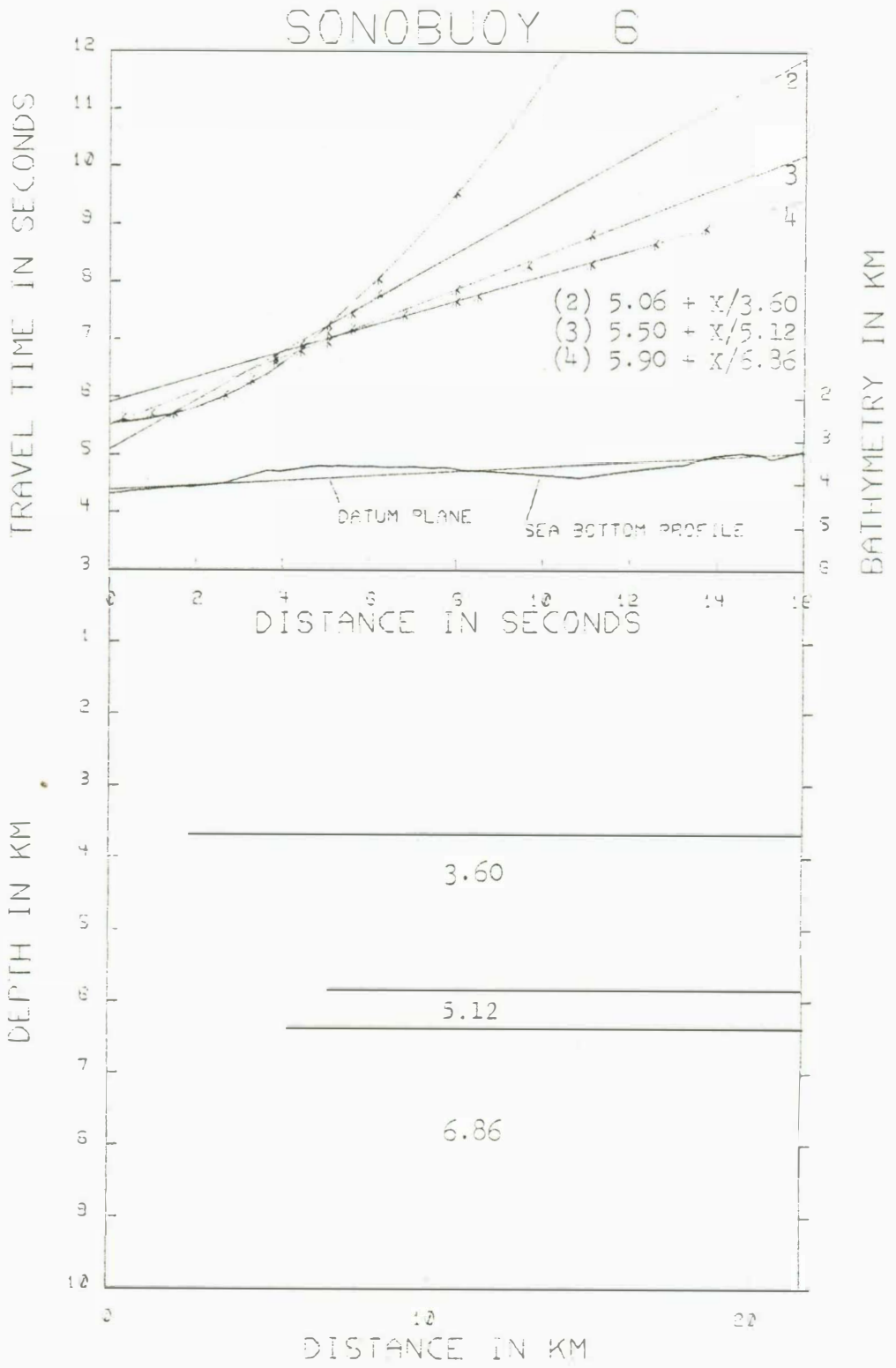
SONOBUOY 6
TRAVEL TIME IN SECONDS
BATHYMETRY IN KM
(2) 5.06 + X/3.60
(3) 5.50 + X/5.12
(4) 5.90 + X/6.86
DATUM PLANE
SEA BOTTOM PROFILE
DISTANCE IN SECONDS
DEPTH IN KM
3.60
5.12
6.86
DISTANCE IN KM

Fig. 44. Interpreted travel time plot with bathymetry and velocity/depth model for Station 5.

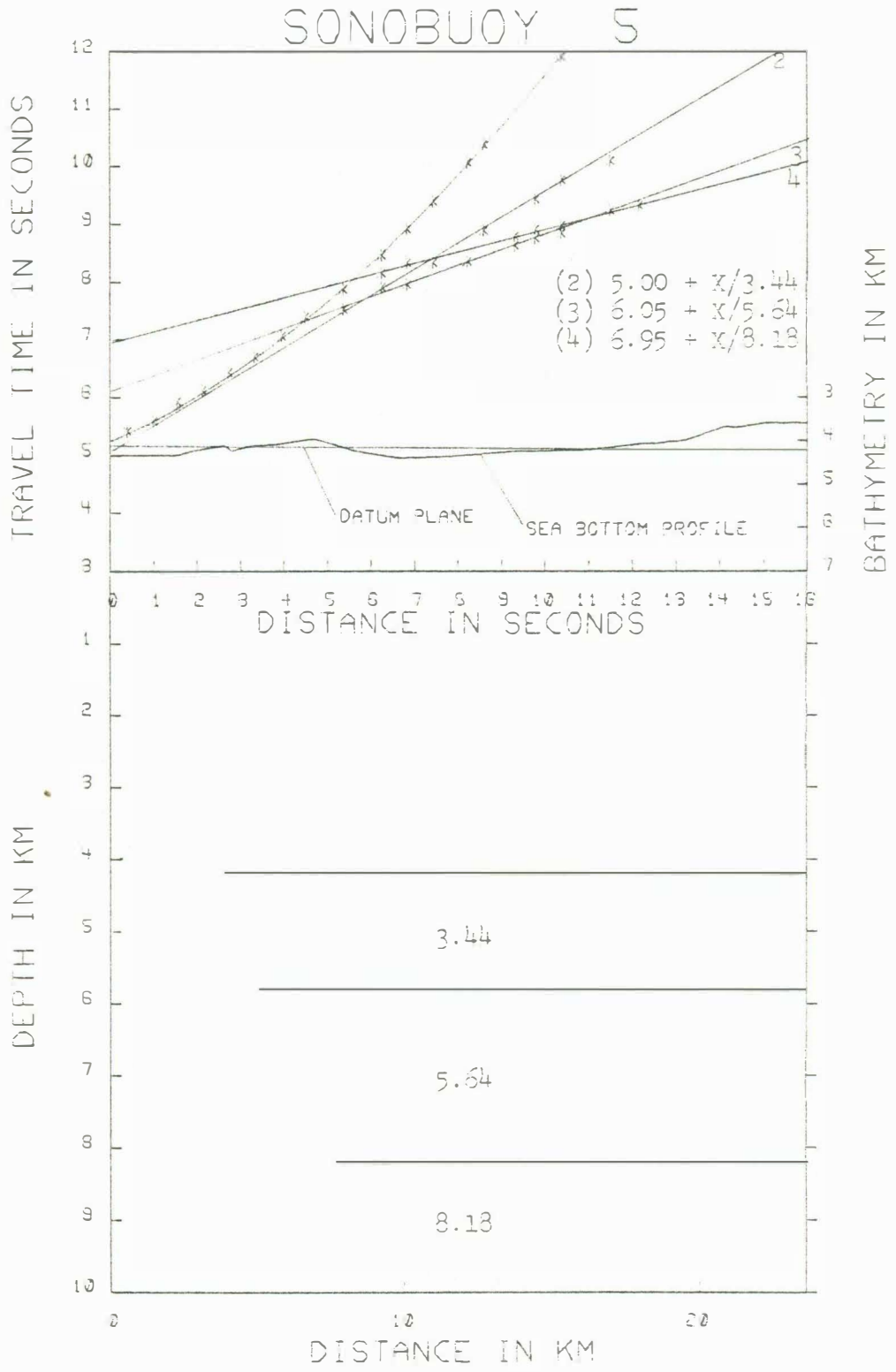
SONOBUOY 5
TRAVEL TIME IN SECONDS
BATHYMETRY IN KM
(2) 5.00 + X/3.44
(3) 6.05 + X/5.64
(4) 6.95 + X/8.18
DATUM PLANE
SEA BOTTOM PROFILE
DISTANCE IN SECONDS
DEPTH IN KM
3.44
5.64
8.18
DISTANCE IN KM

Fig. 45. Interpreted travel time plot with bathymetry and velocity/depth model for Station 4.

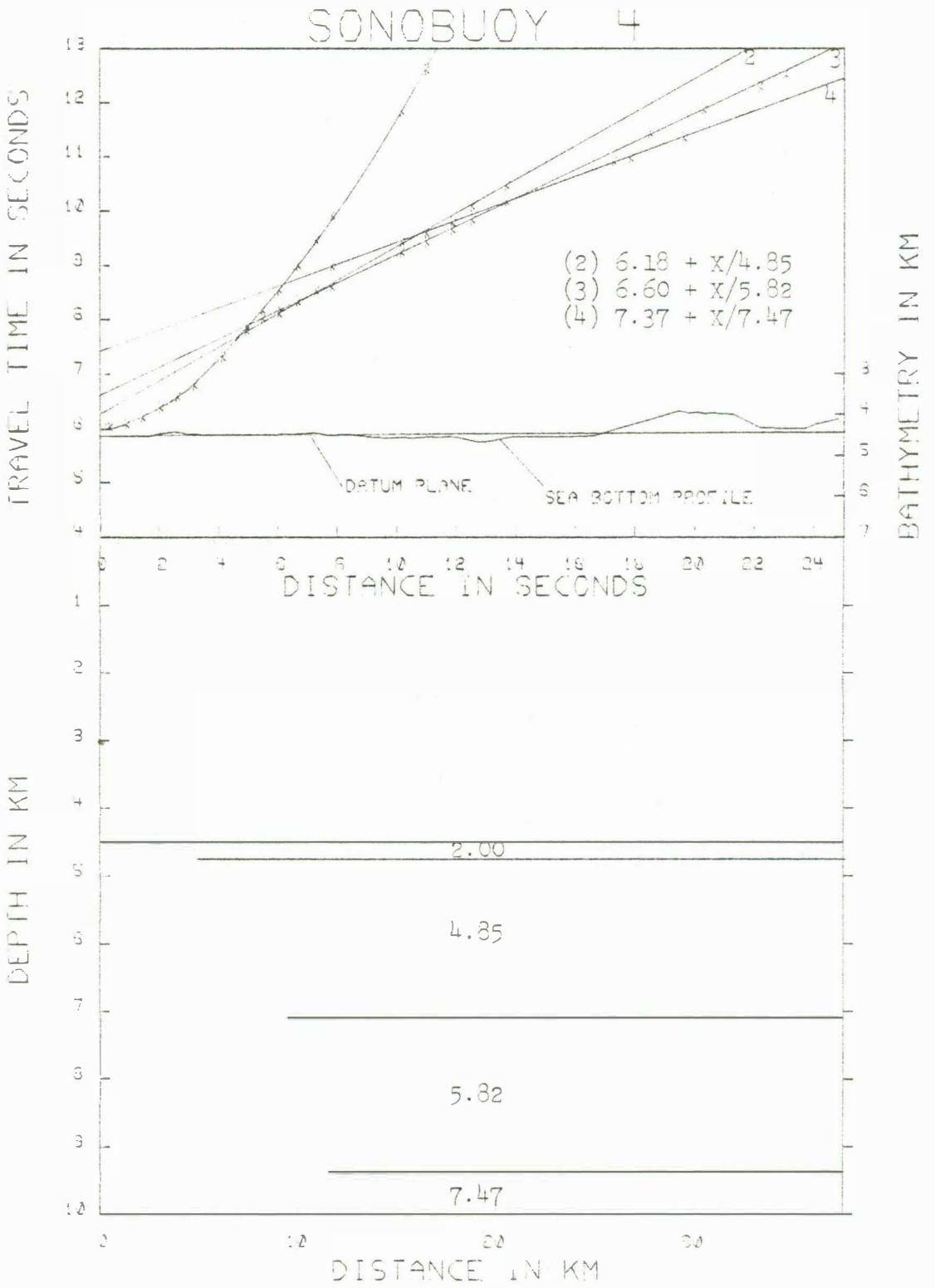
SONOBUOY 4
TRAVEL TIME IN SECONDS
BATHYMETRY IN KM
(2) 6.18 + X/4.85
(3) 6.60 + X/5.82
(4) 7.37 + X/7.47
DATUM PLANE
SEA BOTTOM PROFILE
DISTANCE IN SECONDS
DEPTH IN KM
2.00
4.85
5.82
7.47
DISTANCE IN KM

Fig. 46. Record section for Station 3.

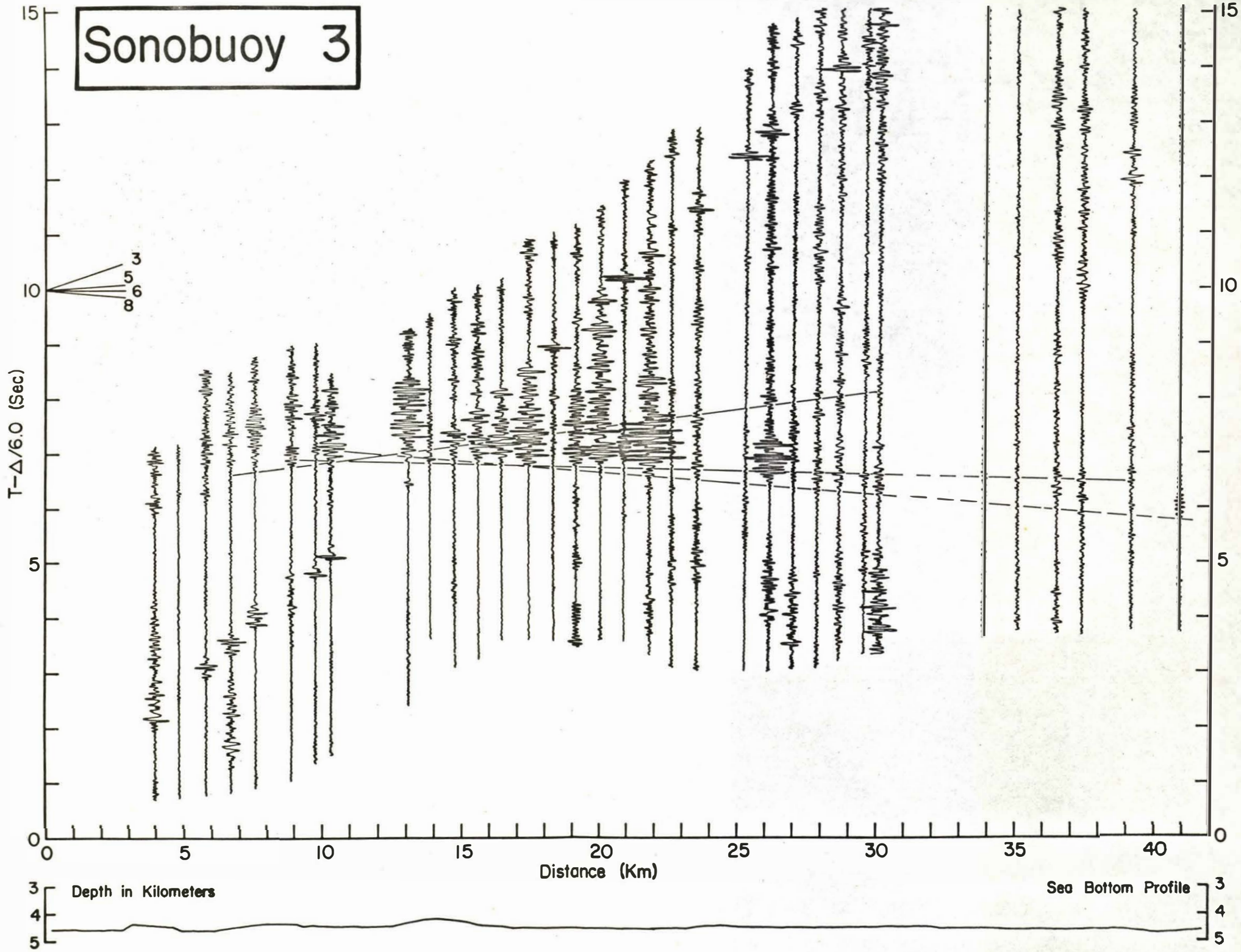
Sonobuoy 3
T−Δ/6.0 (Sec)
3
5
6
8
Distance (Km)
Depth in Kilometers
Sea Bottom Profile

Fig. 47. Interpreted travel time plot with bathymetry and velocity/depth model for Station 3.

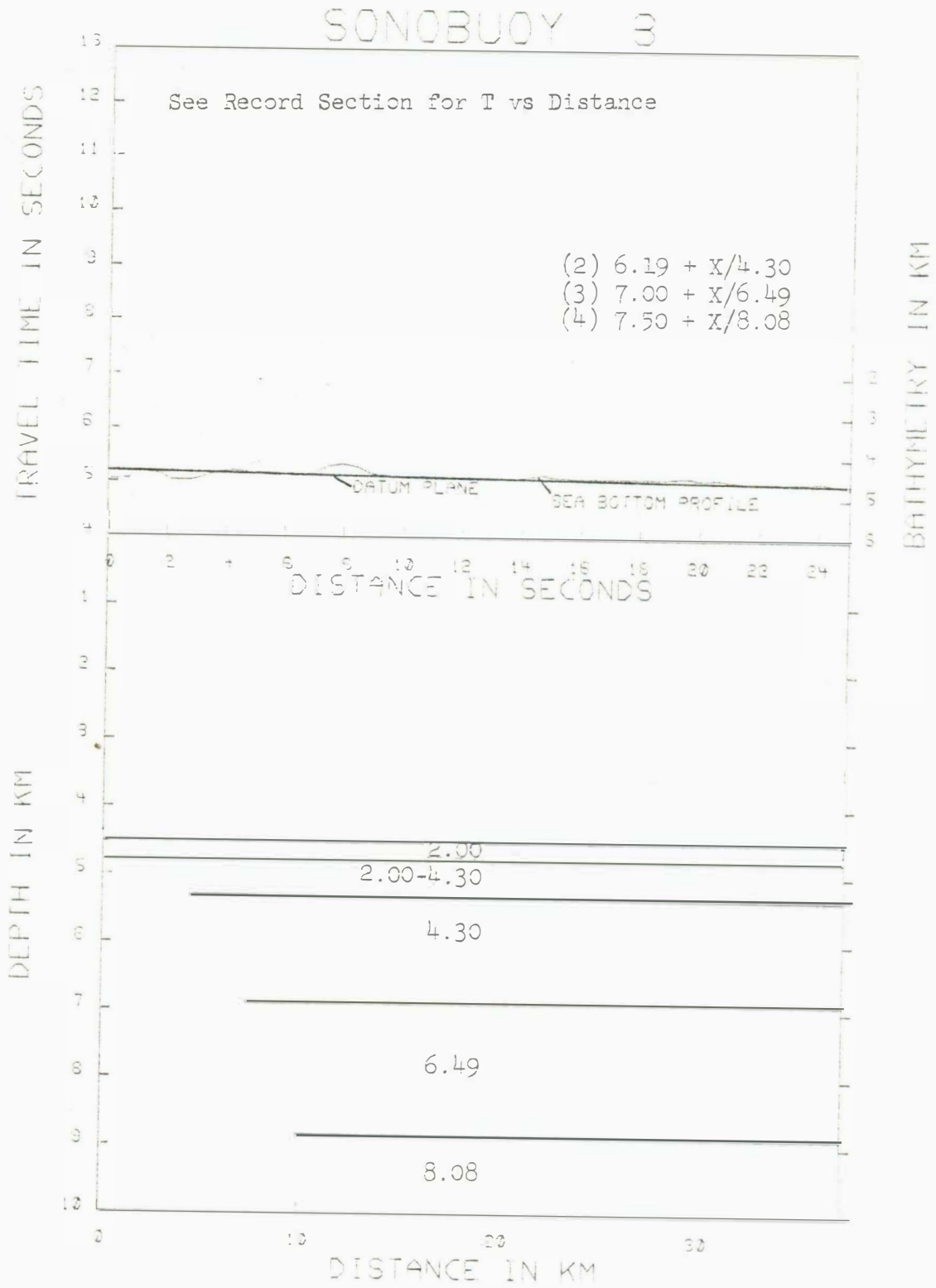
SONOBUOY 3
See Record Section for T vs Distance
(2) 6.19 + X/4.30
(3) 7.00 + X/6.49
(4) 7.50 + X/8.08
DATUM PLANE
SEA BOTTOM PROFILE
TRAVEL TIME IN SECONDS
BATHYMETRY IN KM
DISTANCE IN SECONDS
DEPTH IN KM
2.00
2.00-4.30
4.30
6.49
8.08
DISTANCE IN KM

Fig. 48. Record section for Station 2.

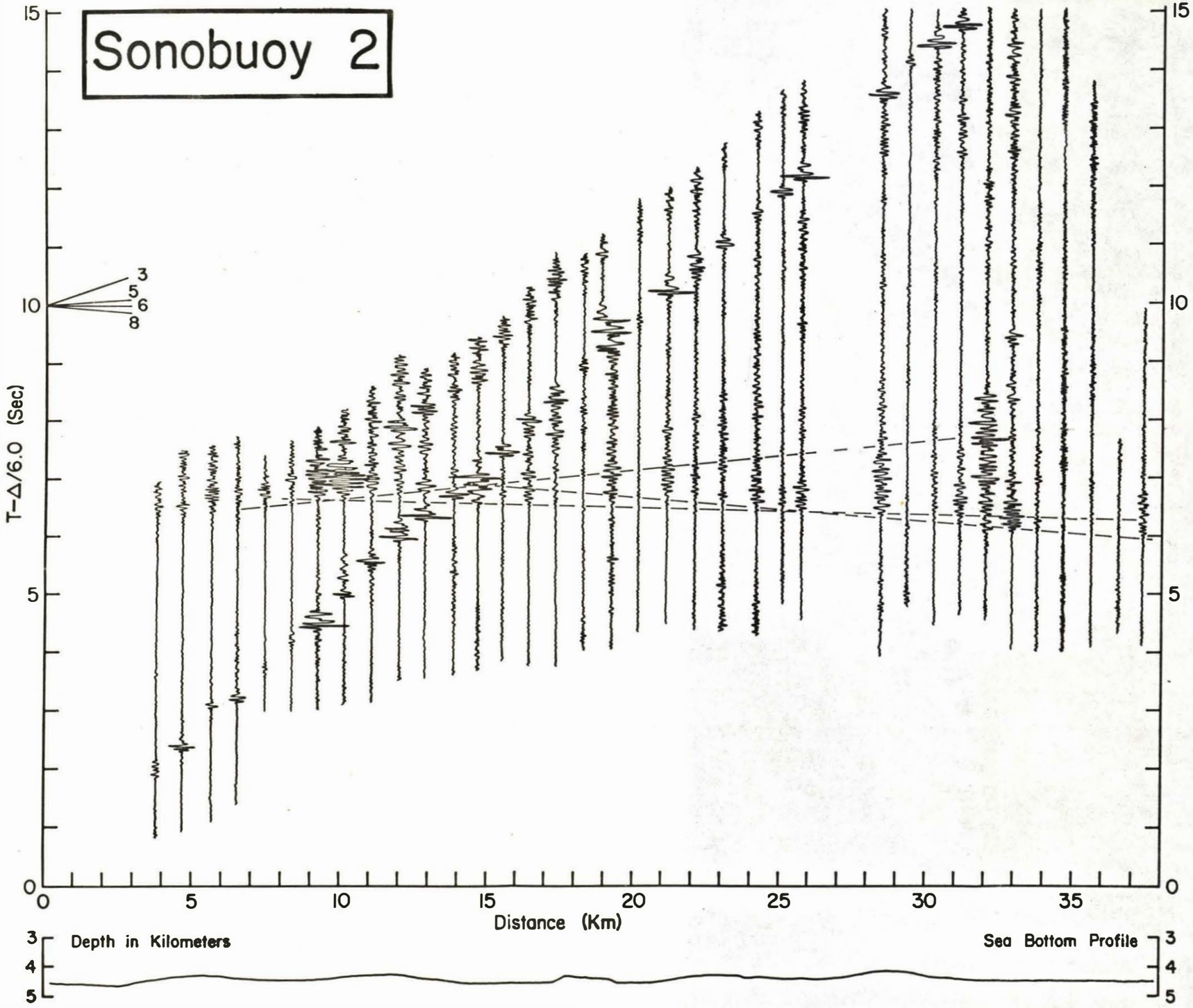
Sonobuoy 2
T-Δ/6.0 (Sec)
15
10
5
0
3
5
6
8
0
5
10
15
20
25
30
35
Distance (Km)
Depth in Kilometers
Sea Bottom Profile
3
4
5

Fig. 49. Interpreted travel time plot with bathymetry and velocity/depth model for Station 2.

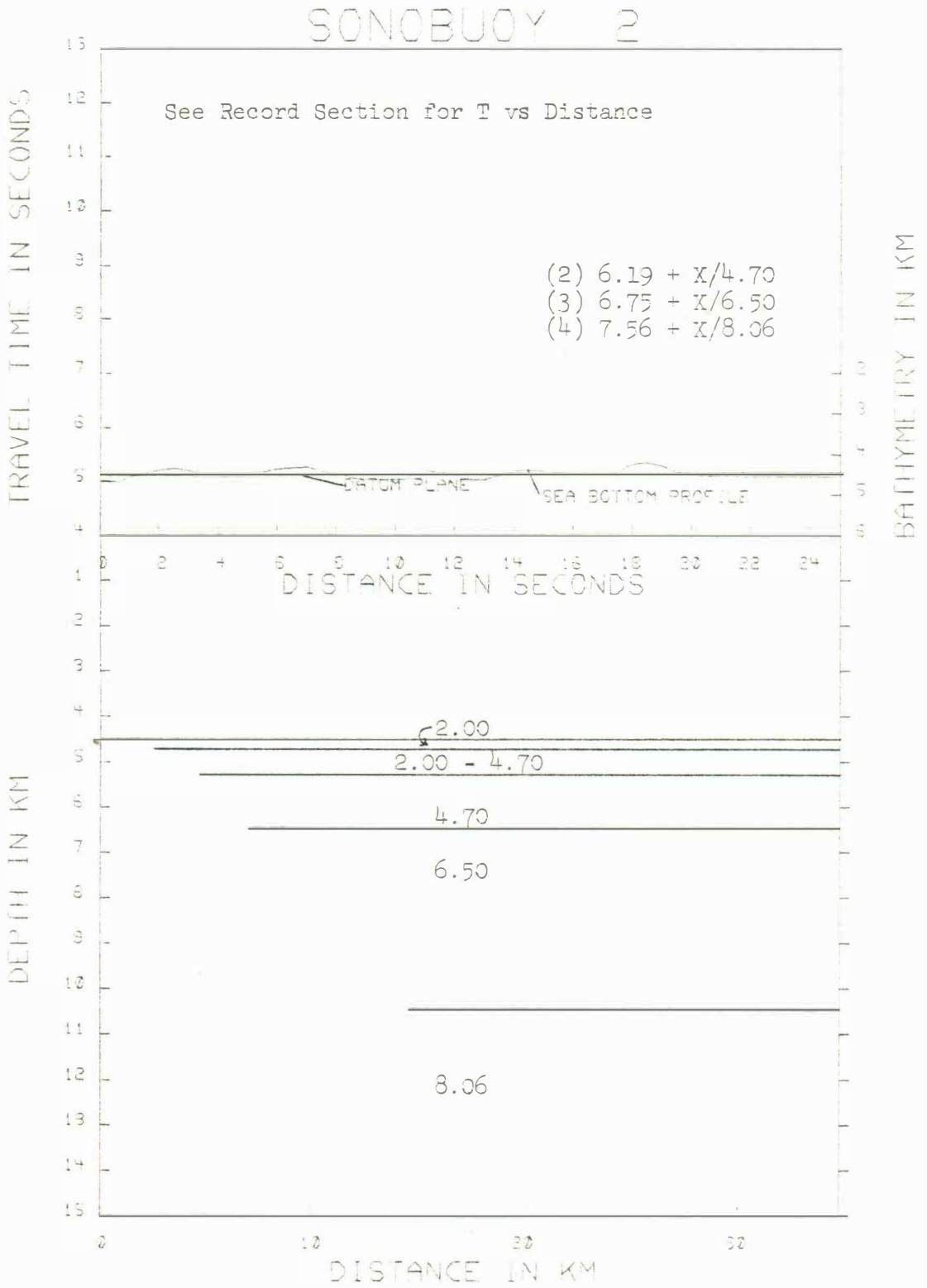
SONOBUOY 2
See Record Section for T vs Distance
(2) 6.19 + X/4.70
(3) 6.75 + X/6.50
(4) 7.56 + X/8.06
DATUM PLANE
SEA BOTTOM PROFILE
TRAVEL TIME IN SECONDS
BATHYMETRY IN KM
DISTANCE IN SECONDS
2.00
2.00 - 4.70
4.70
6.50
8.06
DEPTH IN KM
DISTANCE IN KM

Fig. 50. Interpreted travel time plot with bathymetry and velocity/depth model for Station 1. For this model two datum planes were used because of the deep sediment pond on the western half of the shots. The transition depth from 3.28 km/sec to 3.78 km/sec material is not known.

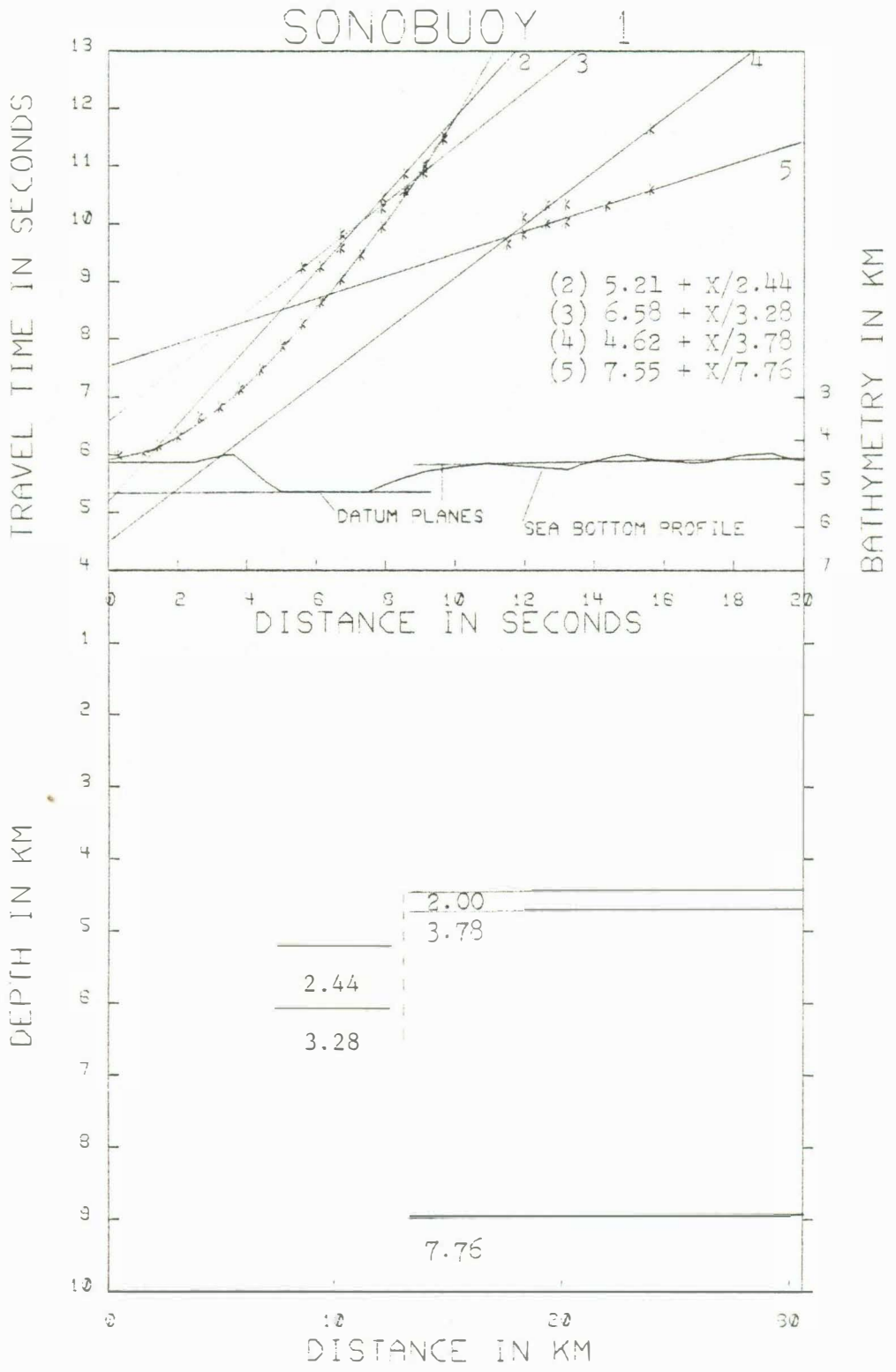
SONOBUOY 1
TRAVEL TIME IN SECONDS
BATHYMETRY IN KM
DISTANCE IN SECONDS
(2) 5.21 + X/2.44
(3) 6.58 + X/3.28
(4) 4.62 + X/3.78
(5) 7.55 + X/7.76
DATUM PLANES
SEA BOTTOM PROFILE
DEPTH IN KM
DISTANCE IN KM
2.00
3.78
2.44
3.28
7.76

BIBLIOGRAPHY

Aggarwal, Y. P., and M. Barazangi, P and S traveltimes in the Tonga-Fiji region: A zone of low velocity in the uppermost mantle behind the Tonga island arc, J. Geophys. Res., 77, 6427-6434, 1972.

Anderson, R. N., Heat flow in the Mariana marginal basin, J. Geophys. Res., 80, 4043-4048, 1975.

Barazangi, M. and B. Isacks, Lateral variation of seismic wave attenuation in the upper mantle above the inclined earthquake zone of the Tonga island arc: Deep anomaly in the upper mantle, J. Geophys. Res. 76, 8493-8515, 1971.

Barazangi, M., W. Pennington and B. Isacks, Global study of seismic wave attenuation in the upper mantle behind island arcs using pP waves, J. Geophys. Res., 80, 1079-1092, 1975.

Clague, D. A., and P.F. Straley, Petrologic nature of the oceanic Moho, Geology, 5, 133-136, 1976.

Epp, D., and W. Suyenaga, Thermal contraction and alteration of the oceanic crust, unpublished manuscript, University of Hawaii, 1978.

Ewing, J. I., Elementary theory of seismic refraction and reflection measurements, in The Sea, vol. 3, edited by M. N. Hill, pp. 3-19, Wiley-Interscience, New York, 1963.

Ewing, M., G. P. Woollard and A. C. Vine, Geophysical investigations in the emerged and submerged Atlantic coastal plain, Part III: Barnegat Bay, New Jersey Section, Geol. Soc. Amer. Bull., 50, 257-296, 1939.

Fisher, R. L., and H. H. Hess, Trenches, in The Sea, vol. 3, edited by M. N. Hill, pp. 411-436, Wiley-Interscience, New York, 1963.

Fryer, P., IPOD site survey report SP 1-4 (Kane Keoki KK770317, legs 3-4), unpublished manuscript, University of Hawaii, 1977.

Goslin, J., et al., Thickening of the oceanic layer in the Pacific ocean, Marine Geophys. Res., 1, 418-427, 1972.

Hart, S. R., W. E. Glassley and D. E. Karig, Basalts and sea floor spreading behind the Mariana island arc, Earth Planet. Sci. Lett., 15, 12-18, 1972.

Henry, M., D. E. Karig and G. G. Shor, Jr., Two seismic refraction profiles in the West Philippine Sea, in Initial reports of the Deep Sea Drilling Project, vol. 31, edited by D. E. Karig, J. C. Ingle et al., pp. 611-614, U.S. Government Printing Office, Washington, D. C., 1975.

Hilde, T. W. C., S. Uyeda and L. Kroenke, Evolution of the western Pacific and its margin, Tectonophysics, 38, 145-165, 1977.

Houtz, R., and J. Ewing, Upper crustal structure as a function of plate age, J. Geophys. Res., 81, 2490-2498, 1976.

Houtz, R. E., Seismic properties of layer 2A in the Pacific, J. Geophys. Res., 81, 6321-6331, 1976.

Hussong, D. M., Detailed structural interpretations of the Pacific oceanic crust using ASPER and ocean bottom seismometer methods, Ph.D. thesis, University of Hawaii, 1972.

Hussong, D. M., et al., Crustal structure of the Peru-Chile trench: 8°-12° S latitude, in The Geophysics of the Pacific Ocean and its Margin, Geophysical Monograph 19, edited by G. H. Sutton, et al., pp. 71-85, American Geophysical Union, Washington, D. C., 1976.

Ingle, J. C., Jr., Summary of Late Paleogene-Neogene insular stratigraphy, paleobathymetry, and correlations, Philippine Sea and Sea of Japan region, in Initial Reports of the Deep Sea Drilling Project, vol. 31, edited by D. E. Karig, J. C. Ingle et al., pp. 837-852, U. S. Government Printing Office, Washington, D. C., 1975.

Isacks, B. L., J. Oliver and L. R. Sykes, Seismology and the new global tectonics, J. Geophys. Res., 73, 5855-5862, 1968.

Karig, D. E., Structural history of the Mariana island arc system, Geol. Soc. Amer. Bull., 82, 323-344, 1971a.

Karig, D. E., Origin and development of marginal basins in the western Pacific, J. Geophys. Res., 76, 2542-2561, 1971b.

Karig, D. E., Site surveys in the Mariana area (Scan IV), in Initial Reports of the Deep Sea Drilling Project, vol. 6, edited by A. G. Fischer, pp. 681-689, U.S. Government Printing Office, Washington, D. C., 1971c.

Karig, D. E., Remnant arcs, Geol. Soc. Amer. Bull., 83, 1057-1068, 1972.

Karig, D. E., Basin genesis in the Philippine Sea, in Initial Reports of the Deep Sea Drilling Project, vol. 31, edited by D. E. Karig, J. C. Ingle et al., pp. 857-879, U. S. Government Printing Office, Washington, D. C., 1975.

Karig, D. E., and G. F. Sharman III, Subduction and accretion in trenches, Geol. Soc. Amer. Bull., 86, 377-389, 1975.

Katsumata, M., and L. R. Sykes, Seismicity and tectonics of the western Pacific: Izu-Mariana-Caroline and Ryukyu-Taiwan regions, J. Geophys. Res., 74, 5923-5948, 1969.

Kroenke, L., and R. Moberly, Jr., Lithologic interpretation of continuous reflection profiling, in Initial Reports of the Deep Sea Drilling Project, vol. 7, edited by E. L. Winterer et al., pp. 1161-1167, U. S. Government Printing Office, Washington, D. C., 1971.

Larson, R. L., Late Jurassic and early Cretaceous evolution of the western central Pacific ocean, J. Geomag. Geoelectr., 28, 219-236, 1976.

Moberly, R., Origin of lithosphere behind island arcs, with reference to the western Pacific, Geol. Soc. of Amer. Memoir 132, edited by R. Shagam et al., pp. 35-55, Geol. Soc. of Amer., 1972.

Mogi, K., Relationship between shallow and deep seismicity in the western Pacific region, Tectonophysics, 17, 1-22, 1973.

Murauchi, S., et al., Crustal structure of the Philippine Sea, J. Geophys. Res., 73, 3143-3171, 1968.

Odegard, M. E., Refraction inversion for a spherical earth, unpublished manuscript, Hawaii Institute of Geophysics, 1975.

Packham, G. H., and D. A. Falvey, An hypothesis for the formation of marginal seas in the western Pacific, Tectonophysics, 11, 79-109, 1971.

Sclater, J. G., Heat flow and elevation of marginal basins of the western Pacific, J. Geophys. Res., 77, 5705-5719, 1972.

Sclater, J. G., and J. Francheteau, The implications of terrestrial heat flow observations on current tectonic and geochemical models of the crust and upper mantle of the earth, Geophys. J. Roy. Astron. Soc., 30, 509-542, 1970.

Seekins, L. C., and T. Teng, Lateral variation in the structure of the Philippine Sea plate, J. Geophys. Res., 82, 317-324, 1977.

Shipboard scientific party, Site 60, in Initial reports of the Deep Sea Drilling Project, vol. 6, edited by A. G. Fischer et al., pp. 587-590, U.S. Government Printing Office, Washington, D. C., 1971.

Shipboard scientific party, Site 61, in Initial reports of the Deep Sea Drilling Project, vol. 7, edited by E. L. Winterer et al., pp. 27-35, U. S. Government Office, Washington, D. C., 1971.

Shor, G. G., Jr., Refraction and reflection techniques and procedure, in The Sea, vol. 3, edited by M. N. Hill, pp. 20-38, Wiley-Interscience, New York, 1963.

Shor, G. G., Jr., H. K. Kirk and H. W. Menard, Crustal structure of the Melanesian arc, J. Geophys. Res., 76, 2562-2590, 1971.

Shor, G. G., Jr., H. W. Menard and R. V. Raitt, Structure of the Pacific basin, in The Sea, vol. 4, edited by A. E. Maxwell, pp. 3-27, Wiley-Interscience, New York, 1971.

Uyeda, S., and Z. Ben-Avraham, Origin and development of the Philippine Sea, Nature Phys. Sci., 240, 176-178, 1972.

Watts, A. B., et al., Sea floor spreading in marginal basins of the western Pacific, Tectonophysics, 37, 167-181, 1977.

Watts, A. B., and J. K. Weissel, Tectonic history of the Shikoku marginal basin, Earth Planet. Sci. Lett., 25, 239-250, 1975.

Woollard, G. P., The interrelationships of crustal and upper mantle parameter values in the Pacific, Rev. Geophys. and Space Phys., 13, 87-137, 1975.